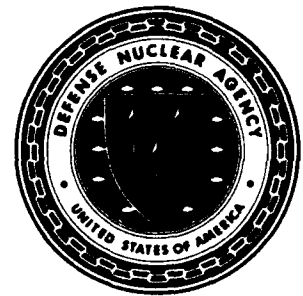Defense Nuclear Agency
Alexandria, VA 22310-3398

AD-A284 231
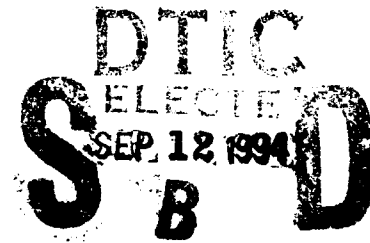
DNA-TR-93-102

Defect Reduction and Back Channel Degradation in SIMOX

Fereydoon Namavar
Spire Corp.
One Patriots Park
Bedford, MA 01730

DTIC
ELECTE
SEP. 12 1994
S B D

August 1994

Technical Report

94-29480

DTIC QUALITY INSPECTED 3

94 9 08 054

Destroy this report when it is no longer needed. Do not return to sender.

DISTRIBUTION LIST UPDATE

This mailer is provided to enable DNA to maintain current distribution lists for reports. (We would appreciate your providing the requested information.)

☐ Add the individual listed to your distribution list.

☐ Delete the cited organization/individual.

☐ Change of address.

> **NOTE:**
> **Please return the mailing label from the document so that any additions, changes, corrections or deletions can be made easily. For distribution cancellation or more information call DNA/IMAS (703) 325-1036.**

NAME: _____

ORGANIZATION: _____

OLD ADDRESS	**CURRENT ADDRESS**
_____	_____
_____	_____
_____	_____

TELEPHONE NUMBER: ( ) _____

DNA PUBLICATION NUMBER/TITLE	**CHANGES/DELETIONS/ADDITIONS, etc.)** *(Attach Sheet if more Space is Required)*
_____	_____
_____	_____
_____	_____

DNA OR OTHER GOVERNMENT CONTRACT NUMBER: _____

CERTIFICATION OF NEED-TO-KNOW BY GOVERNMENT SPONSOR (if other than DNA):

SPONSORING ORGANIZATION: _____

CONTRACTING OFFICER OR REPRESENTATIVE: _____

SIGNATURE: _____

CUT HERE AND RETURN

DEFENSE NUCLEAR AGENCY
ATTN: IMAS
6801 TELEGRAPH ROAD
ALEXANDRIA, VA   22310-3398

REPORT DOCUMENTATION PAGE

1. AGENCY USE ONLY (Leave blank)	2. REPORT DATE 940801	3. REPORT TYPE AND DATES COVERED Technical 900831 – 930930

4. TITLE AND SUBTITLE

Defect Reduction and Back Channel Degradation in SIMOX

5. FUNDING NUMBERS

C - DNA 001-90-C-0080
PE - 62715H
PR - RV
TA - RW
WU - DH303960

6. AUTHOR(S)

Fereydoon Namavar

7. PERFORMING ORGANIZATION NAME(S) AND ADDRESS(ES)

Spire Corp.
One Patriots Park
Bedford, MA 01730

8. PERFORMING ORGANIZATION REPORT NUMBER

FR-10131

9. SPONSORING/MONITORING AGENCY NAME(S) AND ADDRESS(ES)

Defense Nuclear Agency
6801 Telegraph Road
Alexandria, VA 22310-3398
RAES/Palkuti

10. SPONSORING/MONITORING AGENCY REPORT NUMBER

DNA-TR-93-102

11. SUPPLEMENTARY NOTES

12a. DISTRIBUTION/AVAILABILITY STATEMENT

Approved for public release; distribution is unlimited.

12b. DISTRIBUTION CODE

13. ABSTRACT *(Maximum 200 words)*

Because of potential back channel leakage problems and parasitic bipolar effects in silicon-on-insulator (SOI) metal-oxide-semiconductor (MOS) devices, especially n-channel MOS devices which must operate in an ionizing radiation environment, it is desirable to produce SIMOX wafers which have a layer of poor quality silicon near the Si/buried SiO_2 interface. Also, for device fabrication these wafers must have low defect, high quality silicon near the wafer surface.

In this program we have demonstrated, for the first time, that by Ge implantation and solid phase epitaxy regrowth, the surface region of the Si top layer of the SIMOX wafer is improved and the region adjacent to the buried SiO_2 is degraded. N-MOSFETs with and without Ge implantation, were fabricated on SIMOX and Si wafers. Our results show that Ge implantation into SIMOX significantly reduced off-state leakage and parasitic bipolar effects. In addition, gate-induced drain leakage of n-MOSFETs was greatly suppressed and the source-to-drain breakdown voltage was improved.

All devices were irradiated with 100 krad x-ray at RADC. Our measurements show that for devices fabricated on SIMOX with Ge implantation the off-state leakage current was up to 1000 times less than for devices fabricated on SIMOX without Ge implantation.

DTIC QUALITY INSPECTED 3

14. SUBJECT TERMS

Ge Implantation   SOI Devices
Solid Phase Epitaxy   MOS Devices   SIMOX Wafers

15. NUMBER OF PAGES 98

16. PRICE CODE

17. SECURITY CLASSIFICATION OF REPORT	18. SECURITY CLASSIFICATION OF THIS PAGE	19. SECURITY CLASSIFICATION OF ABSTRACT	20. LIMITATION OF ABSTRACT
UNCLASSIFIED	UNCLASSIFIED	UNCLASSIFIED	SAR

CLASSIFIED BY:

N/A since Unclassified.

DECLASSIFY ON:
N/A since Unclassified.

CLASSIFIED BY:

SECURITY CLASSIFICATION OF THIS PAGE

PREFACE

iii

CONVERSION TABLE

Conversion factors for U. S. Customary to metric (SI) units of measurement

MULTIPY ⟶	BY ⟶	TO GET
TO GET ⟵	BY ⟵	DIVIDE
angstrom	$1.000\,000\ \mathrm{X\,E}\text{-}10$	meters (m)
atmosphere (normal)	$1.013\,25\ \ \mathrm{X\,E}\text{+}2$	kilo pascal (kPa)
bar	$1.000\,000\ \mathrm{X\,E}\text{+}2$	kilo pascal (kPa)
barn	$1.000\,000\ \mathrm{X\,E}\text{-}28$	meter^2 (m^2)
British thermal unit (thermochemical)	$1.054\,350\ \mathrm{X\,E}\text{+}3$	joule (J)
calorie (thermochemical)	$4.184\,000$	joule (J)
cal (thermochemical)/cm^2	$4.184\,000\ \mathrm{X\,E}\text{-}2$	mega joule/m^2 (MJ/m^2)
curie	$3.700\,000\ \mathrm{X\,E}\text{+}1$	*giga becquerel (GBq)
degree (angle)	$1.745\,329\ \mathrm{X\,E}\text{-}2$	radian (rad)
degree Fahrenheit	$T_K = (T\,^\circ F + 459.67)/1.8$	degree kelvin (K)
electron volt	$1.602\,19\ \ \mathrm{X\,E}\text{-}19$	joule (J)
erg	$1.000\,000\ \mathrm{X\,E}\text{-}7$	joule (J)
erg/second	$1.000\,000\ \mathrm{X\,E}\text{-}7$	watt (W)
foot	$3.048\,000\ \mathrm{X\,E}\text{-}1$	meter (m)
foot-pound-force	$1.355\,818$	joule (J)
gallon (U.S. liquid)	$3.785\,412\ \mathrm{X\,E}\text{-}3$	meter^3 (m^3)
inch	$2.540\,000\ \mathrm{X\,E}\text{-}2$	meter (m)
jerk	$1.000\,000\ \mathrm{X\,E}\text{+}9$	joule (J)
joule/kilogram (J/kg) (radiation dose absorbed)	$1.000\,000$	Gray (Gy)
kilotons	4.183	terajoules
kip (1000 lbf)	$4.448\,222\ \mathrm{X\,E}\text{+}3$	newton (N)
kip/inch^2 (ksi)	$6.894\,757\ \mathrm{X\,E}\text{+}3$	kilo pascal (kPa)
ktap	$1.000\,000\ \mathrm{X\,E}\text{+}2$	newton-second/m^2 (N-s/m^2)
micron	$1.000\,000\ \mathrm{X\,E}\text{-}6$	meter (m)
mil	$2.540\,000\ \mathrm{X\,E}\text{-}5$	meter (m)
mile (international)	$1.609\,344\ \mathrm{X\,E}\text{+}3$	meter (m)
ounce	$2.834\,952\ \mathrm{X\,E}\text{-}2$	kilogram (kg)
pound-force (lbs avoirdupois)	$4.448\,222$	newton (N)
pound-force inch	$1.129\,848\ \mathrm{X\,E}\text{-}1$	newton/meter (N · m)
pound-force/inch	$1.751\,268\ \mathrm{X\,E}\text{+}2$	newton-meter (N/m)
pound-force/foot^2	$4.788\,026\ \mathrm{X\,E}\text{-}2$	kilo pascal (kPa)
pound-force/inch^2 (psi)	$6.894\,757$	kilo pascal (kPa)
pound-mass (lbm avoirdupois)	$4.535\,924\ \mathrm{X\,E}\text{-}1$	kilogram (kg)
pound-mass-foot^2 (moment of inertia)	$4.214\,011\ \mathrm{X\,E}\text{-}2$	kilogram-meter^2 (kg·m^2)
pound-mass-foot^3	$1.601\,846\ \mathrm{X\,E}\text{+}1$	kilogram/meter^3 (kg/m^3)
rad (radiation dose absorbed)	$1.000\,000\ \mathrm{X\,E}\text{-}2$	**Gray (Gy)
roentgen	$2.579\,760\ \mathrm{X\,E}\text{-}4$	coulomb/kilogram (C/kg)
shake	$1.000\,000\ \mathrm{X\,E}\text{-}8$	second (s)
slug	$1.459\,390\ \mathrm{X\,E}\text{+}1$	kilogram (kg)
torr (mm Hg, 0° C)	$1.333\,22\ \ \mathrm{X\,E}\text{-}1$	kilo pascal (kPa)

*The becquerel (Bq) is the SI unit of radioactivity; 1 Bq = 1 event/s.
**The Gray (Gy) is the SI unit of absorbed radiation.

TABLE OF CONTENTS

FIGURES

FIGURES (Concluded)

SECTION 1

INTRODUCTION

1.1 OBJECTIVE.

The main objectives of this program were to investigate the possibilities of implanting Ge into the silicon top layer of Separation by IMplantation of OXygen (SIMOX) wafers a) to reduce defect density in the surface silicon (the device region) and b) to degrade the quality of silicon near the Si/SiO_2 interface in order to decrease the back-channel leakage current and minimize parasitic bipolar effects.

We also evaluated the effect of a damaged back channel on device performance by fabricating test structures. SIMOX substrates would be implanted with Ge using an optimized process and then sent to an integrated circuits production facility (subcontract) to be run through a device processing line. Several circuits have been fabricated on the substrates, and their electrical characteristics would be evaluated before and after exposure to ionizing radiation.

1.2 BACKGROUND.

The fabrication of silicon-on-insulator (SOI) material with the SIMOX process has gained increasing importance in the fabrication of radiation hard devices. However, one of the obstacles to the more widespread use of SIMOX material is the high density of dislocations in the silicon top layer. Standard SIMOX wafers typically have a silicon surface layer about 1500Å thick and a buried layer about 4000Å thick. The interfaces are generally smooth and sharp, but there are some silicon islands in the buried oxide layer. The density of defects in this material has typically been observed at a level of about 10^8 to 10^{10} dislocations/cm^2.[1,2,3]

Potential back-channel leakage problems in SOI metal-oxide-semiconductor (MOS) devices, especially in n-channel MOS devices which must operate in an ionizing radiation environment, make it desirable to produce SIMOX wafers which have a layer of poor quality silicon near the Si/buried SiO_2 interface. At the same time, these wafers must have low defect, high quality silicon near the wafer surface for device fabrication.

We have demonstrated that with Ge ion implantation and solid phase epitaxy regrowth, the surface region of the silicon top layer of the SIMOX wafer is improved and the region adjacent to the buried SiO_2 is degraded. These results have been observed by Rutherford backscattering spectroscopy (RBS)/channeling, cross-sectional transmission electron microscopy (XTEM), and plan-view TEM (PTEM).

1.2.1 Improving the Crystalline Quality of SOI Material by Implantation.

It has been demonstrated[4] that the crystalline quality of the silicon layer grown on sapphire substrates (SOS) by chemical vapor deposition (CVD) can be improved by implantation of silicon ions and subsequent thermal annealing. Only amorphization and solid phase epitaxy regrowth are necessary to improve the crystalline quality of the silicon because defects in SOS material are planar (twins and stacking faults).[5] Conversely, the threading dislocation defects

1

in the SIMOX material are linear and align along the (110) direction.[1] Therefore, partial amorphization of the silicon top layer is necessary but not sufficient to reduce the density of defects in SIMOX since the threading dislocations will regrow with the Si during solid phase epitaxy.

Threading dislocations are terminated by interfaces which, in SIMOX material, normally are at the buried layer and the wafer surface. Epitaxially-grown layers produced by CVD may also exhibit interface termination if the new layer is sufficiently strained relative to the substrate.[6] We anticipated that Ge implantation would not only produce an amorphized silicon layer (similar to Si implantation but with a lower dose) but would also create a strained layer because of the larger lattice constant of silicon alloyed with germanium as opposed to that of pure silicon. Thus, the strained layer would create an artificial interface and stop the propagation of threading dislocations during solid phase epitaxy regrowth.

Recently, substantial progress has been made in reducing threading dislocation density by using multiple implantation processes.[7,8,9,10,11] Although a Ge implantation process can reduce the density of threading dislocations that reach the surface. Figure 1-1 shows a cross section of a SIMOX wafer implanted with Ge at a dose of 5×10^{14} Ge^+/cm^2 at 150 keV and then annealed for 0.5 hour at 850°C in N_2. Figure 1-2 shows a plan-view TEM of the silicon top layer of the same sample; note the presence of several threading dislocation defects and dislocation loops. Figure 1-3 shows a plan-view TEM of only the surface region of the silicon top layer after the lower part of the sample was thinned; note that no threading dislocation defects can be seen in the Ge-implanted region. However, perhaps more importantly, Ge implantation creates a degraded region near the Si/buried SiO_2 interface which may be advantageous for radiation-hard device applications.

We have studied the effect of Ge implantation into the Si top layer of SIMOX material, followed by solid phase epitaxy regrowth, on reducing the density of threading dislocations that reach the surface. RBS/channeling work on Ge-implanted wafers proves that Ge occupies substitutional sites in Si. Details of this work may be found in the Phase I Final Report, contract # DNA001-88-C-0195, entitled "Defect Reduction in SIMOX Wafers." Figure 1-4 illustrates the angular scans for three different crystalline axes of a si sample implanted with 1×10^{15} Ge^+/cm^2 at 100 keV and annealed for 0.5 hour at 850°C. For these axes, the minimum yield, X_{min}, is quite similar and indicates that, as expected, the Ge dopant atoms are located on lattice sites in the Si.

Although the preliminary Ge doses used appeared too low to produce the desired strain, we did observe a reduction in threading dislocation density (see Figures 1-1, 1-2, and 1-3) which indicated that mechanism(s) other than a strained layer were responsible for the decrease. We believe that the defect density reduction is related to the creation of numerous point defects during Ge implantation and/or to end-of-range damage in the form of dislocation loops near the Si/buried SiO_2 interface which may pin down the dislocations during solid phase epitaxy regrowth.
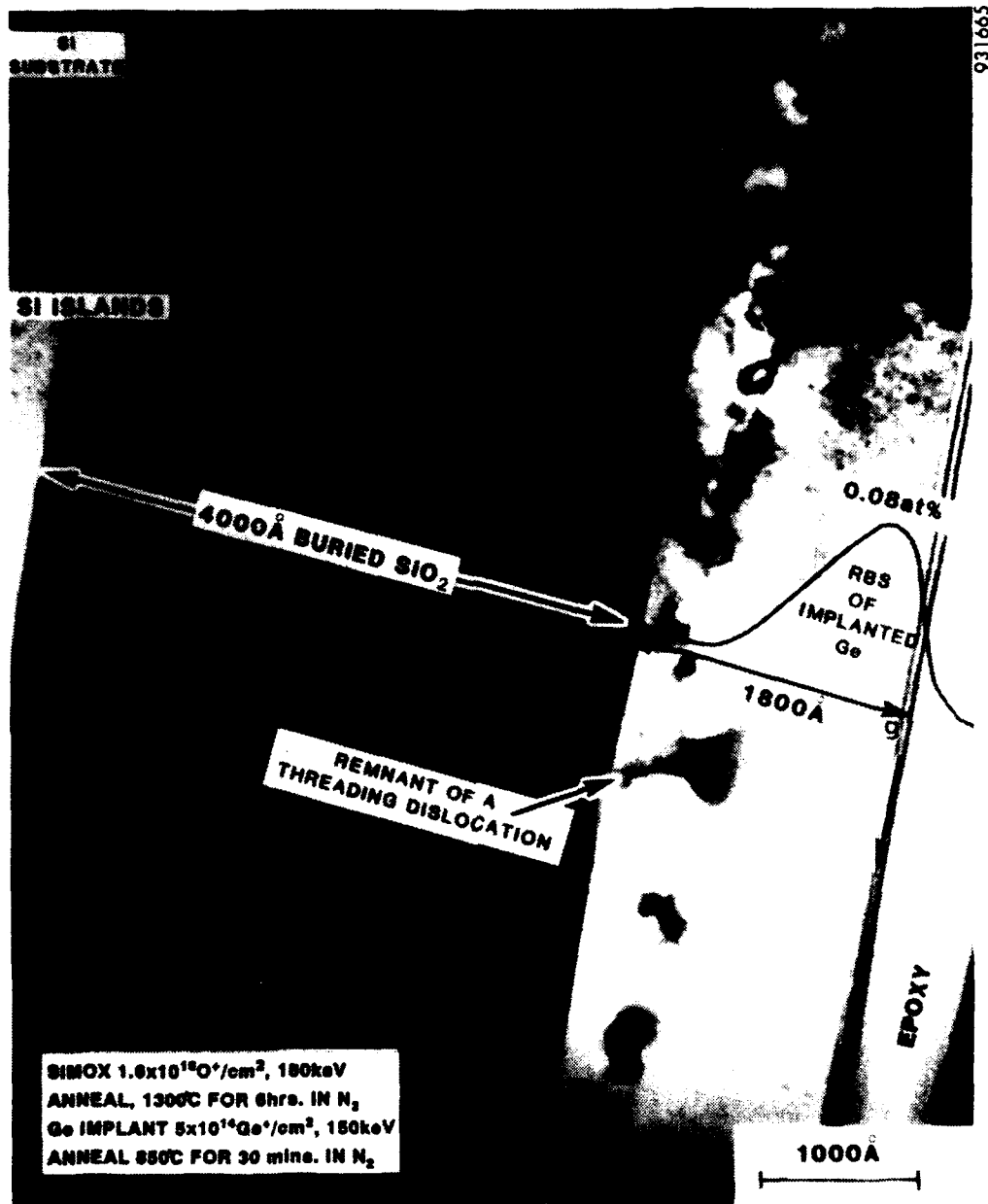
Figure 1-1. *Cross section of SIMOX wafer implanted with Ge at dose of 5 x 10^14 Ge^+/cm^2 at 150 keV and then annealed for 0.5 hour at 850°C in N_2.*

3

THROUGH ENTIRE Si TOP LAYER

2 μm

Dislocation

Dislocation Loop

Figure 1-2. *Plan-view TEM of the silicon top layer.*

NEAR SURFACE LAYER

2 μm

SIMOX $1.6 \times 10^{18} O^+/cm^2$, 180keV
ANNEAL, 1300°C FOR 6hrs. IN N_2
Ge IMPLANT $5 \times 10^{14} Ge^+/cm^2$, 150keV
ANNEAL 850°C FOR 30 mins. IN N_2
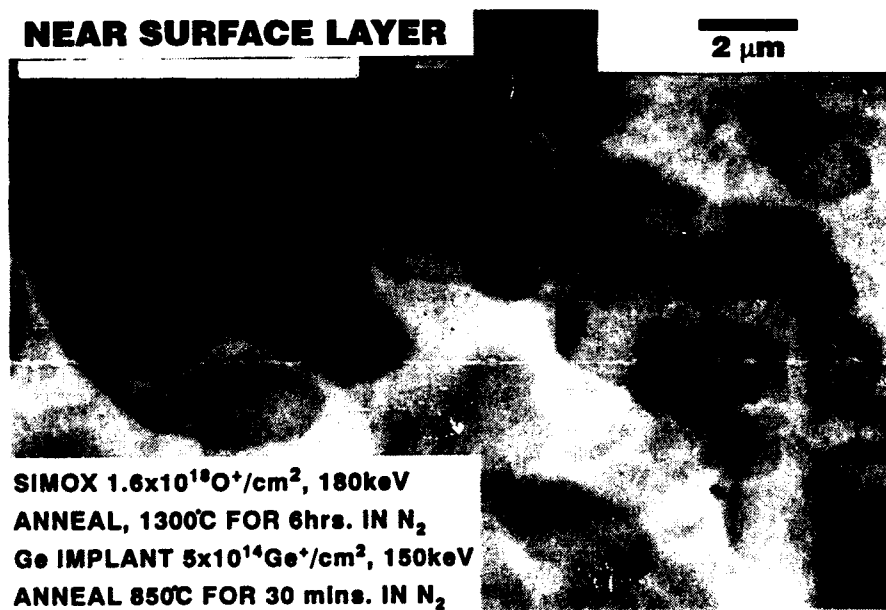
Figure 1-3. *Plan-view TEM of only the surface region of the silicon top layer.*

4
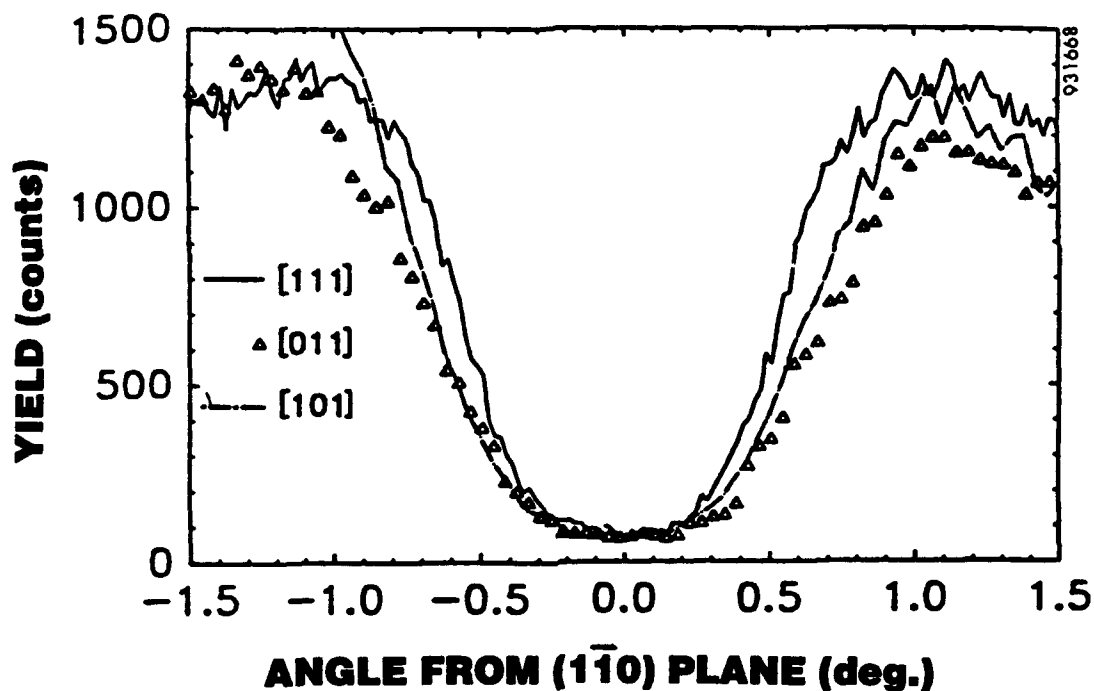
Figure 1-4. *Angular scans for three different crystalline axes of the silicon sample implanted with $1x10^{15}$ Ge^+/cm^2 at 100 keV and annealed for 0.5 hour at 850°C. These scans indicate that germanium is substitutional.*

However, we observed that much higher strain levels (produced, in this case, by the growth of a Ge-doped epitaxial layer) do indeed deflect many threading dislocations away from the surface. Figure 1-5 is an XTEM of such a sample and clearly shows the reduction of the density of defects which reach the surface by the deflection of some of the dislocations away from the surface and back towards the SiO_2 interface. One aspect of Phase II was to use much higher doses of implanted Ge to investigate fully the effect of a sufficiently strained layer in combination with the other mechanisms responsible for reducing defect density.

During the period of Phase I and Phase II of this work, other processes have been developed by Spire and others such as multiple oxygen implantation which appear more effective on defect reduction of SIMOX material.[7-11] Therefore, in this program, we have emphasized creating degradation regions near the SiO_2 interface which are considered advantageous for radiation hard device applications. A variety of ways[12] exist for reducing "back-channeling" in metal-oxide-semiconductor (MOS) devices fabricated in SIMOX, but Ge implantation is more practical and achieves both a higher quality surface Si region and a degraded Si region near the Si/buried SiO_2 interface with one low dose, room temperature implantation.

5
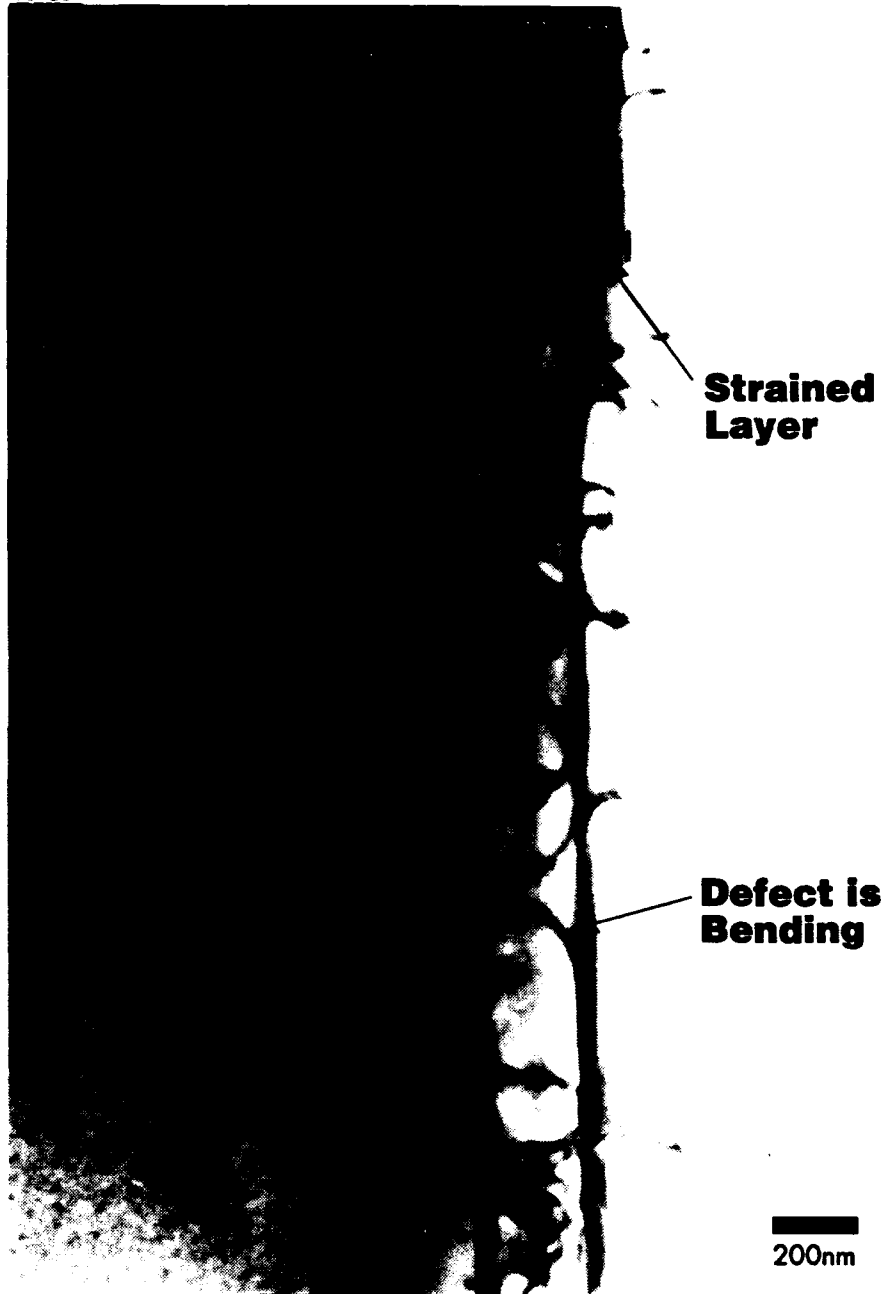
Figure 1-5. *Standard SIMOX wafer on which was epitaxially grown a pure Si layer followed by a Ge-doped Si layer (about 6% Ge) followed by a pure Si layer. This preliminary result clearly demonstrated that by creating a sufficiently strained layer we can deflect threading dislocation defects away from the surface.*

6

1.2.2 Back-Channel Leakage.

An MOS device fabricated in SOI material may have an unwanted parasitic MOS device at the silicon/buried insulator interface after exposure to ionizing radiation.[12,13,14] The passage of ionizing radiation through an insulator such as SiO_2 generates free electrons and holes. The electrons are more mobile and are swept out of the oxide, and the holes tend to be trapped near the silicon interface.[15,16] The trapped positive charge induces a negative charge in the silicon at the insulator interface, which can cause a change in the electrical characteristics of component MOS devices and can create inversion layers in p-type silicon (Figure 1-6).[13] If the inversion layer connects n-type regions of different potentials, a parasitic NMOS can be turned on by ionizing radiation, creating a permanent leakage path (Figure 1-6).
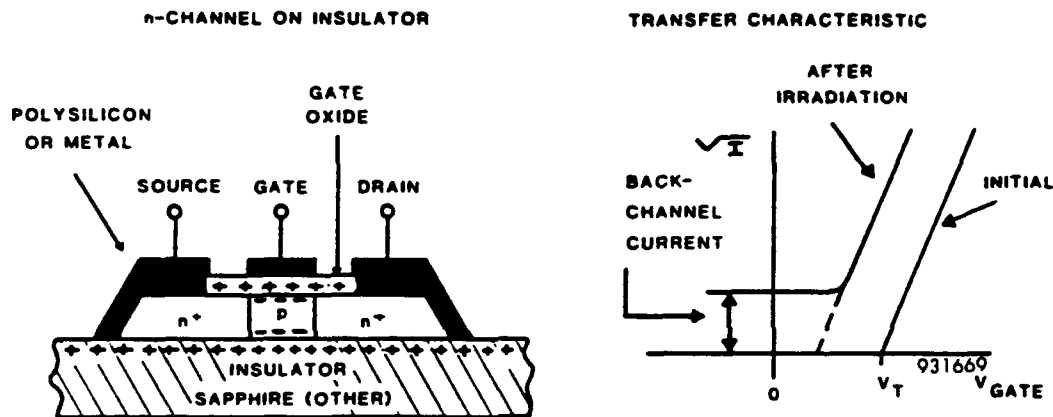
Figure 1-6. *Cross section of NMOS transistor on insulating substrate illustrating the trapped positive charge-induced parasitic back-channel and its effect on transfer characteristics.[13]*

Therefore, we need a silicon top layer which consists of a high quality layer at the surface for device fabrication, adjacent to a damaged layer. The high quality silicon surface layer is used for device fabrication, and the damaged silicon layer, because of reduced mobility, decreases the back-channel current.

Phase II work emphasized the radiation hardening of SIMOX material by reducing mobility in the interface region through degradation, thereby decreasing back-channel leakage current induced by ionizing radiation. Figure 1-7 illustrates another XTEM result of a standard SIMOX wafer Ge-implanted at 80 keV with a higher dose of 1×10^{16} Ge^+/cm^2. Figure 1-7 shows that no threading dislocations occur in the surface region and that a continuous damaged layer with a thickness of about 200 to 400Å has appeared near the Si/SiO_2 interface. The hardening of SIMOX material by the degradation of the Si/SiO_2 interface would be investigated primarily with Ge implanted into SIMOX, with subsequent solid phase epitaxy regrowth.

7

od Quality
stalline Si
Defect Observed
s Region)

aged Si Layer
ocations Loops)
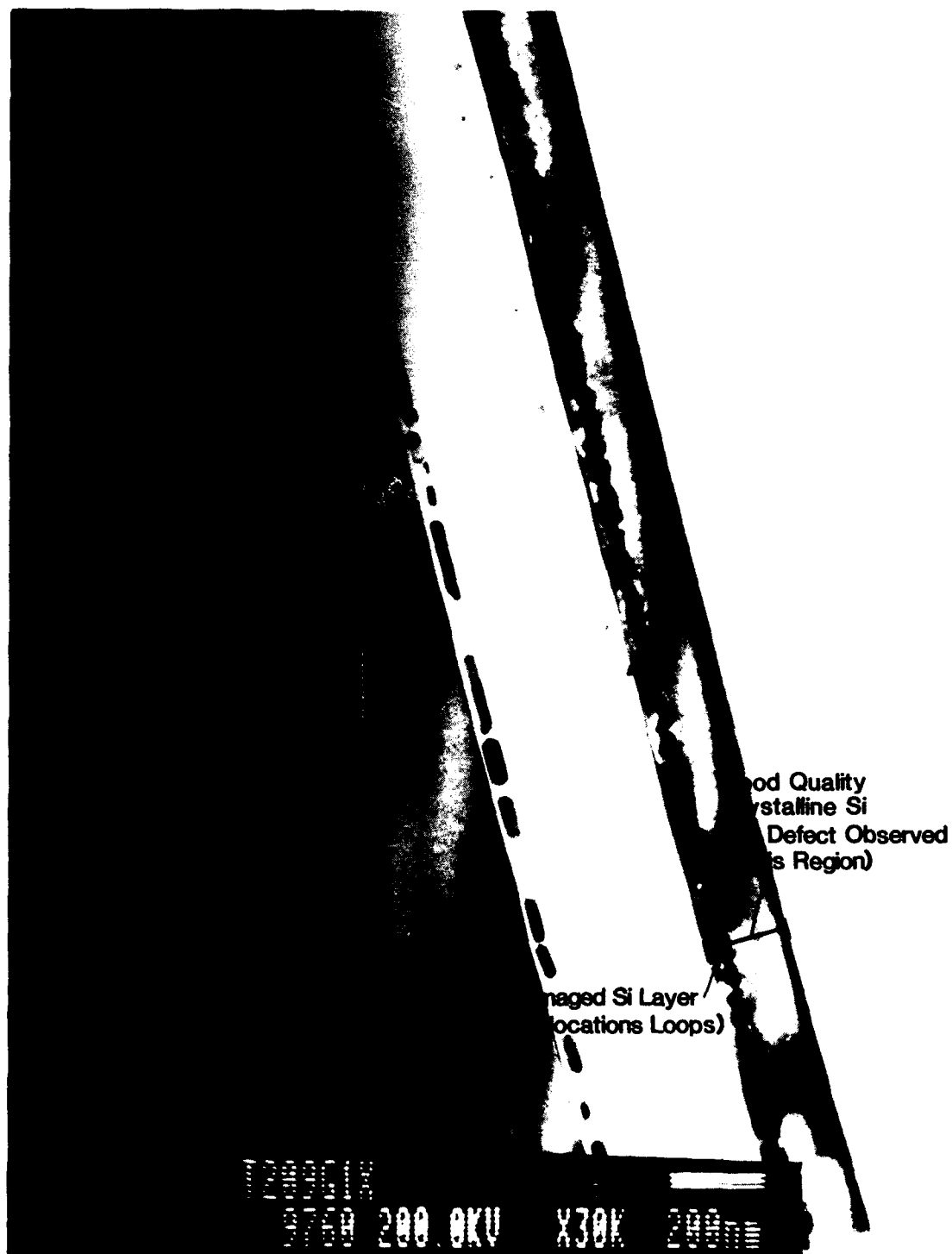
Figure 1-7. *XTEM of a SIMOX sample implanted with a dose of 1 x 10^{16} Ge$^+$/cm^2 at 80 keV and annealed for 0.5 hours at 850°C. Note the absence of threading dislocations in the surface Si region and the damaged layer near the Si/SiO$_2$ interface.*

SECTION 2

EXPERIMENTAL PROCEDURES AND DISCUSSION OF RESULTS

Throughout the Phase II program, we prepared a large number of SIMOX wafers for both materials analysis and device fabrication. These wafers were implanted with germanium under various conditions in order to optimize the parameters for producing SIMOX wafers with reduced defect density near the surface (device region) and a degraded back-channel region for improved radiation hardness and lower bipolar parasitic effects. Tables 2-1 and 2-2 summarize the list of wafers and Ge implantation. Figures 2-1 through 2-6 are representative optical reflectance and RBS data which were used to study the layer structure and composition of these wafers.

2.1   EFFECTS OF Ge IMPLANTATION ENERGY.

In Phase II, we studied the effects of Ge implantation energy on defect formation in the back-channel region of the Si top layer in SIMOX wafers. To reduce the back-channel leakage, the implantation energy must be adjusted so that the end-of-range damage is close to the Si/SiO_2 interface. However, our results indicated that a minimum distance between the amorphous/ crystalline (α/c) and Si/SiO_2 interfaces must be maintained to ensure the formation of dislocation loops resulting from Ge implantation. If the projected depth of the end-of-range damage, as determined by implantation energy, is less than this critical distance, dislocation loop formation may be reduced. Therefore, optimizing the implantation energy and controlling the location of end-of-range damage are greatly significant.

We implanted Ge with a dose of 1×10^{15} Ge^+/cm^2 at 100 keV into both a bulk silicon and a SIMOX wafer with a Si superficial layer about 1700Å thick. The samples were then annealed at 850°C for 0.5 hours in nitrogen. Figures 2-7a and 2-7b show the XTEM results of the Ge-implanted SIMOX and bulk Si samples, respectively. The end-of-range damage (dislocation loops) can be clearly seen in Figure 2-7b. Fewer dislocation loops can be seen in the SIMOX sample as compared to the bulk Si sample. Comparison with the plan-view TEM obtained from these samples (Figures 2-7c and 2-7d) clearly indicates the creation of fewer dislocation loops in SIMOX material than in bulk Si. Dislocation loop densities were about 8×10^9 cm^{-2} in SIMOX and 1.85×10^{10} cm^{-2} in bulk Si.

Fewer dislocation loops may appear in SIMOX as compared to bulk Si because of the distance of the bulk Si dislocation loops from the surface (Figures 2-7a and 2-7b) which, in SIMOX wafers, corresponds nearly to the location of the Si/SiO_2 interface. Dislocation loops are believed to originate from Si interstitials. Based on our results, if the distance between α/c and Si/SiO_2 interfaces in Ge-implanted SIMOX is less than a critical value, the Si/SiO_2 acts as a sink for Si interstitials, resulting in fewer dislocation loops.

To confirm the above notion, we implanted a SIMOX wafer with a Ge dose of 2×10^{15} Ge^+/cm^2 at 80 keV and compared it to a bulk Si sample implanted with the same dose, but at 100 keV. Figures 2-8a and 2-8b show the PTEM results of these samples. The dislocation loop densities for both samples appear comparable; 2.5×10^{10} cm^{-2} for bulk Si and 1.85×10^{15} cm^{-2} for SIMOX.

Table 2-1. *List of Ge$^+$-implanted SIMOX wafers for materials research.*

Wafer	Dose (Ge$^+$/cm^2)	Energy (keV)	Anneal
#SOI3A	1E16	190	0.5 hrs at 850°C in N$_2$
#T240	1E16	190	0.5 hrs at 850°C in N$_2$
#T241	1E16	190	0.5 hrs at 850°C in N$_2$
SiCTL-A	1E15	100	0.5 hrs at 850°C in N$_2$
SIMOX-1	1E15	100	0.5 hrs at 850°C in N$_2$
SIMOX-2	2E15	80	0.5 hrs at 850°C in N$_2$
SIMOX-3	1E16	80	0.5 hrs at 850°C in N$_2$
SIMOX-4	2E16	80	0.5 hrs at 850°C in N$_2$
SIMOX-5	2E16	40	0.5 hrs at 850°C in N$_2$
SiCTL-B	2E16	40	0.5 hrs at 850°C in N$_2$
#T469B	1E15	80	2 hrs. at 850°C in N$_2$
#T469D	1E15	110	2 hrs. at 850°C in N$_2$
MULT-A	2E15	160	0.5 hr. at 850°C in N$_2$
802B	2E15	100	0.5 hr. at 850°C in N$_2$
802C	2E15	80	0.5 hr. at 850°C in N$_2$
802D	3E15	40	0.5 hr. at 850°C in N$_2$ 1 hr. at 1000°C in N$_2$
802E	3E15	120	0.5 hr. at 850°C in N$_2$ 1 hr. at 1000°C in N$_2$
802F	3E15	160	0.5 hr. at 850°C in N$_2$ 1 hr. at 1000°C in N$_2$
#P1047 (p-type)	1E16	160	1 hr at 1000°C in N$_2$
#1047GE			1 hr. at 1000°C in Ar
#N1043 (n-type)	1E16	160	1 hr. at 1000°C in N$_2$
#1043GE			1 hr. at 1000°C in N$_2$
NAS-3	1E16	160	1 hr. at 1000°C in Ar

10

Table 2-2. *List of Ge⁺-implanted SIMOX wafers for device research.*

Wafer	First Half		Second Half		Anneal/N_2 (0.5 hr.)
	Dose (Ge⁺/cm²)	Energy (keV)	Dose (Ge⁺/cm²)	Energy (keV)	
#SOI-1*	0	--	1E15	150	850°C
#SOI-2*	5E15	120	5E15	150	850°C
#SOI-3*	0	--	1E16	150	850°C
#SOI-4**	0	--	1E15	150	850°C
#SOI-5**	1E15	120	1E15	150	950°C
#SOI-6**	5E15	120	5‾15	150	850°C
#SOI-7**	5E15	120	5E15	120	850°C
#SOI-8**	0	--	5E15	120	950°C
#SOI-9**	0	--	5E15	150	950°C
#SOI-10**	0	--	1E16	150	850°C
#SOI-11**	1E16	120	1E16	150	950°C
#SOI-12	0	--	0	--	--
#IBIS-1*	0	--	5E15	150	850°C
#IBIS-2**	0	--	5E15	150	950°C
#IBIS-3**	0	--	1E16	150	850°C
#IBIS-4**	5E15	150	1E15	150	850°C
#BULK-1*	0	--	5E15	150	850°C
#BULK-2**	0	--	5E15	150	850°C
#BULK-3**	0	--	5E15	150	950°C
#BULK-4**	1E16	150	1E15	150	950°C

* Ge implant before LOCOS   ** Ge implant after LOCOS

REFLECTANCE DATA (SYMBOLS) AND FIT (LINE)

N105 PINK   X² = 0.27E-03

DOSE = 1.51E+18   FWHM = 342 nm   DEPTH = 551 nm   CAP THICKNESS = 81 nm

IMPLANTED OXYGEN PROFILE

N105PINK.SOI   P1A451 .TRS

XC = .001 µm   XE = .249 µm   XF = .0174 µm   XI = .321 µm   XB = .103 µm
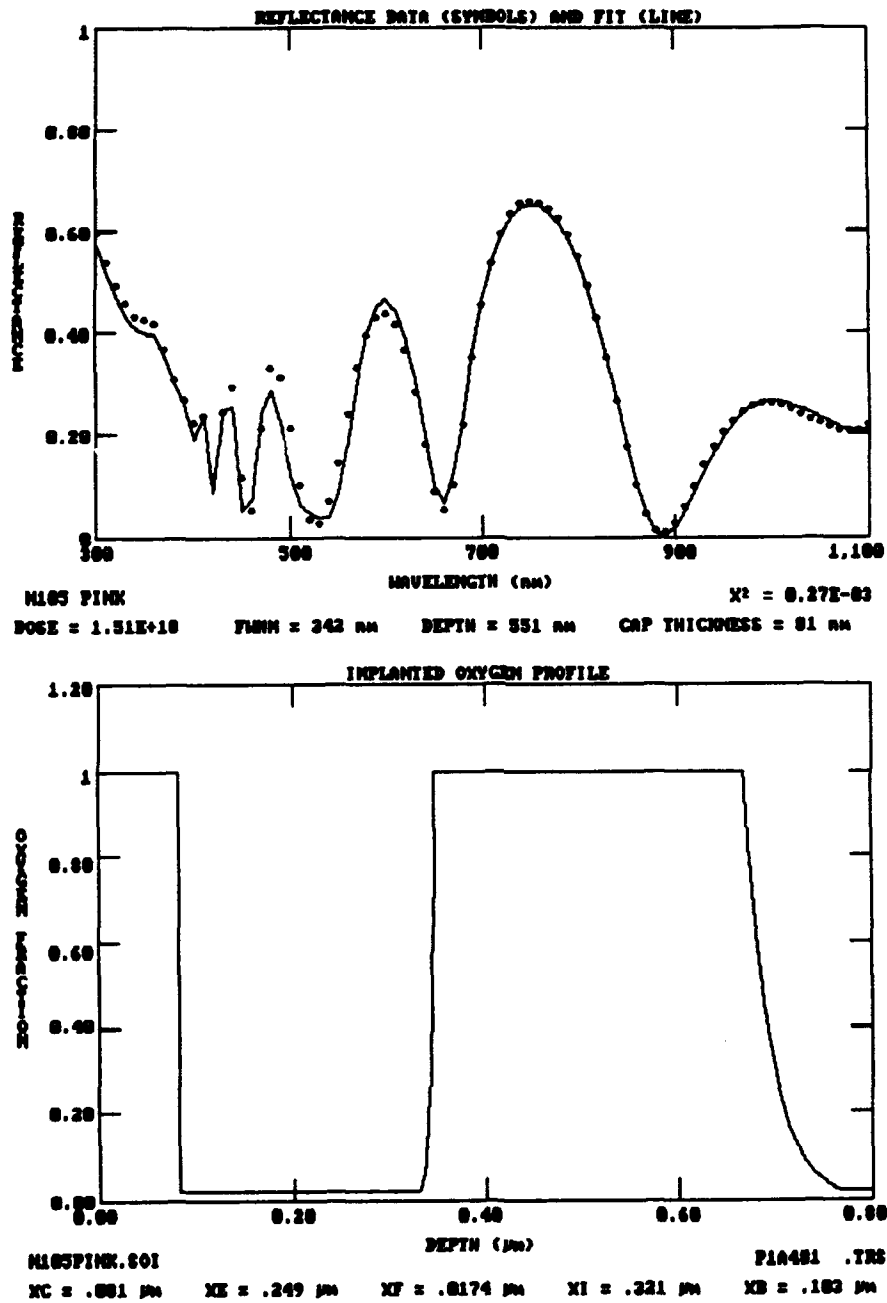
Figure 2-1. *Optical reflectance data with fit and analysis for standard SIMOX wafer #N105 indicating a silicon top layer about 2490Å thick and a buried oxide layer about 3210Å thick.*

12
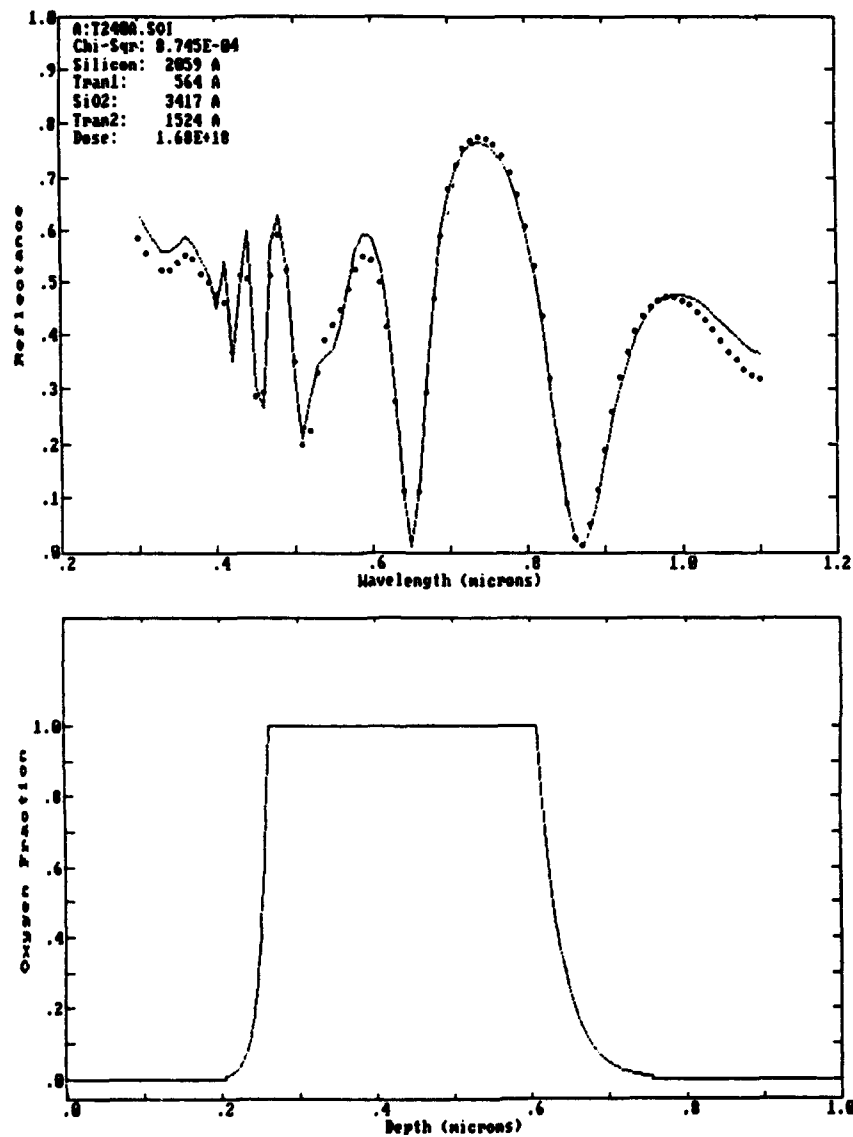
Figure 2-2. *Optical reflectance data with fit and analysis for standard SIMOX wafer #T240 indicating a silicon top layer about 2060Å thick and a buried oxide layer about 3420Å thick.*

13
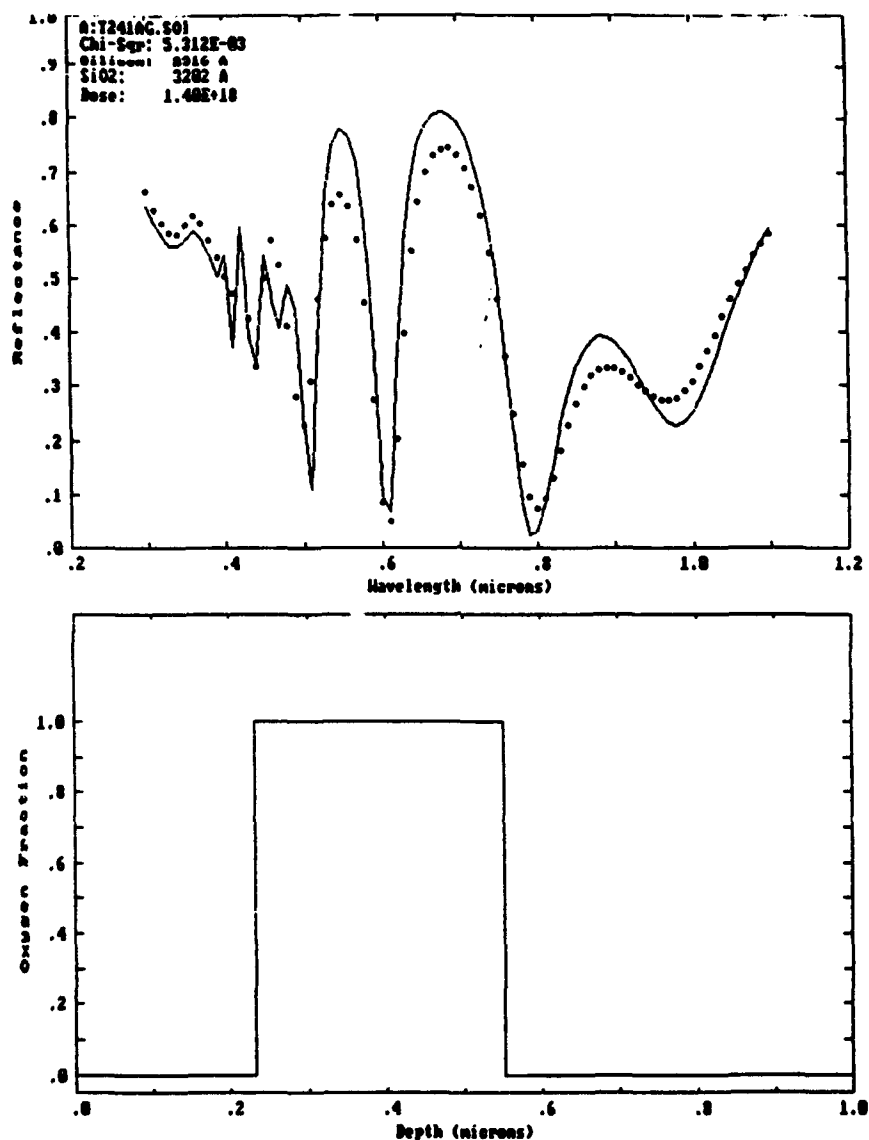
Figure 2-3. *Optical reflectance data with fit and analysis for standard SIMOX wafer #T241 indicating a silicon top layer about 2200Å thick and a buried oxide layer about 3200Å thick.*

14
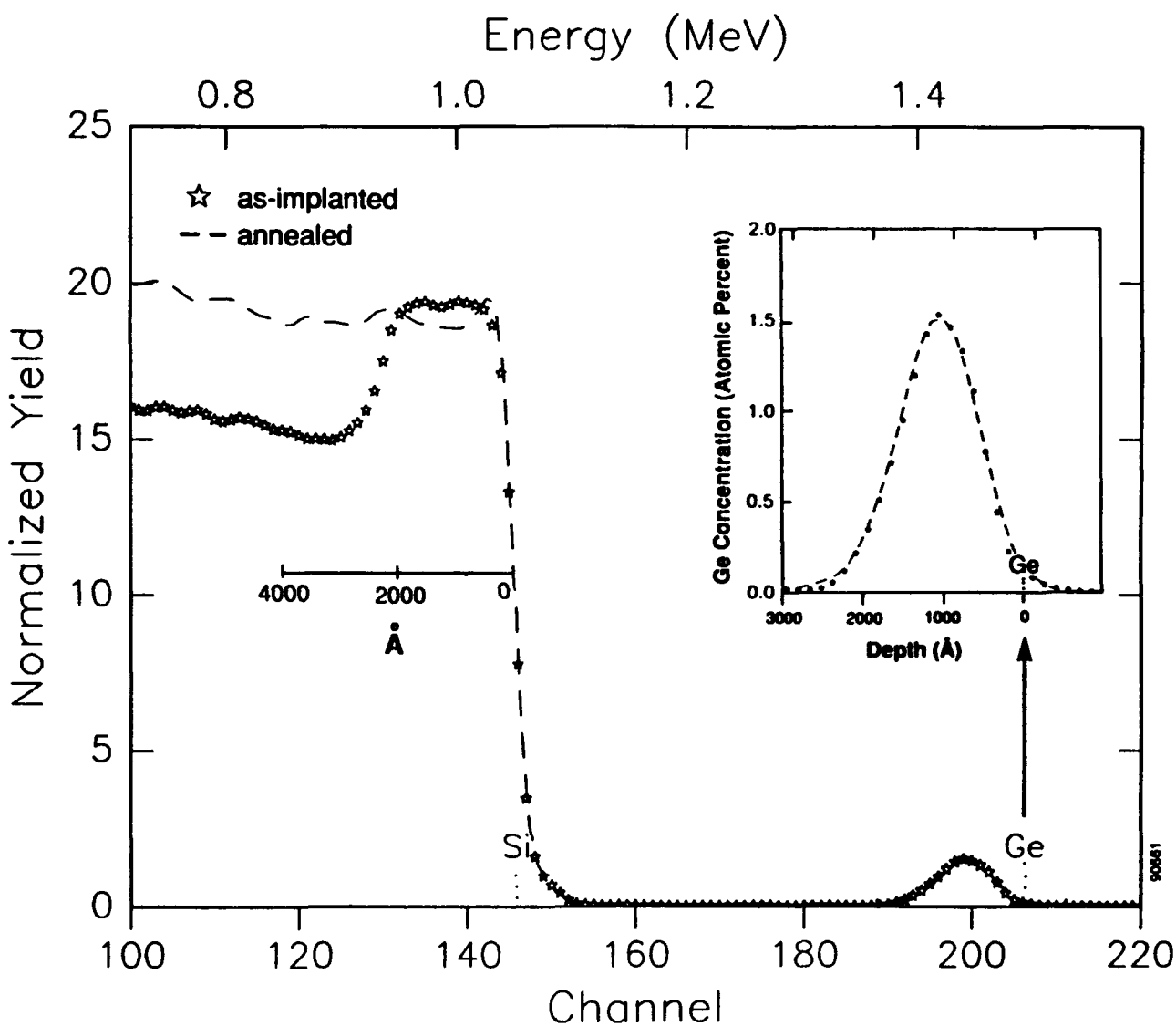
Figure 2-4. *RBS results for Si control sample #CTL1 implanted with a Ge dose of 1 x 10^16 Ge+/cm^2 at 190 keV before and after annealing for 0.5 hour at 850°C in N2. No redistribution of Ge resulting from annealing can be observed.*

15
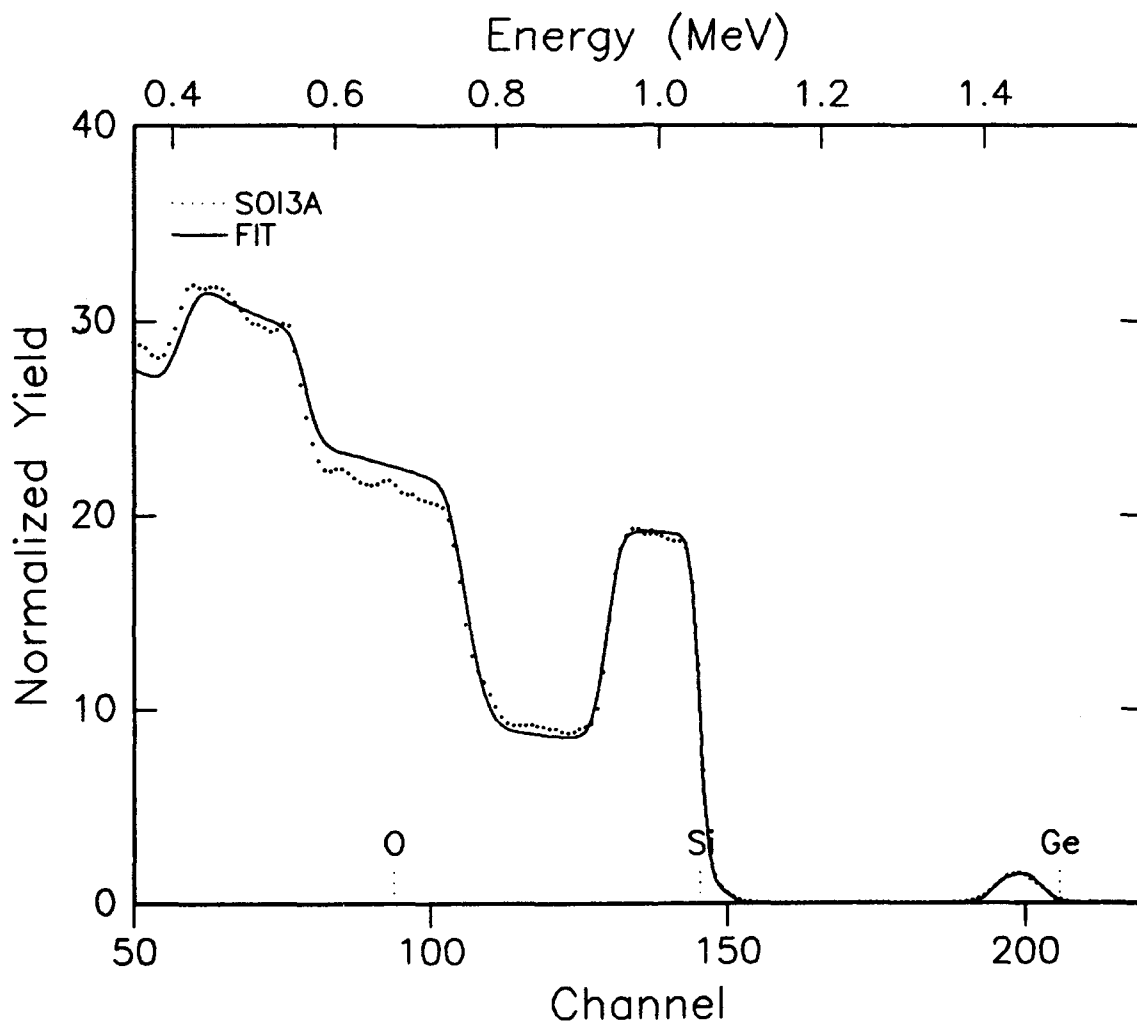
Figure 2-5. *RUMP code fit to RBS results for SIMOX sample #SOI3A (a piece of #N105) implanted with a dose of 1 x 10^16 Ge^+/cm^2 at 190 keV and annealed for 0.5 hours at 850°C in N_2. Results show a Si-Ge layer about 1240Å thick with Ge concentration of 1.54 atomic percent, 400Å below the surface. Total Si top layer thickness is about 2450Å which is in agreement with optical reflectance results.*

16
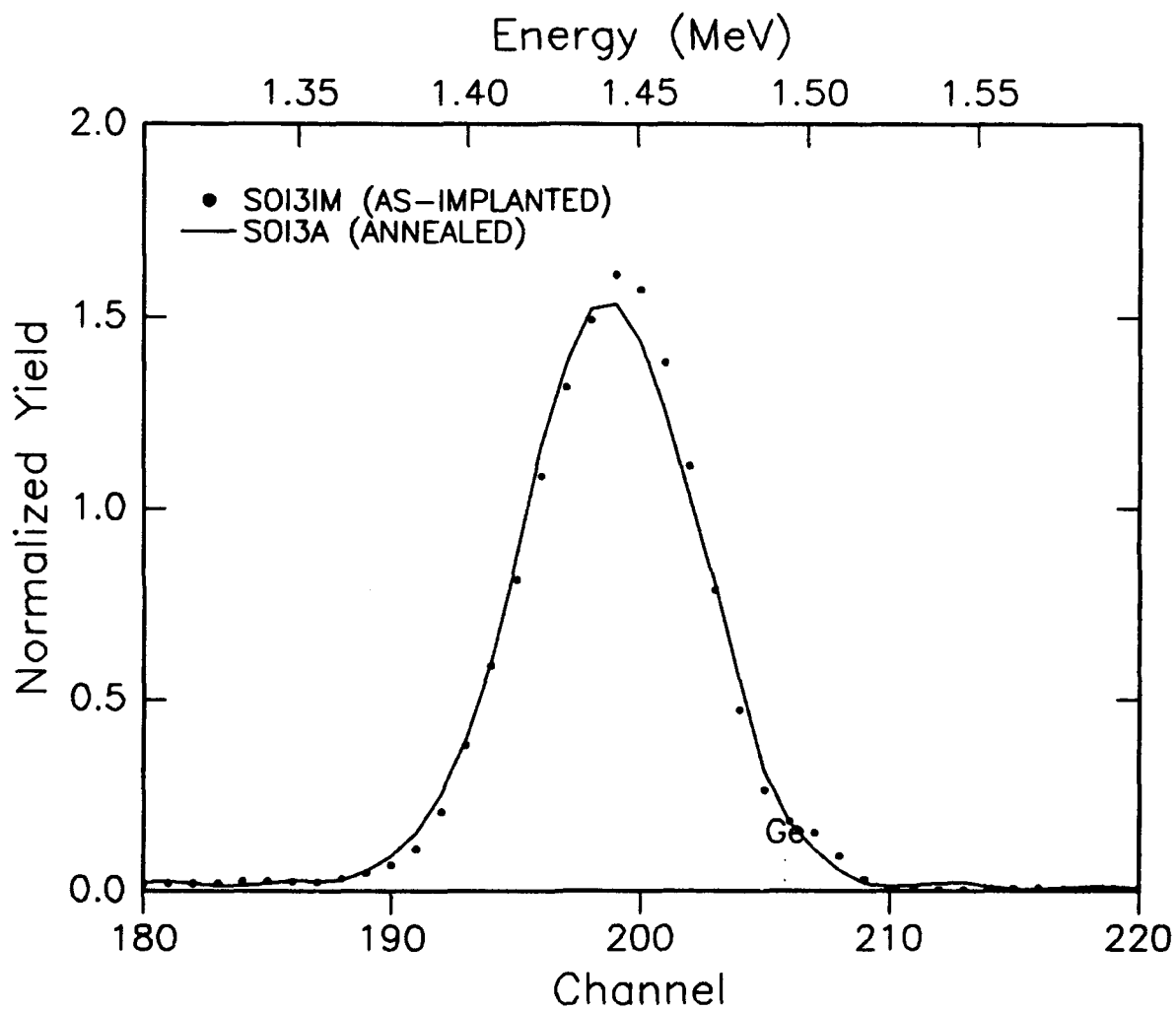
Figure 2-6. *RBS spectra of the Ge profile in as-implanted and annealed pieces of SIMOX sample (#SOI3) implanted with a dose of 1 x 10¹⁶ Ge⁺/cm² at 190 keV. As in the control Si sample shown in Figure 2-1, no significant redistribution of Ge resulting from annealing can be observed.*

SIMOX   **Bulk Si**

a.   **c.**   0.1 μm

b.   **d.**   0.2 μm
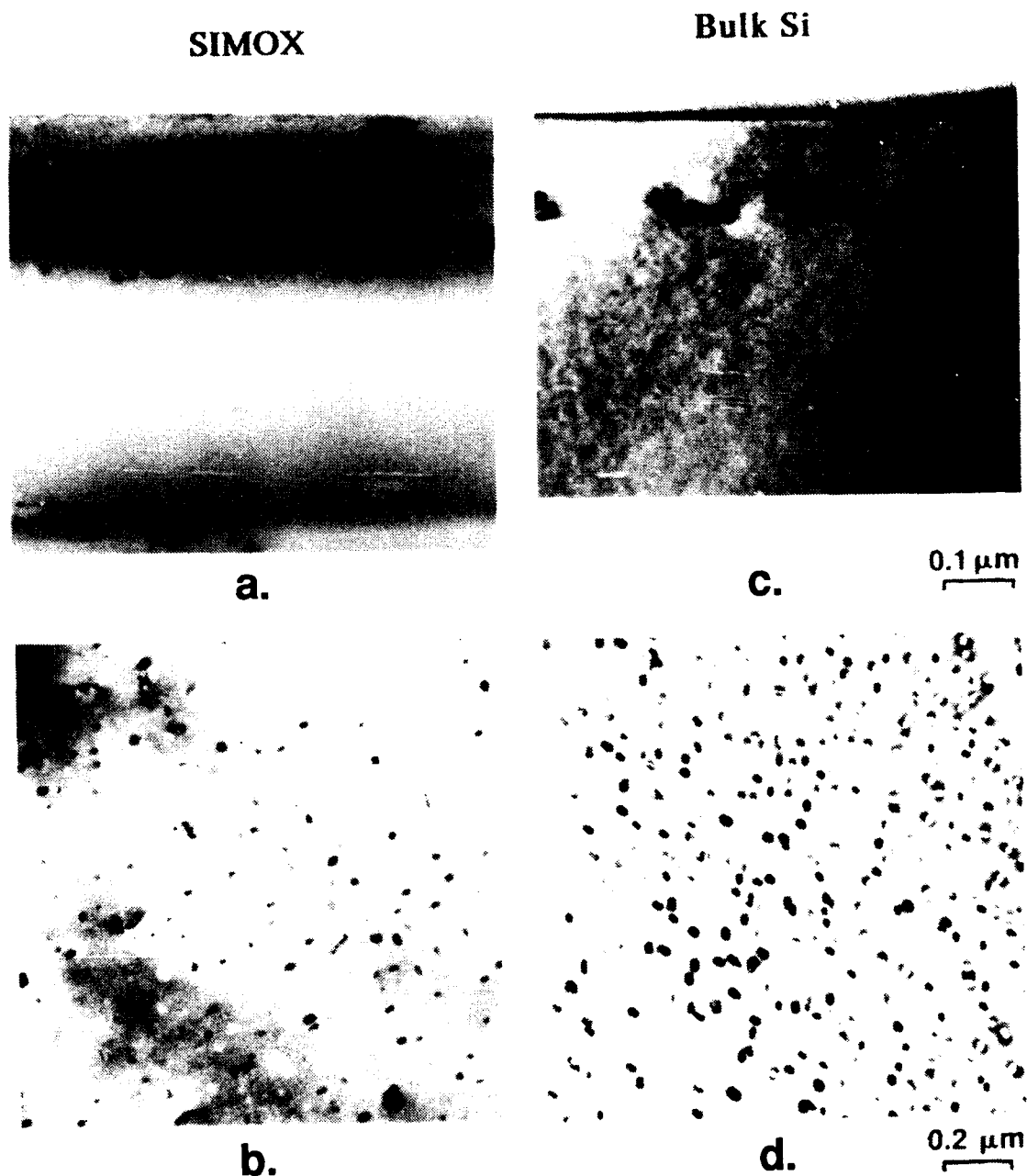
Figure 2-7. *Cross-sectional and plan-view TEMs show effect of Si/SiO₂ interface on dislocation loop formation. a) XTEM of SIMOX sample implanted with 1x10¹⁵ Ge⁺/ cm² at 100 keV and annealed for 0.5 hour at 850°C in N₂. b) XTEM of bulk Si sample implanted with Ge and annealed under above conditions. c) and d) Plan-view TEMs of samples in a and b, respectively. The fewer dislocation loops in SIMOX as compared to bulk Si may be explained by distance of dislocation loops from surface, which, in SIMOX wafers, closely corresponds to location of Si/SiO₂ interface.*
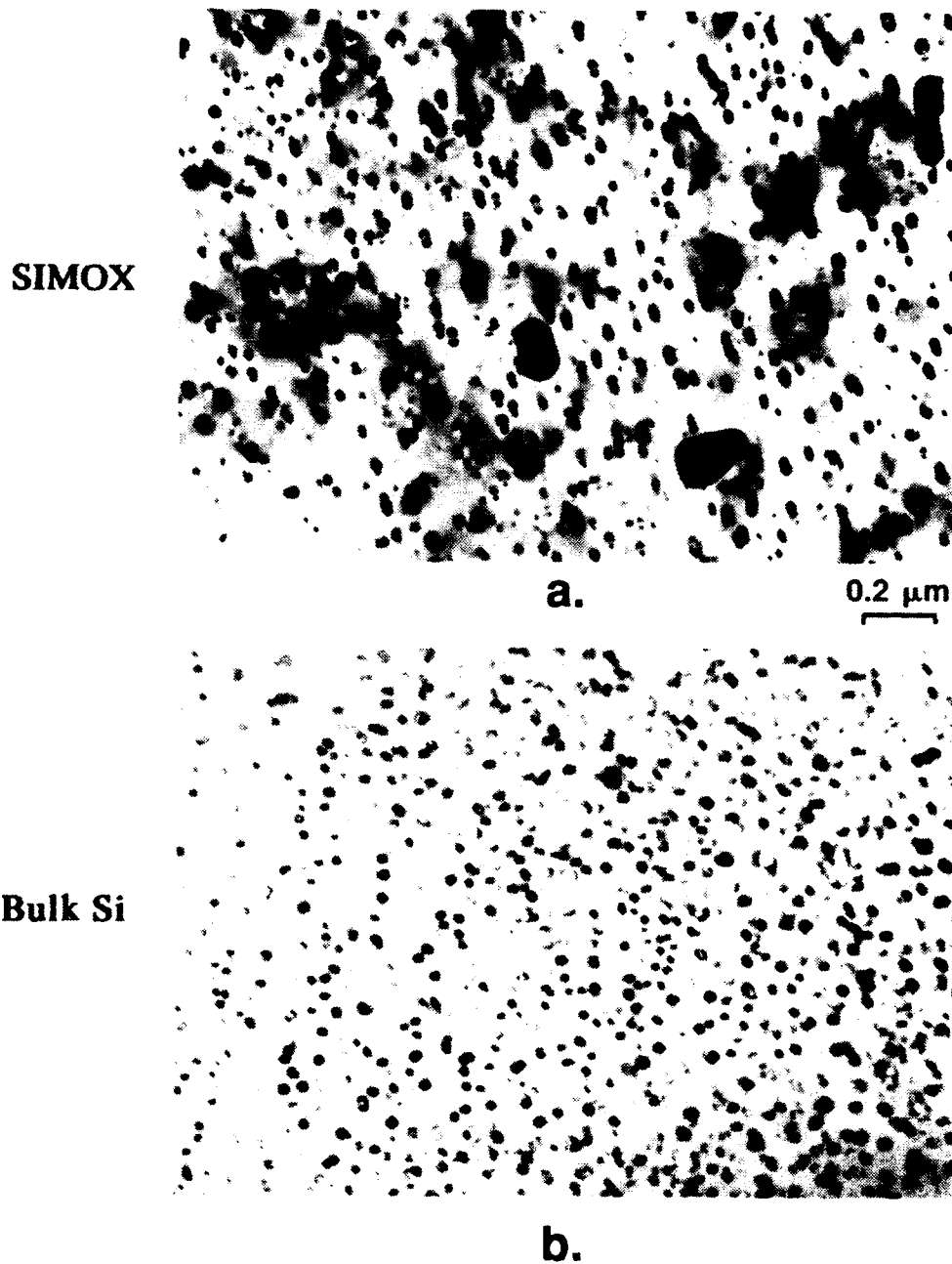
Figure 2-8. *Plan-view TEM results from a) SIMOX sample implanted with a dose of $2x10^{15}$ Ge^+/cm^2 at 80 keV and b) bulk silicon sample implanted with the same Ge dose but at 100 keV. When, by lowering the implantation energy, the α/c interface in SIMOX wafers moves away from the Si/SiO_2 interfaces, the dislocation loop density becomes comparable to that in bulk Si.*

These results indicate that the creation of the dislocation loops strongly depends on the location of the α/c interface relative to the buried oxide layer. If Ge implantation into SIMOX is carried out so that the α/c interface is closer to the buried oxide interface than the critical distance, fewer dislocation loops will be created.

2.2 EFFECTS OF Ge IMPLANTATION DOSE.

Following the study of the effect of Ge implantation energy, we studied the effect of Ge implantation dose on the formation of a degraded back-channel region in SIMOX structures. We implanted several SIMOX samples with various Ge doses at 80 keV and annealed them for 30 minutes at 850°C in nitrogen. These samples were studied by PTEM and XTEM to characterize the defect formation in the back-channel region as a function of Ge implantation dose. Some samples were also produced by implanting Ge at 40 keV.

Figure 2-9a shows the dislocation loops produced by end-of-range damage resulting from implanting a SIMOX sample with a Ge dose of 2×10^{15} Ge$^+$/cm^2 at 80 keV. As the Ge dose increases to 1×10^{16} Ge$^+$/cm^2, the dislocation loop density increases significantly (Figure 2-9b). Figure 2-9c illustrates that if the Ge dose is further increased to 2×10^{16} Ge$^+$/cm^2, no individual dislocation loops are observed. In the latter sample, the dislocation loops appear to overlap and form a network of defects. These results can also be seen in Figures 2-10a and 2-10b which depict XTEM micrographs from the SIMOX samples implanted with Ge doses of 2×10^{15} and 2×10^{16} Ge$^+$/cm^2, respectively. Only individual dislocation loops can be seen in the sample with 2×10^{15} Ge$^+$/cm^2, while defects in the sample implanted with 2×10^{16} Ge$^+$/cm^2 appear extended and continuous.

The defect structure resulting from end-of-range damage in the SIMOX sample implanted at 80 keV with 2×10^{16} Ge$^+$/cm^2 may have been partially influenced by the Si/SiO$_2$ interface. When comparing PTEMs from this sample and those from a Si control sample implanted under the same conditions, we saw slightly different defect structures (Figures 2-11a and 2-11b). Also, threading dislocations in SIMOX wafers may possibly play a role in structuring the end-of-range damage. However, this effect is not fully understood.

Conversely, PTEM results from a SIMOX sample and a Si control wafer implanted under identical conditions with a dose of 2×10^{16} Ge$^+$/cm^2 at an implantation energy of 40 keV show no difference in the structure of end-of-range damage (Figure 2-11c and 2-11d). As shown in these figures, only individual dislocation loops can be observed in both the SIMOX and the Si samples.

We also studied the relationship between the dislocation loop defect density and the Ge implantation dose and energy. The effect of the damaged layer formed by Ge implantation must be related to the electrical properties of the back-channel region. One of the best approaches for investigating the back-channel region in SIMOX is by using back-gate MOSFET structures. However, we also attempted to study various electrical properties of Ge-implanted samples using simpler test structures and several characterization techniques such as spreading resistance and C-V measurements.

(a) $2 \times 10^{15}/cm^2$

(b) $1 \times 10^{16}/cm^2$

(c) $2 \times 10^{16}/cm^2$

0.2 μm
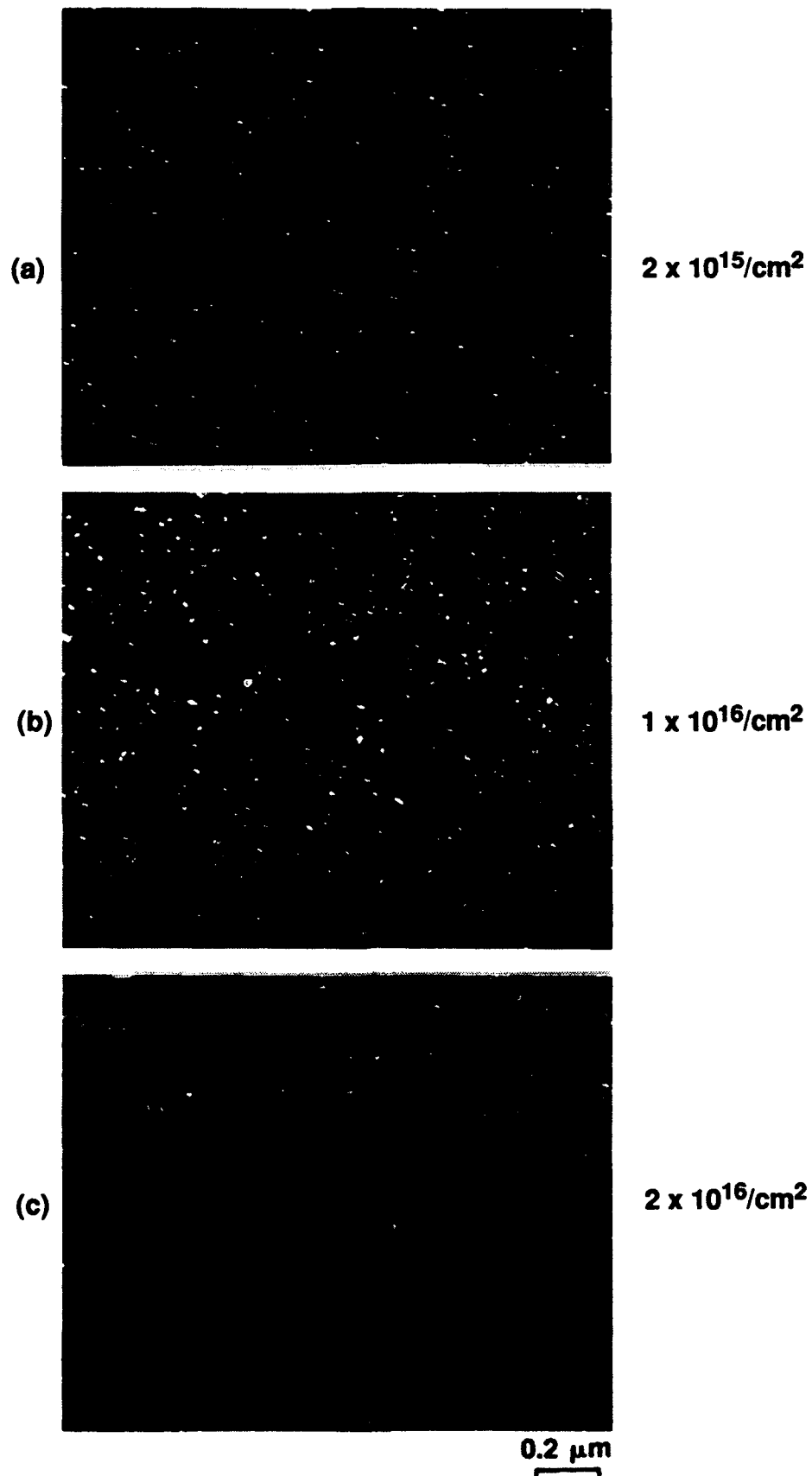
Figure 2-9. *PTEM micrographs of SIMOX samples implanted with Ge at 80 keV with doses of a) 2×10^{15} Ge⁺/cm², b) 1×10^{16} Ge⁺/cm², and c) 2×10^{16} Ge⁺/cm².*

21

80 keV

(a)   2 x 10^{15}/cm^2

80 keV

(b)   2 x 10^{16}/cm^2
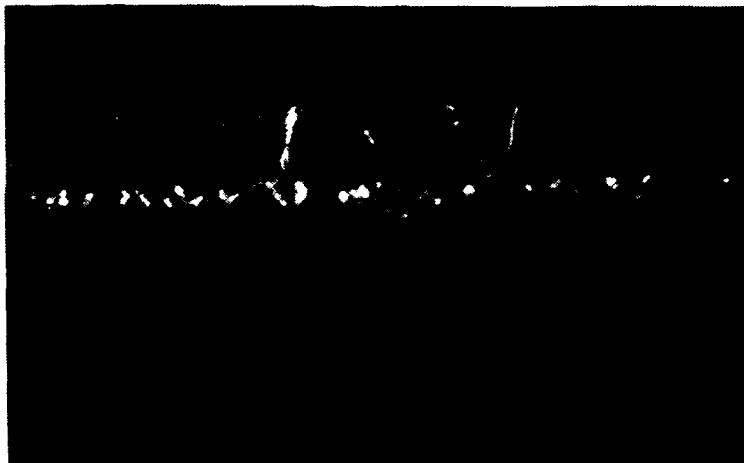
0.1 μm

Figure 2-10. *XTEM micrographs of SIMOX samples implanted with Ge at 80 keV with doses of a) 2 x 10^{15} Ge$^+$/cm^2 and b) 2 x 10^{16} Ge$^+$/cm^2.*

22

80 keV
2 x 10¹⁶/cm²
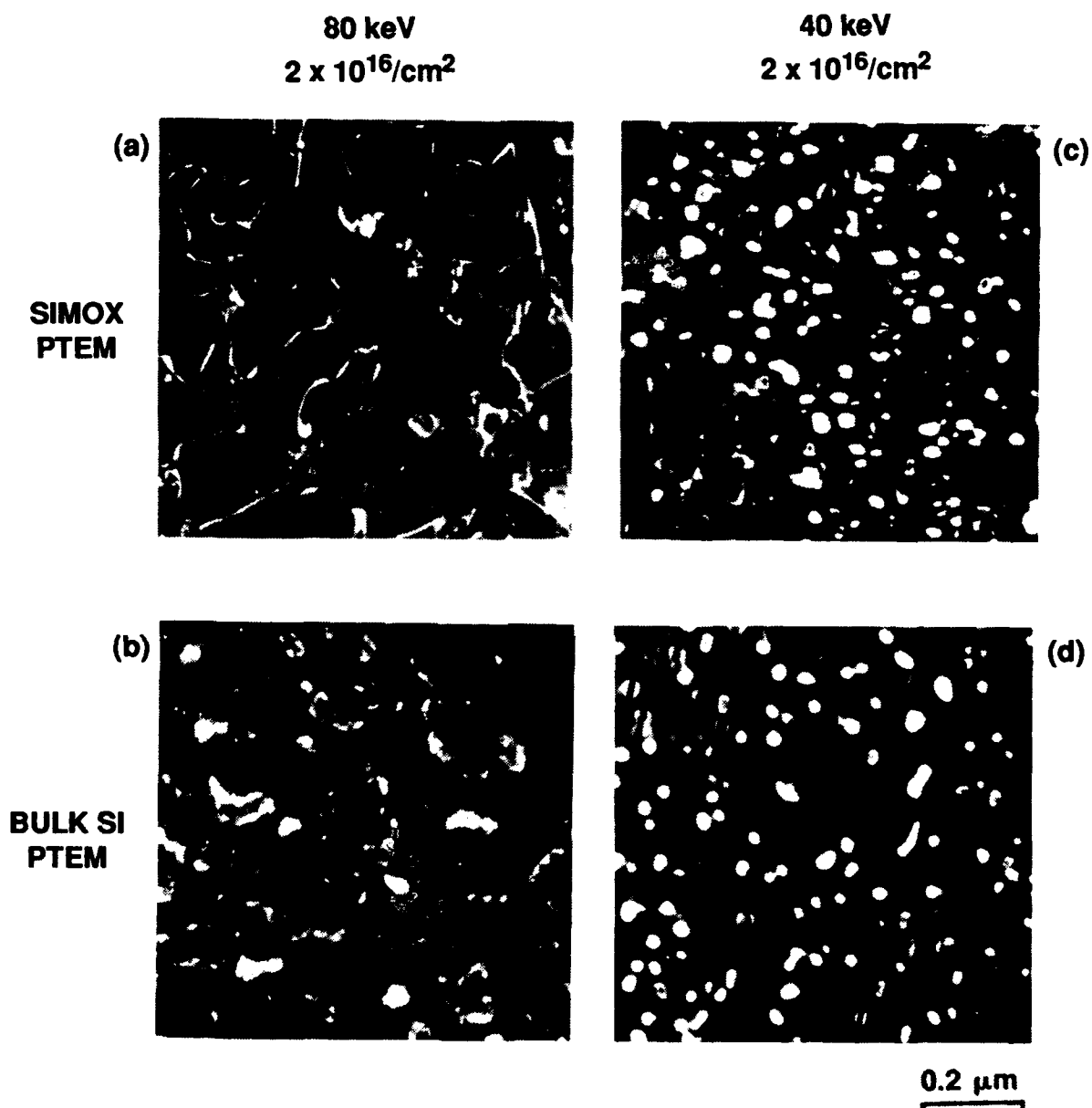
40 keV
2 x 10¹⁶/cm²

Figure 2-11. *PTEM results for samples implanted with 2 x 10^{16} Ge$^+$/cm^2; a) SIMOX sample implanted at 80 keV, b) Si sample implanted at 80 keV, c) SIMOX sample implanted at 40 keV, and d) Si sample implanted at 40 keV.*

23

2.3   EFFECTS OF HAZE.

One objective of this program has been to study and compare the effects of Ge implantation on the degradation of the back-channel region in SIMOX wafers produced at Spire and other companies in the US and overseas. We used multiple-implant SIMOX wafers from a commercial vendor to verify that back-channel degradation by Ge-implantation applies universally to all SIMOX wafers.

As noted above, we studied the layer structure of the wafers using optical reflectance and Rutherford backscattering spectroscopy (RBS). The results showed SIMOX wafers with Si top layers about 1800Å thick and buried oxide layers about 4500Å thick. We implanted a piece from one of these wafers with a dose of 2 x 10^{15} Ge$^+$/cm^2 at 160 keV and annealed the sample at 850°C for 30 minutes in N$_2$.

After Ge implantation, we studied the layer and crystalline structure of this sample using RBS and XTEM. The RBS results shown in Figure 2-12 indicated that after Ge implantation and annealing a Si:Ge layer about 1160Å thick, with a peak Ge concentration of about 0.5 at.%, formed close to the wafer surface. The results also suggested that the end-of-range damage, as determined by the penetration depth of Ge ions, should be about 500Å from the upper Si/SiO$_2$ interface.

Figure 2-13 is an XTEM micrograph of the multiple-implant SIMOX sample after Ge implantation and annealing. The buried oxide layer appears of very good quality and is continuous with no Si islands, but the Si top layer does not have good crystallinity and seems either amorphous or poly-crystalline. These results were inconsistent with our established results for Ge implantation into single-implant SIMOX wafers with similar layer thicknesses (as determined by optical reflectance and RBS). We repeated the XTEM analysis of the sample, with the same results. We speculated that the results related to the degree of "haze" on the commercial multiple-implant wafers. Before Ge implantation, we had noticed a considerable amount of haze on the wafer surfaces and, therefore, studied the surface morphology using an optical microscope. Figure 2-14 compares the optical micrographs (1000x magnification) from the surface of the commercial multiple-implant SIMOX wafer with those from a similar non-Ge-implanted wafer produced at Spire.

We discussed our findings with technical personnel from the SIMOX vendor. They indicated that the upper Si/SiO$_2$ interface in their multiple-implant wafers is generally wavy, and that this waviness produces haze at the wafer surface. After further discussion, we attempted to find an explanation for the resulting amorphous/poly-crystalline Si top layer after Ge implantation and annealing.

One possible explanation is that the waviness at the upper Si/SiO$_2$ interface plays an important role in the solid phase epitaxy (SPE) regrowth of the Si top layer. Figures 2-15a and 2-15b show schematics of two SIMOX structures, one with a smooth upper Si/SiO$_2$ interface and the other with a wavy interface, implanted with Ge under identical conditions. If Ge implantation amorphizes the Si layer as indicated in the figures, problems will arise during SPE regrowth of the sample with the wavy interface. Since only pockets of single-crystal Si remain after Ge implantation, rather than a continuous layer, these regions can only recrystallize the
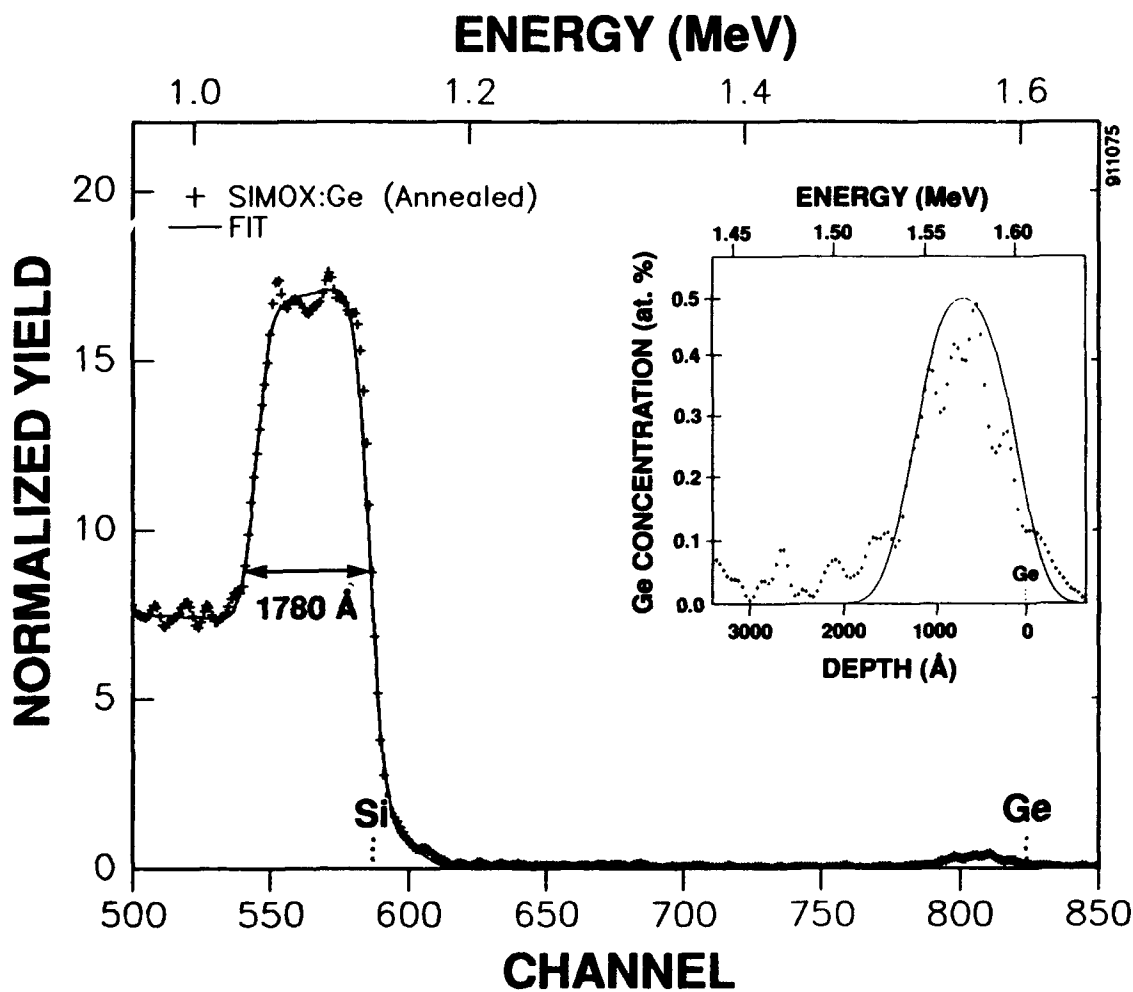
Figure 2-12. *RBS result for a commercial multiple-implant SIMOX sample both Ge-implanted and annealed. A fit to data indicates a Si:Ge layer about 1160Å thick with a peak Ge concentration of 0.5 at.%, formed about 100Å from the surface and 520Å from the upper Si/SiO₂ interface.*

Figure 2-13. *XTEM micrograph of a commercial multiple-implant SIMOX wafer both Ge-implanted and annealed. The buried SiO_2 layer is continuous and of good quality, but the Si top layer appears amorphous or poly-crystalline.*

26

(a)
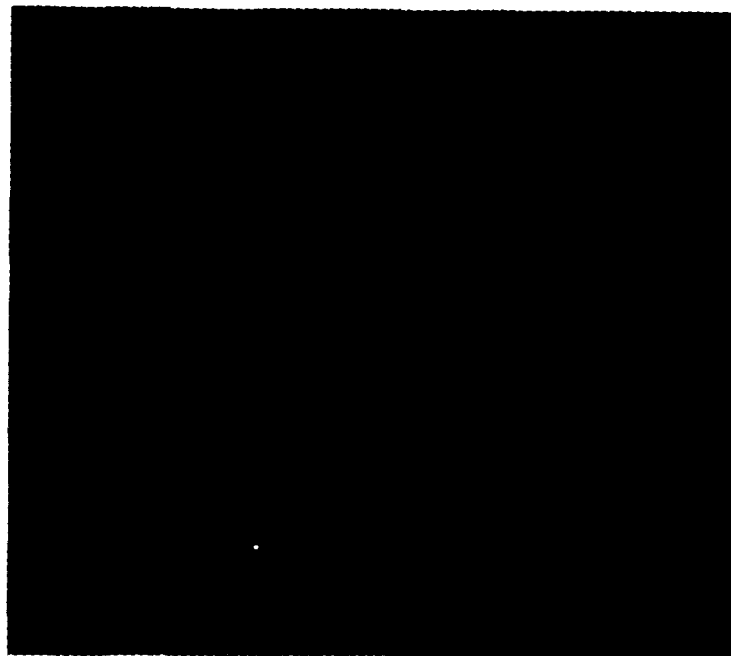
(b)
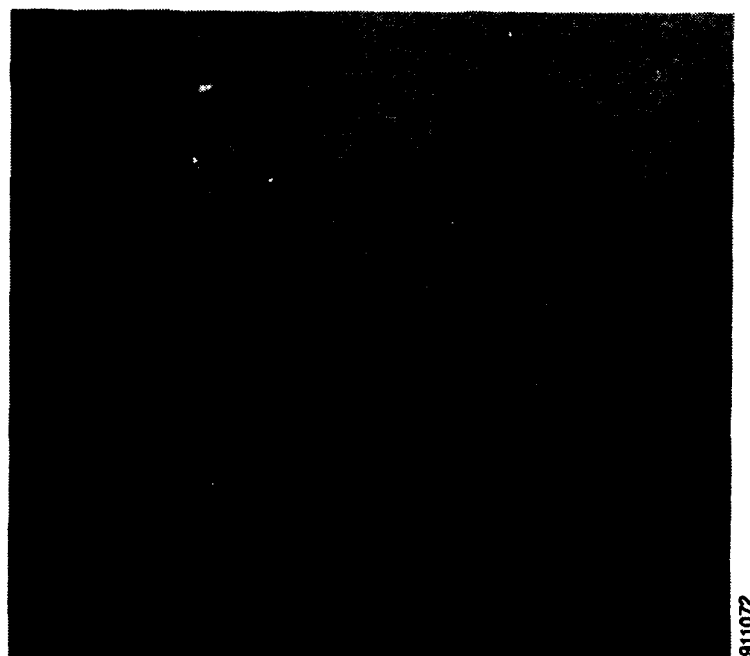
911072

Figure 2-14. *Comparison of the optical micrographs (1000x magnification) from surface of a) commercial multiple-implant SIMOX and b) multiple-implant SIMOX wafer produced at Spire. The surface of the commercial multiple-implant wafer appears to be relatively hazy and rough.*
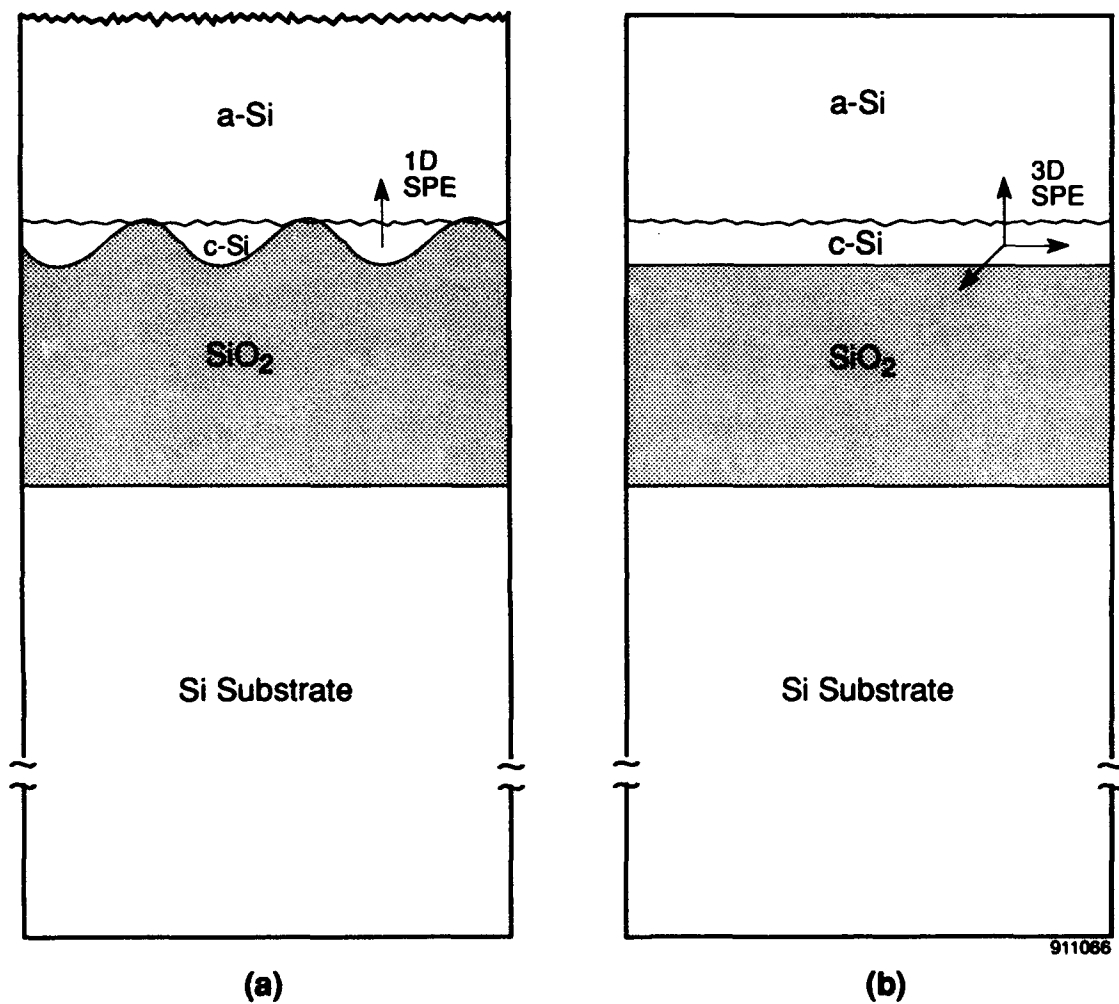
Figure 2-15. *Cross-sectional schematics of Ge-implanted SIMOX wafers with a) wavy upper Si/ SiO₂ interface and b) smooth upper Si/SiO₂ interface. Only vertical (1D) recrystallization may be possible in sample a, but the adjacent Si in sample b can recrystallize in all directions (3D).*

adjacent Si vertically. Lateral recrystallization will be inhibited by the surrounding SiO_2 walls. In fact, the scientists from the SIMOX vendor agreed with this hypothesis and further hypothesized that, due to the strain present in these pockets, even the vertically-recrystallized Si may not have the same orientation as the original Si. On the other hand, the sample with a smooth interface and a continuous single-crystal layer (seed) remaining after Ge implantation can recrystallize the adjacent Si in three dimensions, resulting in a single-crystal Si top layer. Thus, a lower Ge implantation energy should be used for multiple-implant SIMOX wafers with wavy upper Si/SiO_2 interfaces rather than for standard SIMOX wafers with similar layer thicknesses.

SECTION 3

ELECTRICAL CHARACTERIZATION

3.1 C-V MEASUREMENTS.

During Phase II, we made several simple test structures and used various techniques to evaluate the effects of Ge implantation on the electrical properties of the back-channel region.

We fabricated several simple test capacitors on p-type SIMOX wafers, with and without Ge implantation, for C-V measurements. These capacitors were formed by a) evaporating aluminum on the p-type SIMOX samples; b) masking and isolating device regions using photolithography; c) removing excess Al; d) selectively etching off the Si top layer using an ethylene-diamine-based mixture, and finally, e) evaporating Al to the back side of the wafer. Figure 3-1 shows a schematic of these test structures. We used a Model 565 MSI Electronics C-V Meter connected to a Hewlett-Packard Model 85B computer and operated at 1 MHz to measure the C-V characteristics.

Figure 3-2 compares the high frequency C-V characteristics for a) p-type standard SIMOX sample without Ge implantation (#T469E), b) a piece of the same SIMOX wafer with 1×10^{15} Ge^+/cm^2 implanted at 80 keV (#T469B), and c) another piece of the same wafer with 1×10^{15} Ge^+/cm^2 implanted at 110 keV (#T469D). The standard single-implant SIMOX wafer (#T469) was produced at Spire by implanting a four-inch p-type Si(100) substrate with an oxygen dose of 1.6×10^{16} O^+/cm^2 at 160 keV followed by annealing for six hours at 1300°C in nitrogen. The Ge-implanted samples were annealed for two hours at 850°C in nitrogen. As shown in Figure 3-2, Ge implantation appears to shift the C-V curve toward the more positive voltage region. In addition, as the implantation energy increases from 80 to 110 keV, a larger positive shift in the C-V curve occurs. These results may be due to the charge-trapping behavior of the defects formed by Ge implantation near the Si/SiO_2 interface.

For more conclusive C-V measurements, we also fabricated new test capacitors with an n-type Si top layer and n-type Si substrate (N-on-N structure) after preparing single-implant SIMOX wafers with n-type substrates. To form the n-type Si top layer, we implanted pieces of the wafer with a dose of 6×10^{14} As^+/cm^2 at 110 keV. The samples were then annealed for 30 minutes at 900°C in N_2 to activate the dopants and remove the implantation damage. We then implanted the Si top layer with a dose of 2×10^{15} Ge^+/cm^2 at 100 keV and annealed the samples for 30 minutes at 850°C in N_2. RBS analyses and results from a surface morphology study of these wafers showed relatively good quality material with the desired layer structure. A fit to the RBS data, shown in Figure 3-3, indicates a Si top layer about 2200Å thick and a buried SiO_2 layer about 3550Å thick.

30
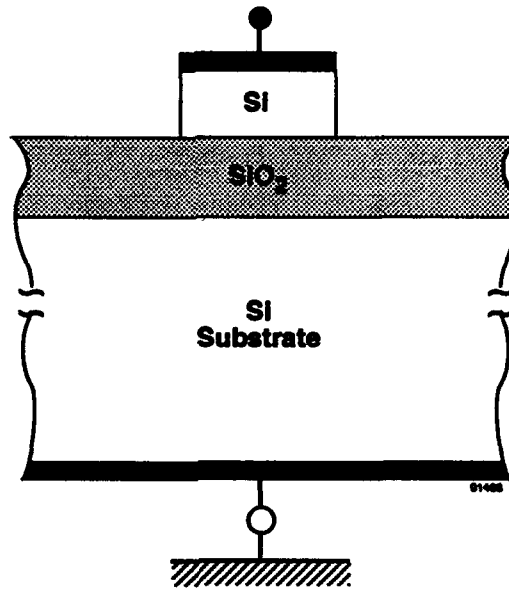
Figure 3-1. *Schematic of test structures used for C-V measurements.*
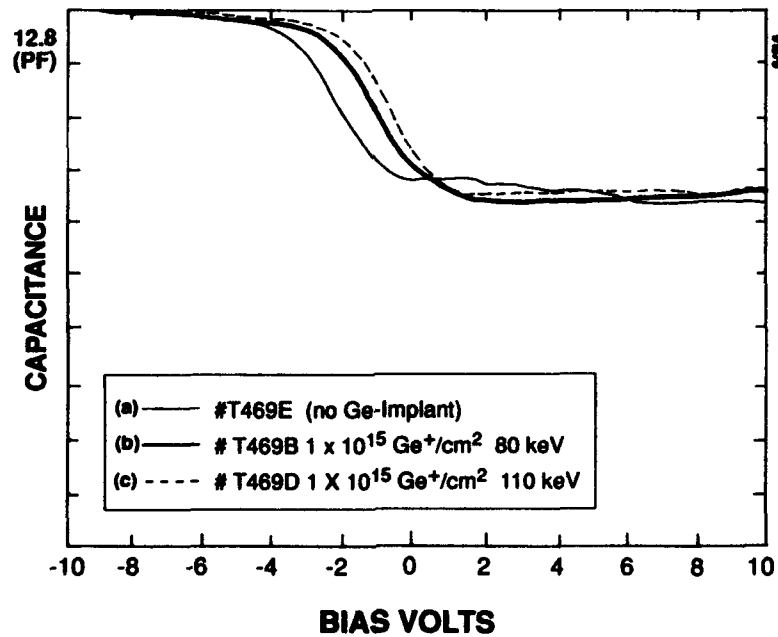
Figure 3-2. *High frequency C-V curves for SIMOX samples a) with no Ge implant (#T469E), b) with 1 x 10^{15} Ge$^+$/cm^2 implanted at 80 keV (#T469B), and c) with 1 x 10^{15} Ge$^+$/ cm^2 implanted at 110 keV (#T469D). All samples are pieces of the same SIMOX wafer (#T469).*

31
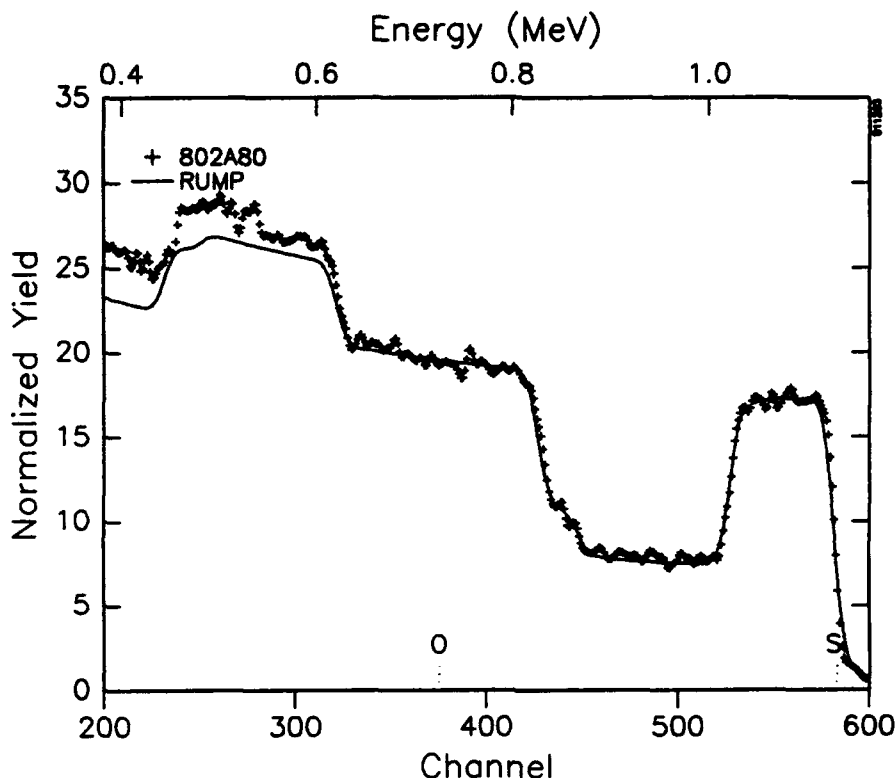
Figure 3-3. *RBS results of the single-implant, n-type standard SIMOX wafer used for C-V cha-racterization. A fit to the RBS results indicates a Si top layer about 2200Å thick and a buried SiO$_2$ layer about 3550Å thick.*

We fabricated test capacitors on SIMOX samples implanted with As$^+$ and Ge$^+$ as well as on samples without any such implantations. To fabricate these devices, we deposited Al onto the samples using an electron-beam evaporator and then photolithographically-masked isolated regions of the samples using a photomask (see Figure 3-4) provided by Dr. Frank Sinclair of Eaton Corporation, Beverly, MA. We then removed the excess Si (regions not masked with Al) using an ethylene-diamine-based preferential etchant at 100°C to form isolated Si top layer regions with Al contacts.

We studied the capacitance-voltage (C-V) characteristics of the devices using a Materials Development Model SCM/16 Semiconductor Measurement System. This system is equipped with a Boonton Model 72C capacitance meter, an MDC model RM-1600 computer, and an MSI Electronics Model WF-2 probe station. For C-V measurements, we first swept the voltage across each capacitor from -100V to +100V and then retraced it by sweeping the bias from +100 to -100 volts.

Figure 3-5 shows the C-V characteristics of capacitors fabricated on SIMOX wafers without As$^+$ and Ge$^+$ implantation. The results indicate that the Si substrate is indeed n-type material, but that the Si top layer appears to be p-type. Conversely, the C-V characteristics of devices fabricated on samples implanted with both As$^+$ and Ge$^+$ (as shown in Figure 3-6) suggest that the Si top layer has converted to a lightly doped n-type material. In both C-V curves, an unusually large stretch-out exists between the depletion regions of the Si top layer and the Si substrate.
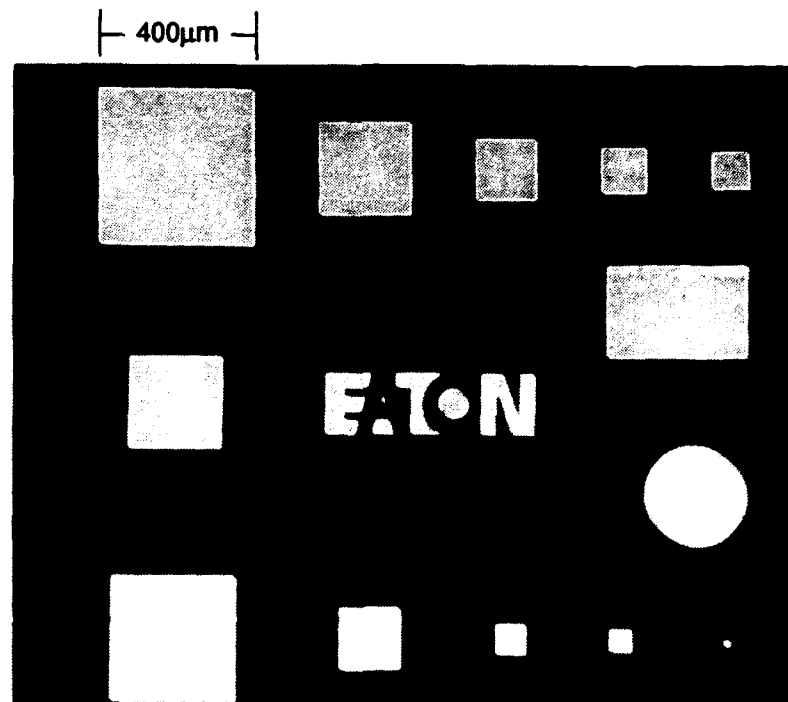
Figure 3-4. *The photomask pattern used for fabricating SIMOX capacitors. The photomask was provided by Dr. Frank Sinclair of Eaton Corporation, Beverly, MA.*
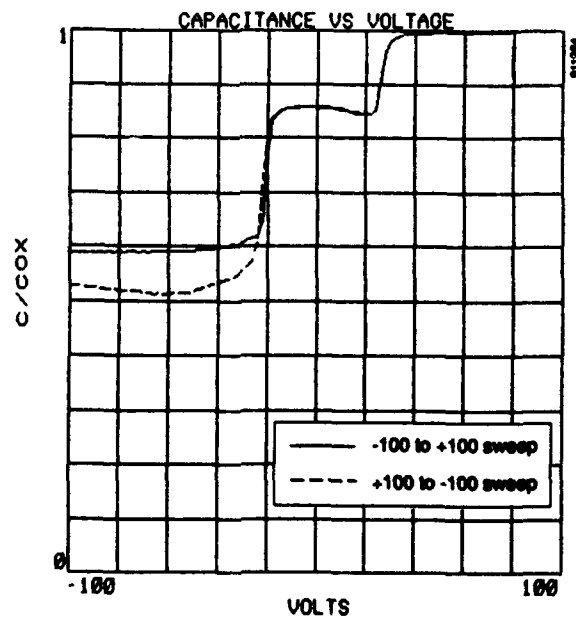
Figure 3-5. *C-V characteristics for as-fabricated SIMOX capacitors without As and Ge implantations. Results indicate an n-type Si substrate and a p-type Si top layer. The stretch-out in the C-V curve suggests process-induced ionizing radiation effects.*
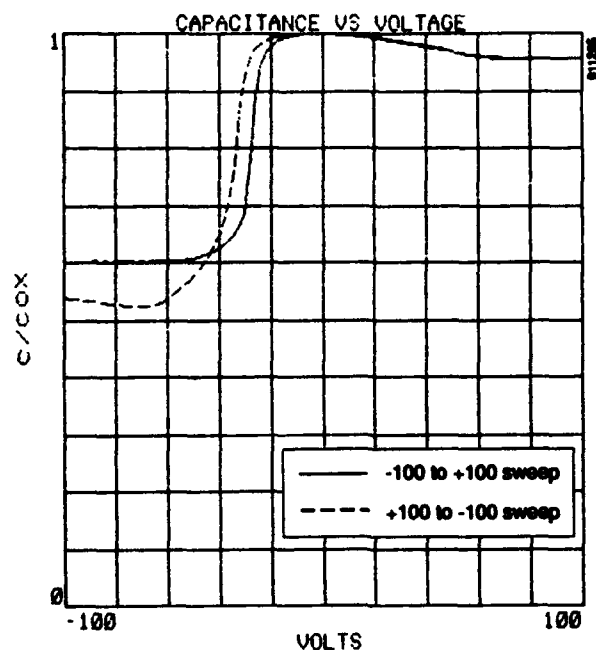
Figure 3-6. *C-V characteristics for as-fabricated SIMOX capacitors implanted with both As and Ge. The results indicate an n-type Si substrate and a lightly doped n-type Si top layer. These results also suggest that the capacitors were irradiated during the fabrication process.*

Since the stretch-out may have resulted from irradiation of the samples by the electron-beam during Al evaporation, we annealed the samples for periods of up to eight hours at an average temperature of about 225°C to remove the irradiation damage.

Figures 3-7 and 3-8 show the C-V characteristics of the same devices used for the measurements in Figures 3-5 and 3-6, respectively, after annealing for eight hours at an average temperature of about 225°C. As shown, annealing results in a significant reduction in the stretch-out of the C-V curves.

By comparing the results shown in Figures 3-5 and 3-7 to the results shown in Figures 3-6 and 3-8, we see that the C-V curve of devices with both As$^+$ and Ge$^+$ implants shifts when the direction of the sweeping bias changes, while the C-V curves of devices without As$^+$ and Ge$^+$ implants remain relatively stable.

In general, the C-V analyses were not very helpful for quantitatively evaluating the effect of Ge implantation on the electrical properties in the back-channel region of SIMOX wafers. Therefore, we focused our remaining efforts on more suitable characterization techniques.
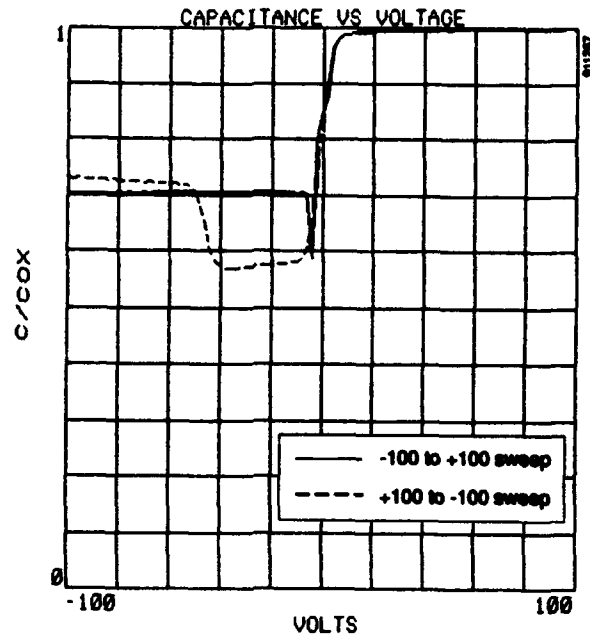
Figure 3-7. *C-V characteristics for capacitors of Figure 3-5 after annealing for eight hours at an average temperature of about 225°C. Annealing resulted in a significant reduction in the C-V curve stretch-out.*
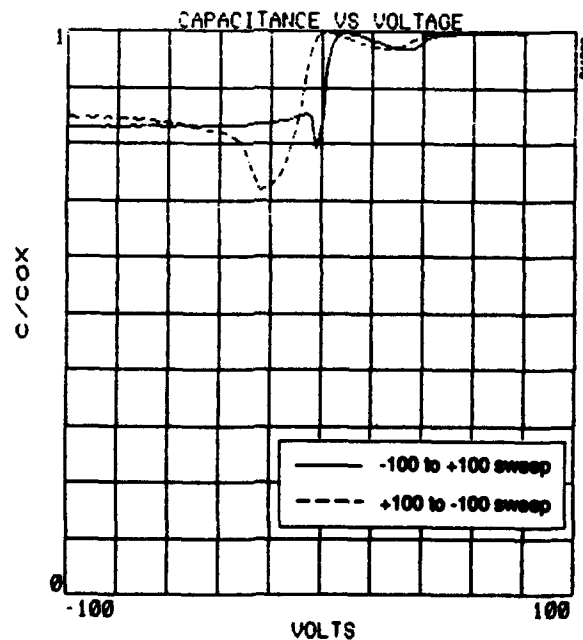
Figure 3-8. *C-V characteristics for capacitors of Figure 3-6 after annealing for eight hours at an average temperature of about 225°C. Again, annealing resulted in a significant reduction in the C-V curve stretch-out.*

35

3.2   POINT-CONTACT MOS TEST.

We used the point-contact MOS transistor (PCMOST) method to study the electrical properties of Ge-implanted samples in order to characterize and compare their current-voltage (I-V) characteristics with those from unimplanted samples.

We used a standard single-implant SIMOX wafer produced by implanting an oxygen dose of 1.8×10^{18} O^+/cm^2 at 200 keV followed by annealing at 1300°C for six hours. Rutherford backscattering spectroscopy (RBS) results for this sample indicated a Si top layer about 2200Å thick and a buried oxide layer about 3550Å thick. We also used a multiple-implant SIMOX wafer with a Si top layer of about 1800Å thick and a buried oxide layer about 4500Å thick.

We then implanted pieces of the above SIMOX wafers with a dose of 2×10^{15} Ge^+/cm^2 at 80 keV and annealed them for 30 minutes at 850°C in N_2. These implanted and unimplanted SIMOX pieces were then used for test device fabrication to evaluate the effect of Ge implantation on the electrical properties of the back-channel region. The devices used in this study were fabricated by first thermally evaporating Al on the samples through a shadow mask and then selectively etching off, in a preferential Al etchant (ethylene-diamine-based), the excess Si top layer regions not covered with Al down to the buried oxide layer. Finally, we removed the Al from the remaining isolated Si top layer regions using a phosphoric-acid based mixture.

To perform the PCMOST measurements, two probes were pressure-contacted onto the Si top layer at a distance of about 0.5 mm from each other. A third contact was made to the Si substrate on the back side of the sample. Figure 3-9 shows a diagram of the PCMOST system used at Spire. We used a Hewlett-Packard Model 6113A DC power supply to provide a constant bias to the drain, while a Hewlett-Packard Model 6216B power supply provided the back-gate bias. The current at the source was then measured as a function of the gate bias using a Keithley Model 485A picoammeter. In this study, we applied a 1 volt bias to the drain and varied the gate voltage from -30V to +30V.

We measured the I-V characteristics of several test devices on each sample. The I-V curves obtained from different devices on SIMOX samples without Ge implantation behaved very similarly and resembled a "gull wing" with a minimum current at zero bias ($V_G = 0V$). Conversely, we recorded two distinct I-V behaviors from devices fabricated on SIMOX wafers with Ge implantation.

Figures 3-10a and 3-10b compare the I-V characteristics of devices fabricated on standard SIMOX samples with and without Ge implantation. As shown, both I-V curves have a minimum current at $V_G = 0V$, but the leakage current in the device with Ge implantation is generally smaller than that of the unimplanted device, particularly for positive V_G region. Although the I-V curve of the Ge-implanted device still has the "gull wing" shape, the minimum leakage current occurs at $V_G = -5V$ instead of at $V_G = 0V$.

We obtained similar results for devices fabricated on multiple-implant SIMOX samples with and without Ge implantation. Figures 3-11a and 3-11b compare the I-V curves of a device fabricated on multiple-implant SIMOX without Ge implantation with those from two different devices with Ge implantation. Our results showed that the amount of leakage current in devices

36
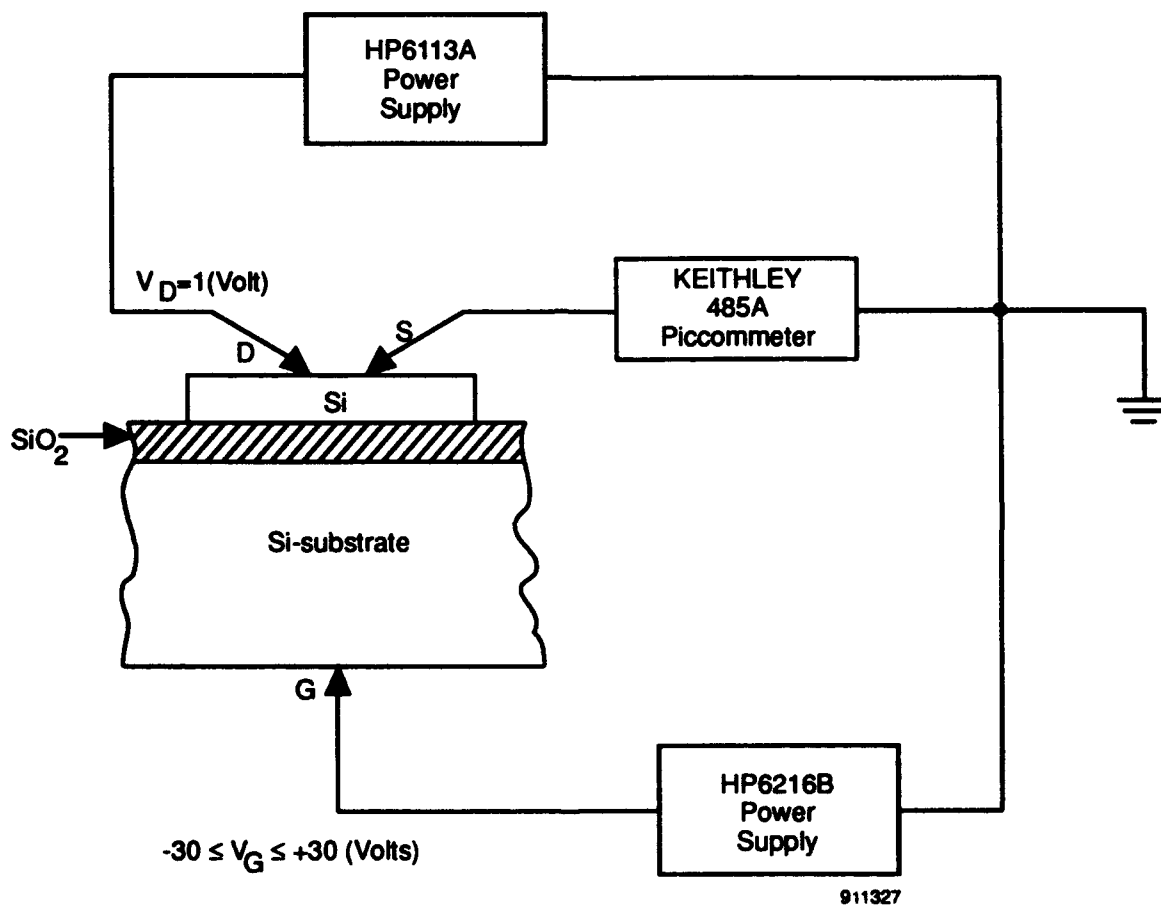
Figure 3-9. *Schematic diagram of the point-contact MOS transistor (PCMOST) measurement system used to study the electrical characteristics of the back-channel region in SIMOX wafers.*

37
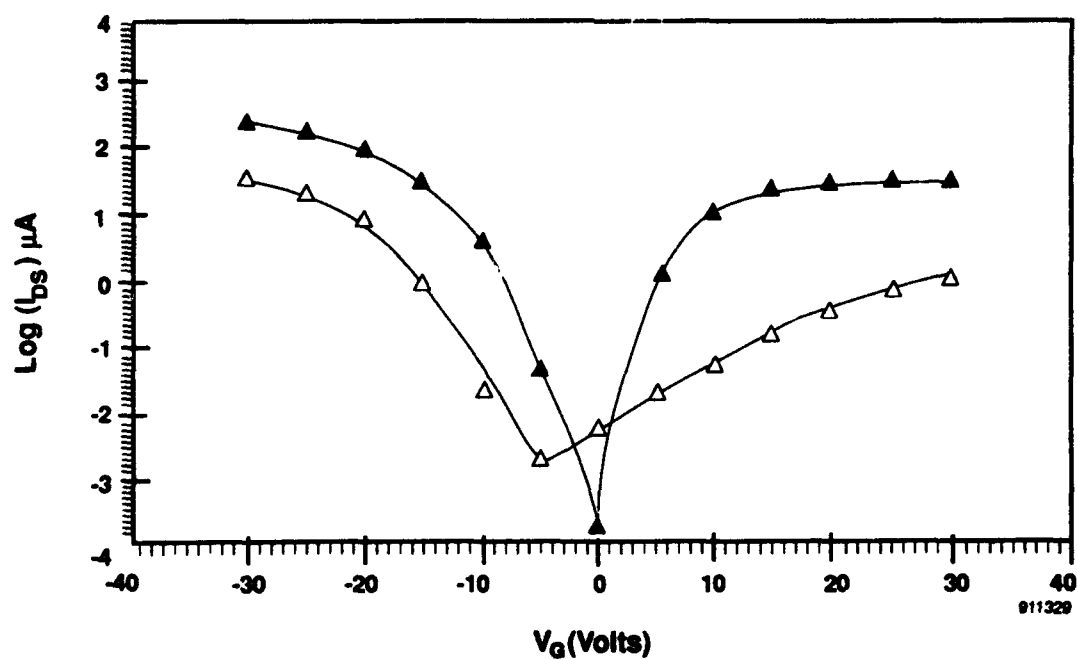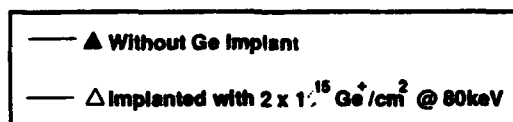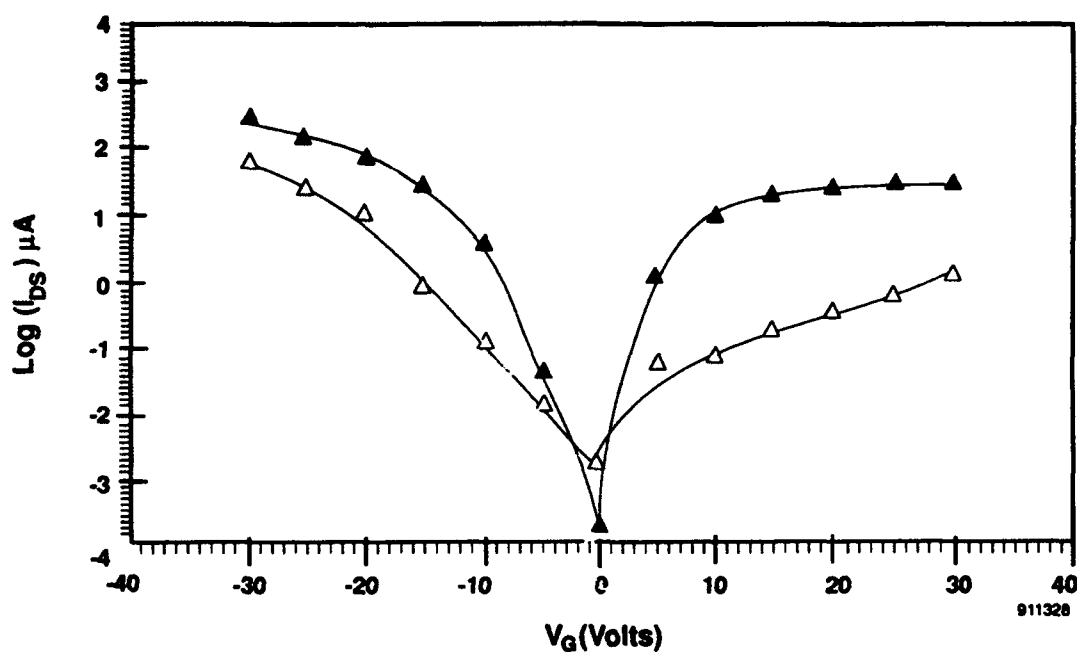
Figure 3-10. *Comparison of the I-V curves of a standard SIMOX PCMOST device without Ge implantation and two different devices from a sample with Ge implantation. The leakage current in Ge-implanted devices is generally smaller than that in non-Ge-implanted devices.*

38
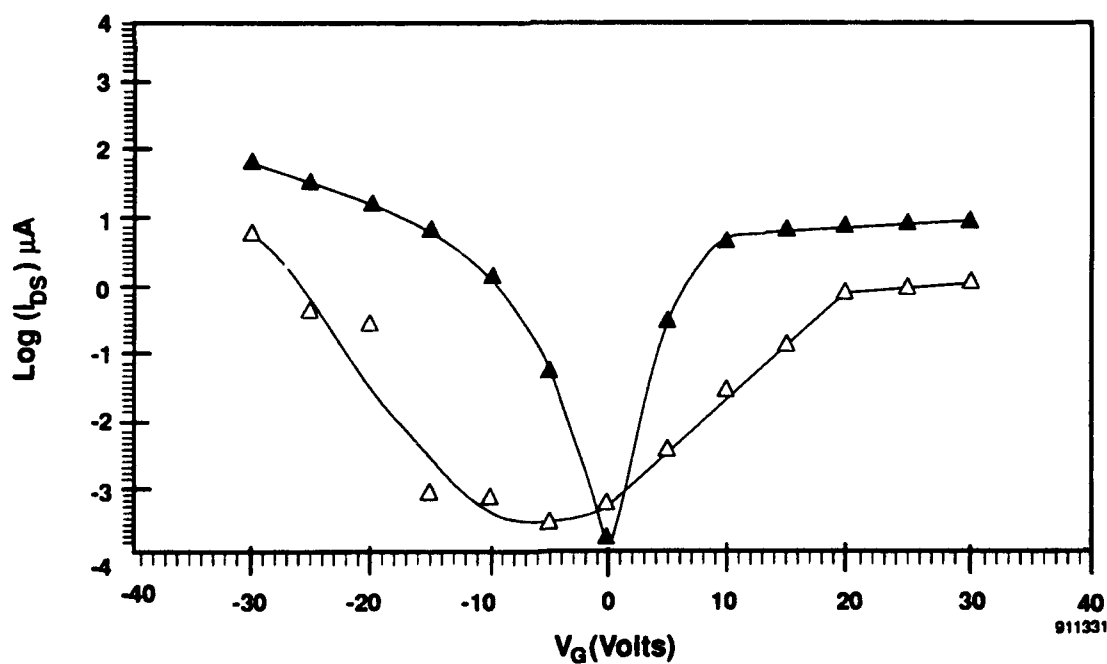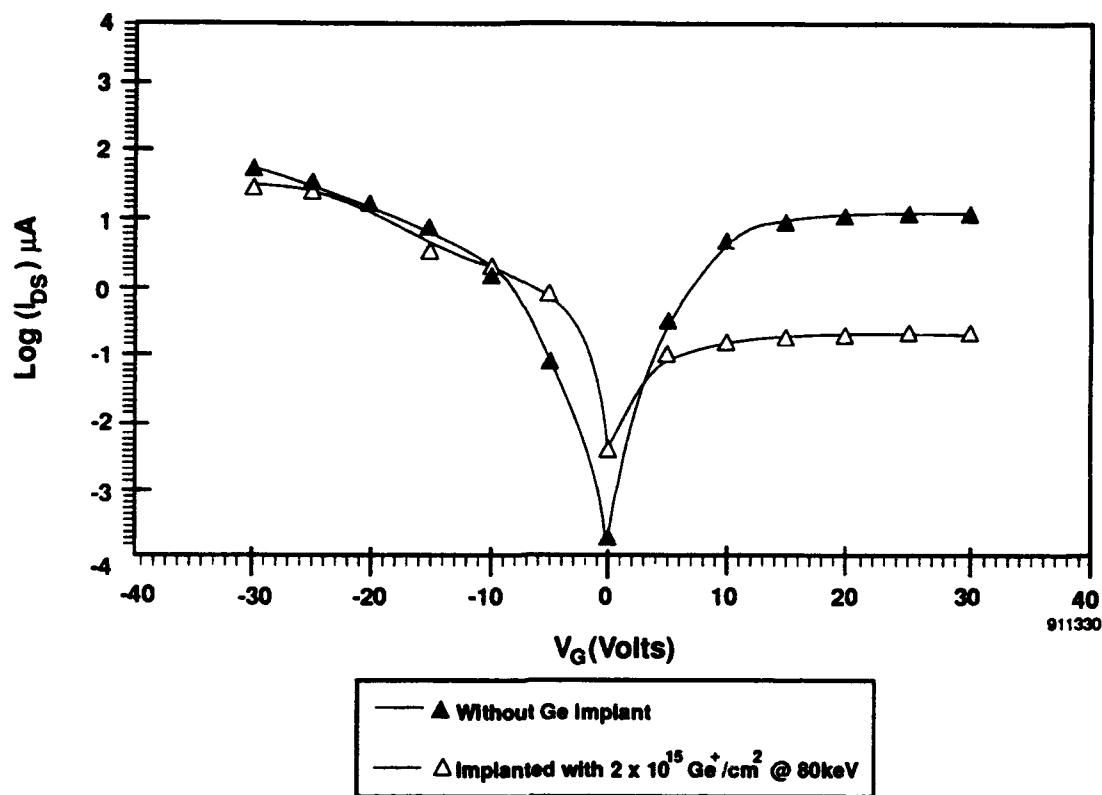
Figure 3-11. *Comparison of the I-V curves of a multiple-implant SIMOX PCMOST device without Ge implantation and two different devices from a sample with Ge implantation. Again, the leakage current in Ge-implanted devices is generally smaller than that in non-Ge-implanted devices.*

39

with Ge implantation is generally smaller than that for devices without Ge. This supports the concept that Ge implantation can be used effectively for degrading the back-channel region in SIMOX wafers.

3.2.1 Improved Point-Contact MOS Transistor.

The preliminary results of our work in the previous section demonstrated the feasibility of studying the back-channel region using PCMOST. However, the measurement system required various improvements before quantitative data could be recorded. For example, the current-voltage characteristics were to be recorded and plotted continuously using a computer-controlled procedure rather than by measuring drain-to-source current (I_{DS}) at discrete incremental points of applied gate voltage. In addition, the updated system was to enable bipolar sweeping of the voltage.

We concentrated on two directions: 1) improving the PCMOST measurement system and 2) Ge-implanting several standard SIMOX wafers using different implantation conditions as well as fabricating test structures on both Ge-implanted and untreated SIMOX wafers for PCMOST measurements. The layer structures of selected Ge-implanted samples were studied by XTEM.

Figure 3-12 is the schematic of the improved PCMOST measurement system. In this system, a Kepco bipolar operational power supply enables DC voltage sweeping in the range from -20V to +20V, and, vice versa, across the back-gate of the SIMOX test structures. The constant bias of about 1V between the drain and source (V_D) of the PCMOST is provided by an HP6113A DC power supply. Drain-to-source current and the back-gate voltage (V_G) are monitored with a Keithley 485 auto-ranging picoammeter and a Keithley 195A digital multimeter. As shown in the figure, the test equipment and procedures are computer-controlled through IEEE 488 bus lines.

We implanted germanium into three standard SIMOX samples (all from one wafer) with a dose of 3 x 10^{15} Ge+/cm^2 at energies of 40, 120, and 160 keV. The three samples were then annealed for 30 minutes at 850°C in N_2.

To fabricate the PCMOST test structures, we photolithographically masked the surfaces of the above Ge-implanted samples and a SIMOX sample from the same original wafer but without Ge-implantation. Aluminum was then thermally evaporated onto the samples, and the excess was removed using a lift-off process. The remaining Al masked square regions had a surface area of about 0.25 mm^2. Using a preferential etchant, the unmasked Si top layer regions were etched off to expose the buried SiO_2. Finally, all the remaining Al was etched off to create isolated square Si top layer regions for PCMOST measurements (see Figure 3-12).

Figure 3-13 shows the I-V characteristics from a test device on the standard single-implant SIMOX sample without Ge implantation. The solid I-V curve is recorded when V_G is swept from negative to positive voltages, followed by the dashed curve which indicates the I-V behavior when the voltage is swept in the reverse direction. As shown, both curves appear similar with a small current minimum at a V_G value near 0V. However, when a small bias is applied to the back-gate, a large current flows in the back-channel region with a rate (slope of the linear region on the curve) of about 3 decade/V.
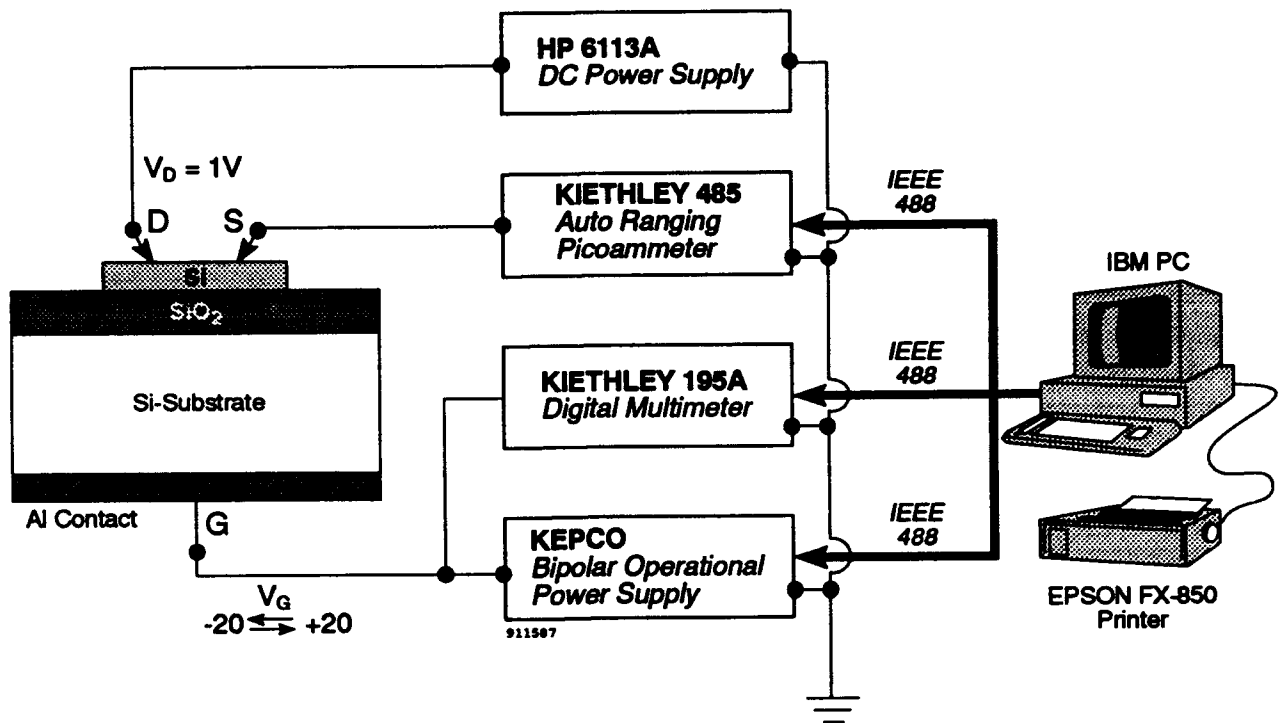
Figure 3-12. *Schematic of the improved point-contact MOS transistor measurement system.*
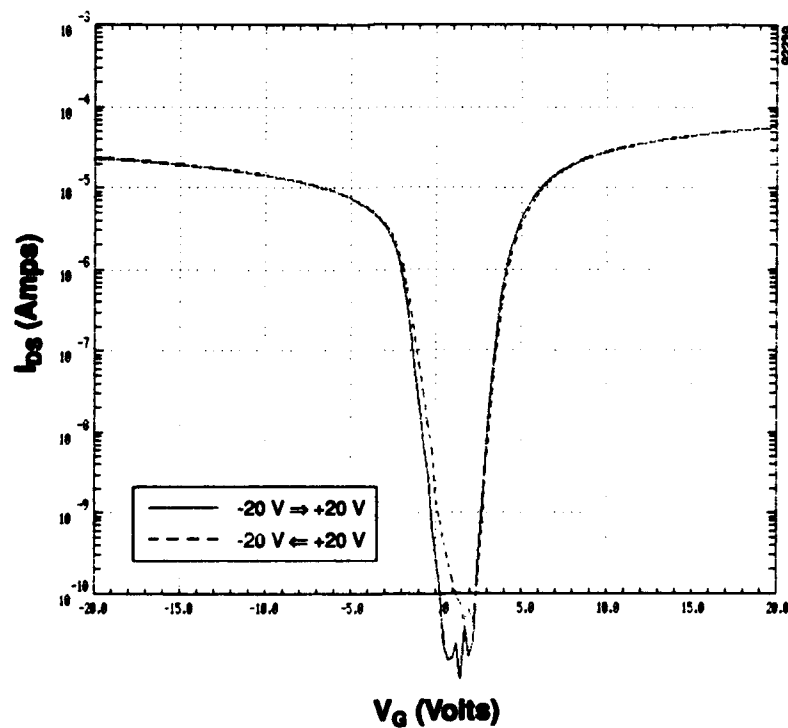
Figure 3-13. *Current-voltage characteristics from a PCMOST structure fabricated on a standard SIMOX sample without Ge implantation.*

41

Figures 3-14a, 3-15a, and 3-16a show the I-V characteristics of the samples implanted with a Ge dose of 3×10^{15} Ge$^+$/cm^2 at 40, 120, and 160 keV, respectively, and annealed for 30 minutes at 850°C. As shown, several differences exist between these I-V curves and the ones obtained from the sample without Ge implantation. One obvious difference is that when the gate voltage sweep shifts direction, the I-V curve shifts toward the negative voltages. When we discussed these results with Dr. H. Hughes from the Naval Research Laboratories, he speculated that the shift may have resulted from the residual implantation damage caused inadequate post-implantation annealing. He suggested that annealing the samples at a temperature of 1000°C for one hour might eliminate the shift between I-V curves. Therefore, we followed Dr. Hughes advice and tested the I-V characteristics of the reannealed samples. The results of this work will be discussed in the next section.

From the linear regions of the I-V curves shown in Figures 3-14a, 3-15a, and 3-16a, one can also discern that the flow of current in the back-channel region increases at a much slower rate (about 0.75 decade/V) than that measured in Figure 3-13 for the sample without Ge implantation. Significantly, this result may indicate that Ge implantation actually does result in the degradation of the back-channel region, thus inhibiting current leakage channel formation in the back interface.

The I-V curves of the Ge-implanted and non-Ge-implanted samples differ again in that the I_{DS} value at $V_G=0$ is lower for the sample without Ge than for the Ge-implanted sample. Implanting Ge into the Si top layer and then annealing the wafer may have improved the quality of the Si near the surface layer, enhancing the carrier life-time and, thus, forming a current path near the surface between the source and drain. We have discussed earlier that adequate Ge implantation into the Si top layer of SIMOX wafers may result in bending the threading dislocation defects and stopping their propagation to the surface layer.

3.2.2 Effect of Annealing on PCMOST Characteristics.

As mentioned above, we annealed the Ge-implanted samples for one hour further at 1000°C in N_2 and again measured their PCMOST characteristics. Figures 3-14b, 3-15b, and 3-16b show I-V characteristics of these samples after the second annealing, clearly indicating that the second annealing eliminated the shift between the individual I-V curves (solid and dashed curves) in each sample. However, after the second annealing, a significant change in the location of the minimum I_{DS} appears to occur, shifting to large positive voltage regions. We speculate that some impurities may have contaminated the Si top layer during the second annealing process, thus causing the shift in I-V curves. The large leakage current at $V_G = 0$ may also be caused by further improvements in the quality of the Si surface layer. As shown, the rate at which the current increases as a function of the applied gate voltage becomes even slower after the second annealing, making it more difficult to control the current path from the back-channel region.
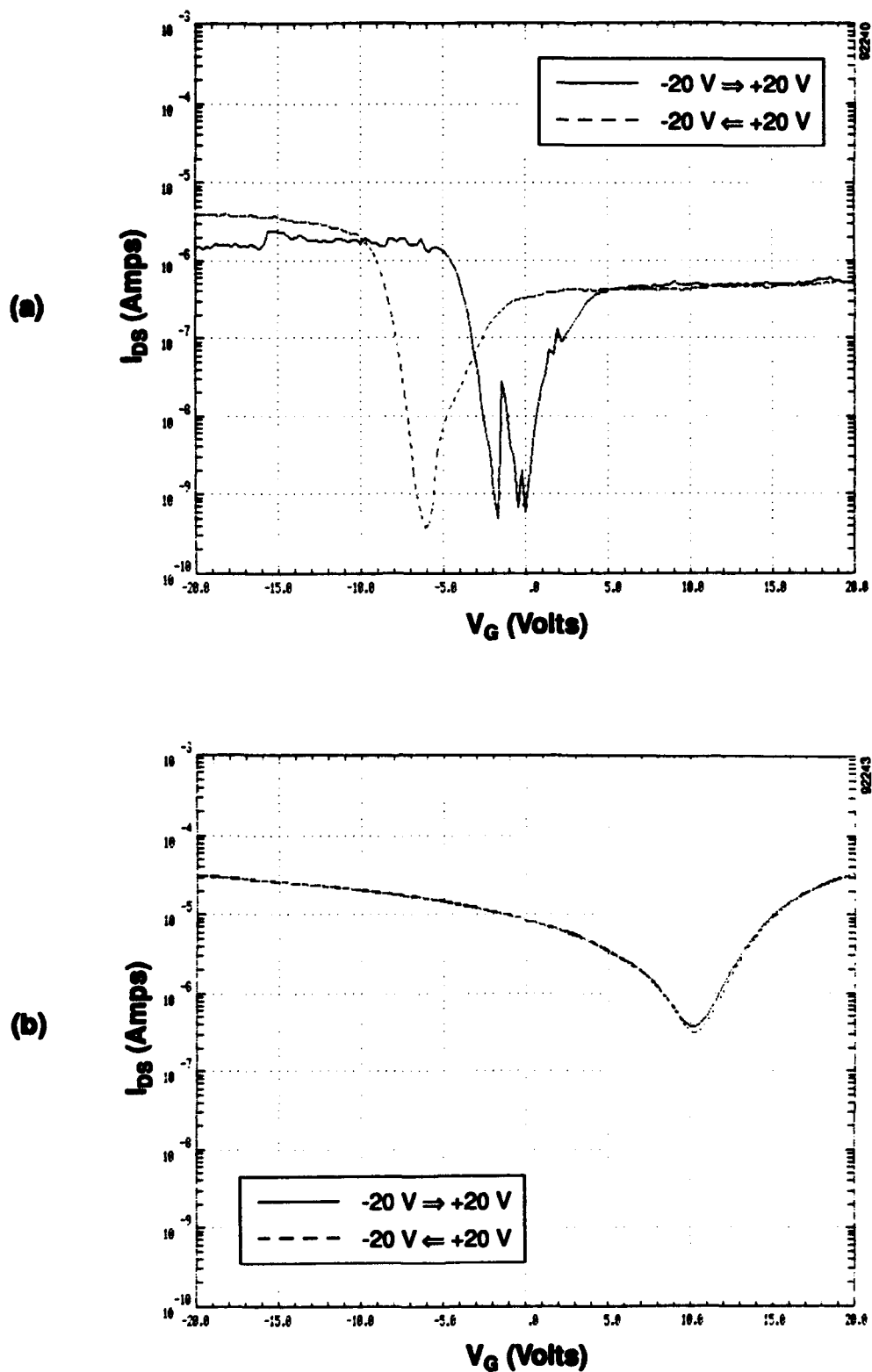
Figure 3-14. *Current-voltage characteristics from a PCMOST structure fabricated on standard SIMOX samples implanted with a dose of $3x10^{15}$ Ge^+/cm^2 at 40 keV and annealed for a) 30 minutes at 850°C in N_2 and b) 30 minutes at 850°C followed by one hour at 1000°C in N_2.*
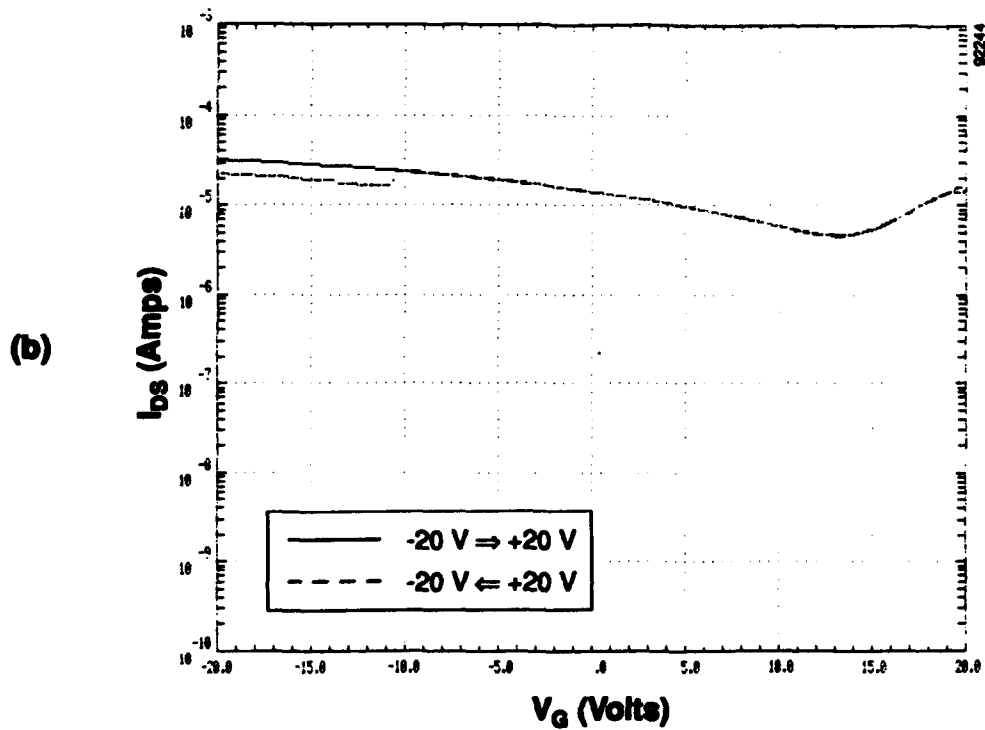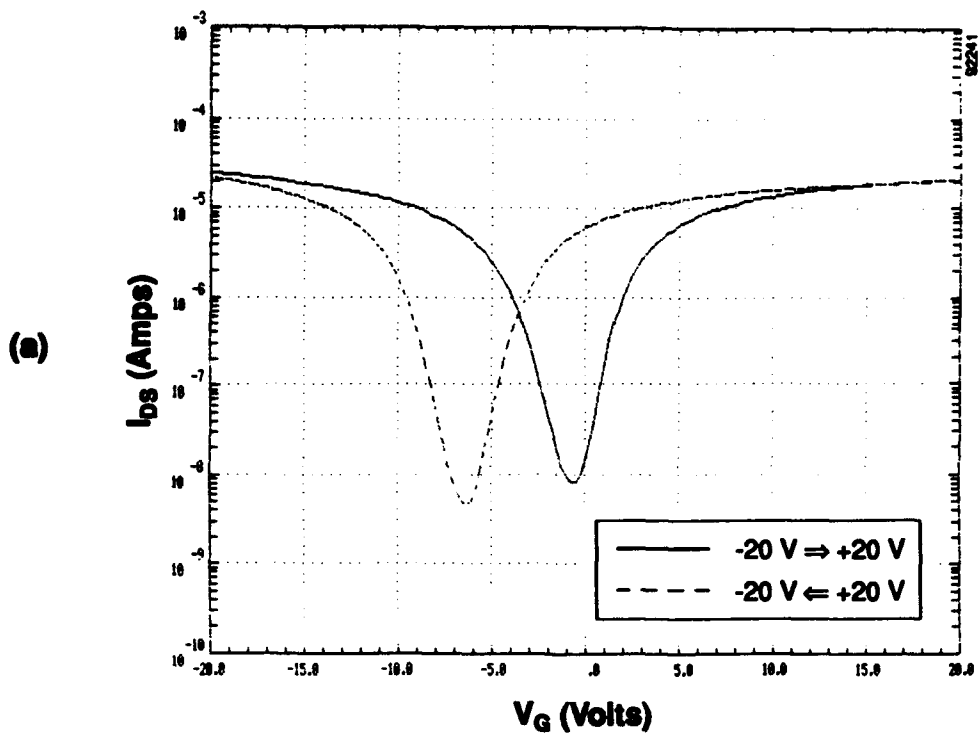
Figure 3-15. *Current-voltage characteristics from a PCMOST structure fabricated on standard SIMOX samples implanted with a dose of 3 x 10^{15} Ge$^+$/cm^2 at 120 keV and annealed for a) 30 minutes at 850°C in N$_2$ and b) 30 minutes at 850°C followed by one hour at 1000°C in N$_2$.*

44
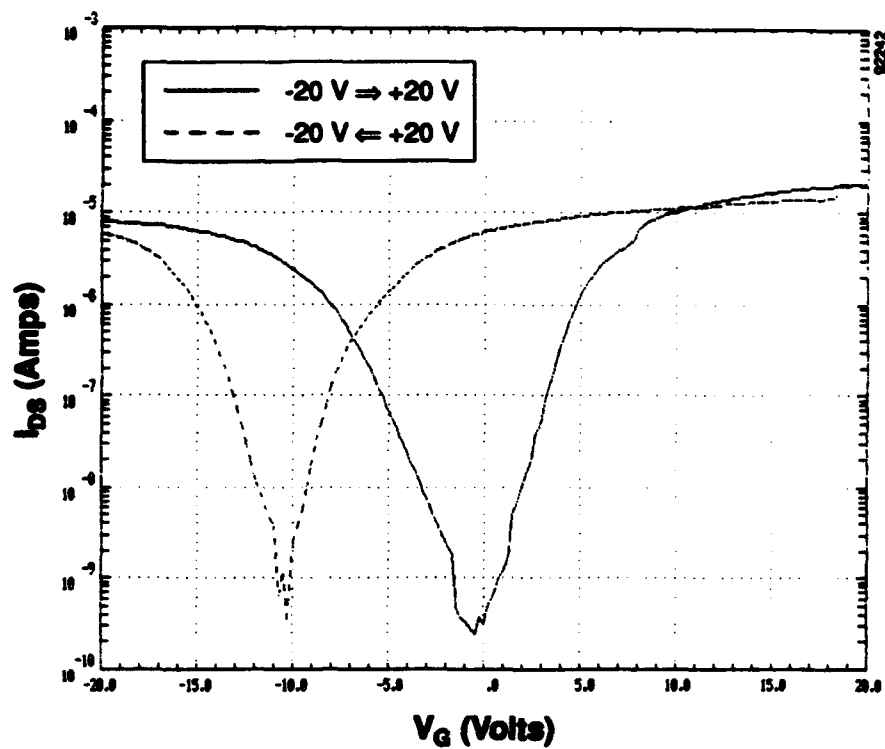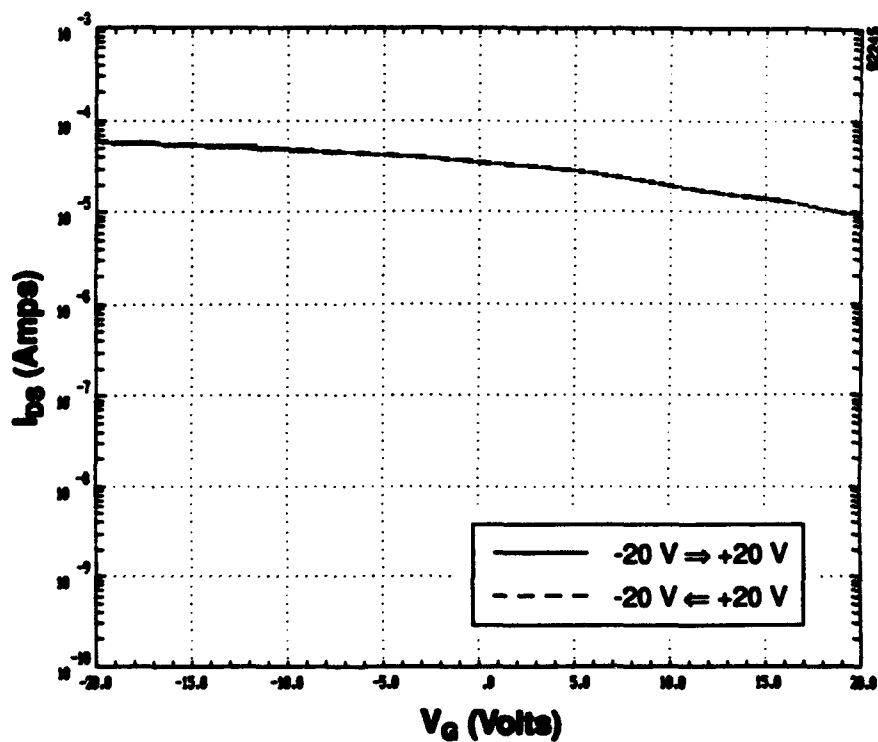
Figure 3-16. *Current-voltage characteristics from a PCMOST structure fabricated on standard SIMOX samples implanted with a dose of $3x10^{15}$ Ge^+/cm^2 at 160 keV and annealed for a) 30 minutes at 850°C in N_2 and b) 30 minutes at 850°C followed by one hour at 1000°C in N_2.*

We implanted additional SIMOX wafers with Ge, fabricated new test structures, and continued to measure PCMOST characteristics to understand better the effects of Ge implantation on the electrical properties of the Si top layer, especially close to the SiO_2 interface region.

We implanted Ge into samples from two standard SIMOX wafers (#P1047, a p-type <100> wafer and #N1043, an n-type <100> wafer) with a dose of 1 x 10^{16} Ge^+/cm^2 at 160 keV. Both implanted samples were then annealed at 1000°C for one hour. However, one sample (#1043GE) was annealed in N_2 ambient, while the other (#1047GE) was annealed in Ar ambient with about 0.5% O_2 gas flowing.

To fabricate test structures on Ge-implanted samples (#1043GE and #1047GE) and non-Ge-implanted samples (#1043 and #1047), we deposited 5000Å of SiO_2 (instead of Al) onto the surface layer for masking in the EDP silicon etchant. We patterned the samples photolithographically and then placed them in buffer HF solution to remove the oxide from non-device regions and expose the Si. The samples were then etched in EDP solution to remove the Si and expose the buried SiO_2 layer. Finally, the oxide layer covering the isolated Si top layer islands was removed in buffer HF.

Using our improved PCMOST measurement system, we measured the dependence of drain current I_{DS} on gate voltage V_G, where the Si substrate serves as a gate contact and V_{DS} was taken as an adjustable parameter. Figure 3-17a and 3-178b shows representative PCMOST results obtained from devices fabricated on SIMOX samples without Ge implantation, with V_{DS} adjusted to 0, 0.2, 0.5, and 0.9V. Figure 3-18a and 3-18b, conversely, shows the PCMOST results from Ge-implanted devices with Ar and N_2 anneal ambient, respectively. Despite the difference in annealing ambient, results from the Ge-implanted structures appear similar; however, they reveal several important differences when compared with results for non-Ge-implanted SIMOX structures (Figure 3-17a and 3-17b).

As shown in Figure 3-18a and 3-18b, the I-V curves measured at V_{DS} values above zero (0.2, 0.5 and 0.9V) for Ge-implanted samples typically indicated a minimum I_{DS} at V_G values near 10V and the current leakage increase with the applied V_{DS} for all V_G biases. In the SIMOX samples without Ge implantation (Figure 3-17a and 3-17b), a minimum I_{DS} of about 10 nA occurs at V_G values near zero, regardless of the applied V_{DS} value (though current leakage increases with V_{DS} for other V_G biases).

We observed a most interesting difference in the magnitude of the drain current when comparing devices without and with Ge implantation under zero bias applied between the source and drain (V_{DS} = 0V). The drain current under zero bias can only originate from the gate bias supply through the implanted SiO_2 layer. This very significant accomplishment implies that the parasitic gate leakage current was reduced by more than an order of magnitude due to the Ge implantation. The Ge seems to form a high resistivity region in the Si/SiO_2 interface region, blocking the gate leakage current flow.
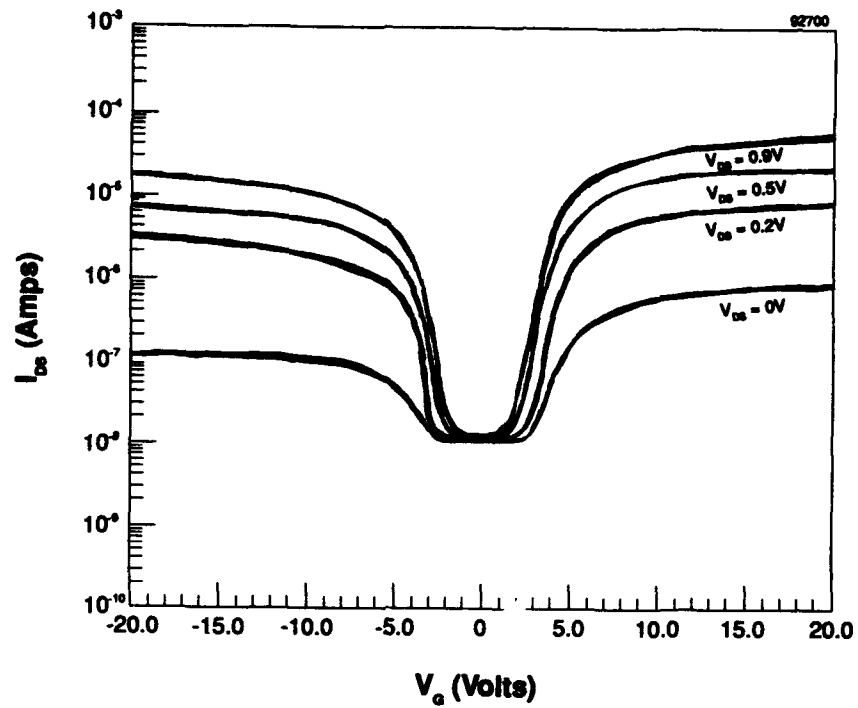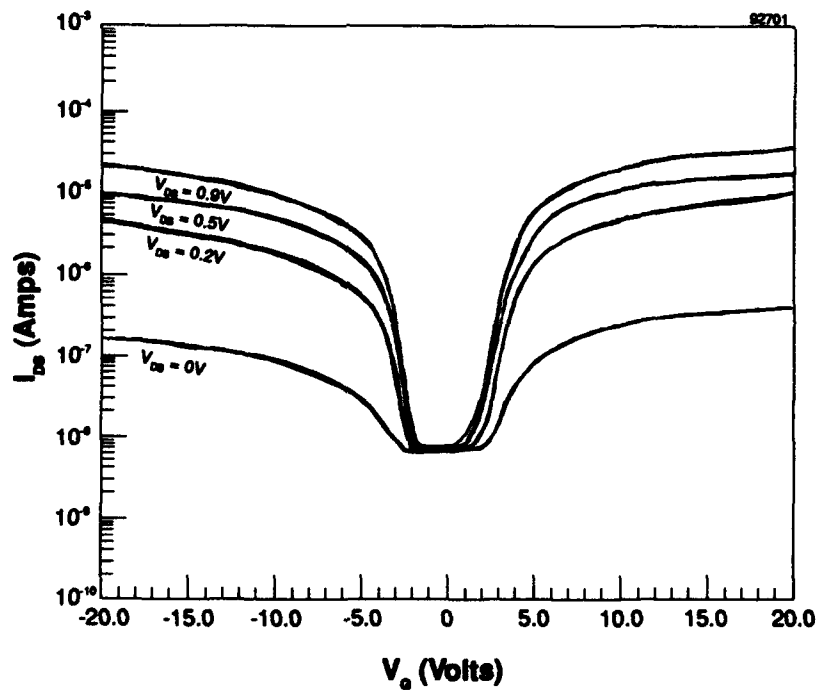
Figure 3-17. *PCMOST characteristics of structures fabricated on standard SIMOX samples without Ge implantation: a) sample #1047 and b) sample #1043.*

47

A

I_{DS} (Amps)

10^{-3}
10^{-4}
10^{-5}
10^{-6}
10^{-7}
10^{-8}
10^{-9}
10^{-10}

$V_{DS} = 0.9V$
$V_{DS} = 0.5V$
$V_{DS} = 0.2V$
$V_{DS} = 0V$

-20.0 -15.0 -10.0 -5.0 0 5.0 10.0 15.0 20.0

V_G (Volts)

A

B

I_{DS} (Amps)

10^{-3}
10^{-4}
10^{-5}
10^{-6}
10^{-7}
10^{-8}
10^{-9}
10^{-10}

$V_{DS} = 0.9V$
$V_{DS} = 0.5V$
$V_{DS} = 0.2V$
$V_{DS} = 0V$

-20.0 -15.0 -10.0 -5.0 0 5.0 10.0 15.0 20.0

V_G (Volts)
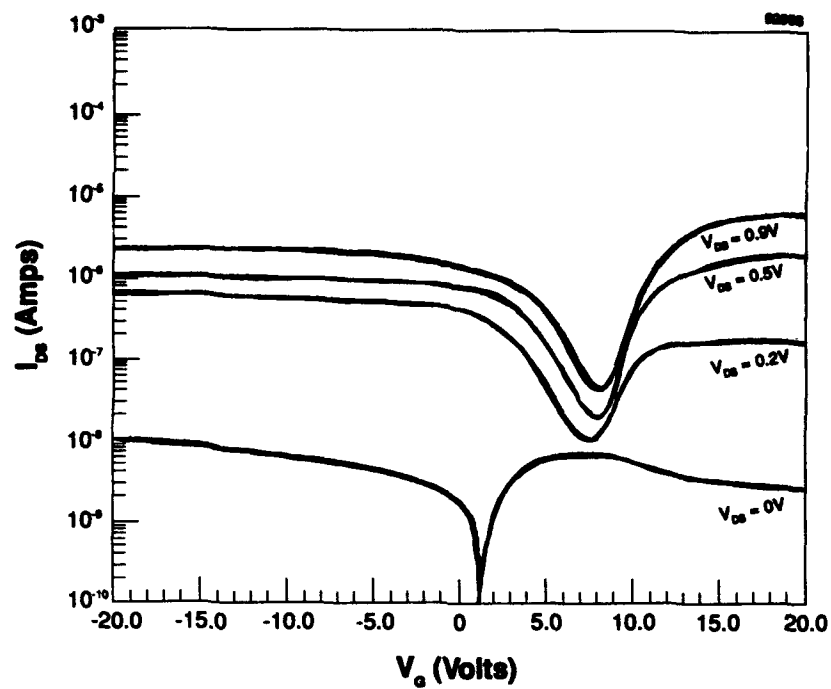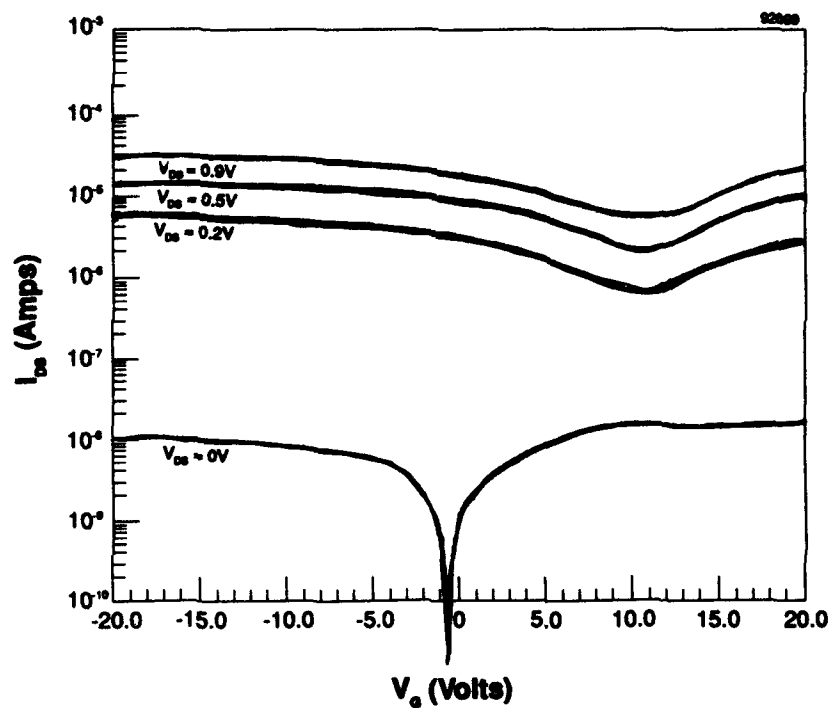
B

Figure 3-18. *PCMOST characteristics of structures fabricated on standard SIMOX samples implanted with a dose of $1x10^{16}$ Ge^+/cm^2 at 160 keV and annealed for one hour at 1000°C in a) argon (sample #1047GE) and b) nitrogen (sample #1043GE).*

48

Also, Ge implantation seems to create a depletion mode FET. Results shown in Figure 3-18a and 3-18b demonstrates that a hole current can flow between the source and drain even without a gate bias, indicating the presence of an accumulation channel. When the gate bias becomes increasingly positive, this hole current decreases and, in fact, will vanish at gate voltages over +10V. At strong positive biases, electrons accumulate and I_{DS} increases, thus demonstrating a back-channel depletion-mode FET. When measuring the Hall effect in the top Si layer as a function of gate bias, if the mobile carriers change from holes to electrons as V_G exceeds +10V, Hall voltage polarity should be reversed. Furthermore, the measurement provides magnitudes of both electron and hole mobilities, confirming that Ge can improve the crystalline quality of the Si top surface film.

SECTION 4

SUBCONTRACT AGREEMENTS FOR DEVICE FABRICATION

4.1 QUICK TURNAROUND MOSFET DEVICES.

Though we initiated arrangements for a subcontract with Massachusetts Institute of Technology (MIT) Lincoln Laboratories, Lexington MA, for device and circuit processing, no agreement was finalized. However, we did collaborate briefly with Dr. Pramod C. Karulkar to study the effect of Ge implantation on back-channel degradation in SIMOX wafers.

We implanted a three-inch standard SIMOX wafer with a Ge dose of 1×10^{16} Ge^+/cm^2 at 160 keV and annealed it at 1000°C in Ar for one hour, along with another SIMOX wafer without Ge implantation from the same lot. Dr. Karulkar used both wafers for test device fabrication and testing; his preliminary results follow.

The test devices were very simple, quick turnaround MOSFETs fabricated only on small areas of the SIMOX wafers to allow further processing steps and the future use of such wafers. Figure 4-1 shows a schematic for the quick turnaround test MOSFETS. To fabricate these test devices, they patterned the SIMOX wafers and etched the Si mesa. They then applied a photoresist layer as an implantation mask. To form the source and drain, boron was implanted with a dose of 2×10^{15} B^+/cm^2 at 30 keV into the wafers through windows in the photoresist. Finally, the photoresist was removed, and the wafers were annealed for 30 minutes at 900°C. The buried SiO_2 functions as the back-gate oxide and the substrate as the back-gate electrode in this device. During electrical characterization, probes were pressure-contacted to the source, drain, and back gate. No metallization or doping of the channel region was performed.

The C-V measurements of these simple devices seemed to indicate good MOSFET characteristics. Figure 4-2 (a and b) compares the I_D-V_{DS} curves, and Figure 4-3 (a and b) compares the I_D-V_B curves of the two types of devices. The carrier mobilities in the devices' inversion layers (both with and without Ge implantation) appear identical with values of 160 to 200 cm^2/V-S. The kink effect related to the floating body can be observed in the I-V results, especially those from the SIMOX devices without Ge implantation.

4.2 SUBCONTRACT WITH DEVICE PROCESSING INSTITUTION.

Under Dr. Karulkar's direction, MIT Lincoln Laboratory would have fabricated and tested several devices and circuits to evaluate the effect of Ge implantation in reducing back-channel leakage in SIMOX structures. Unfortunately, Lincoln Laboratory was unable to finalize the agreement because of its Air Force contract which prevents it from directly competing with industry or from functioning as a subcontractor on any government contract.

We arranged a subcontract agreement with Prof. James E. Chung of the Dept. of Electrical Engineering and Computer Science at MIT. Under Professor James Chung's supervision, the MIT group would fabricate and test a number of devices and circuits on SIMOX wafers, provided by Spire, in order to determine the effectiveness of Ge implantation for reducing back-channel leakage in NMOS SIMOX devices and for improving radiation hardness.

50
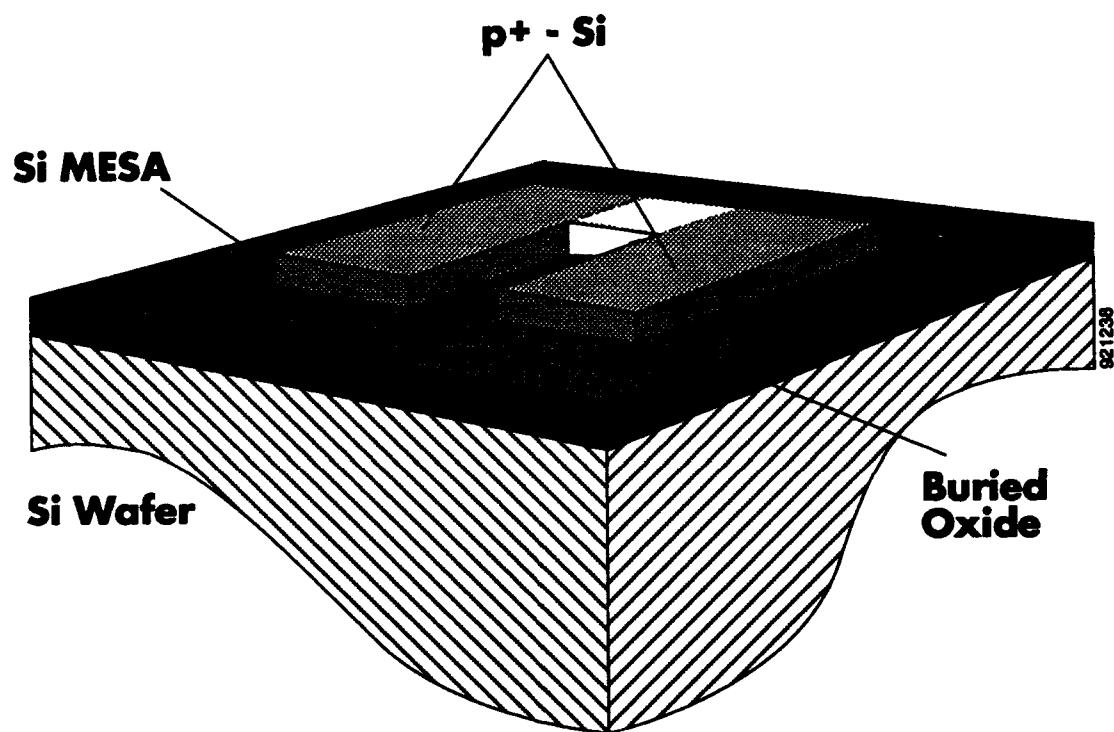
Figure 4-1. *Schematic of the quick turnaround MOSFETs fabricated on SIMOX wafers.*

51
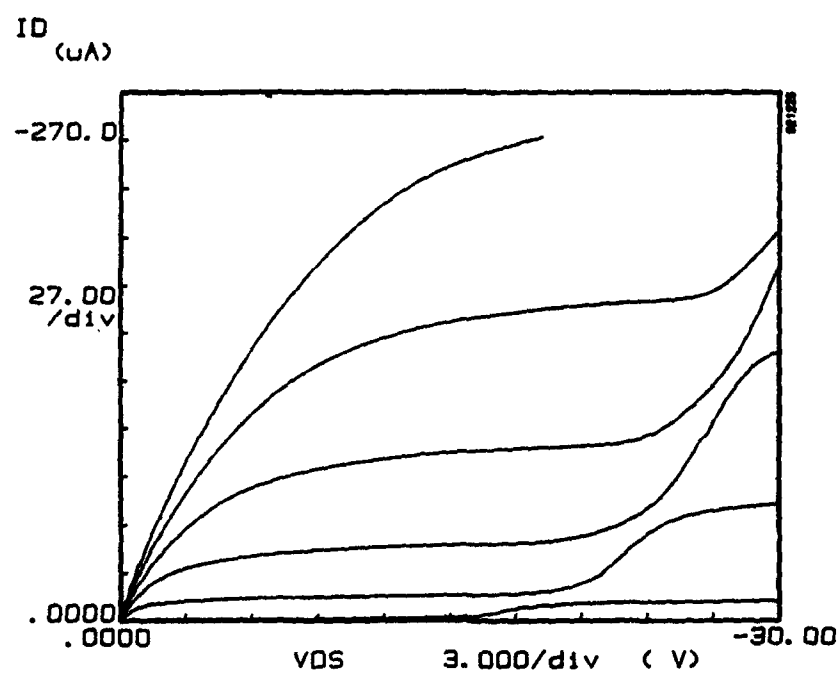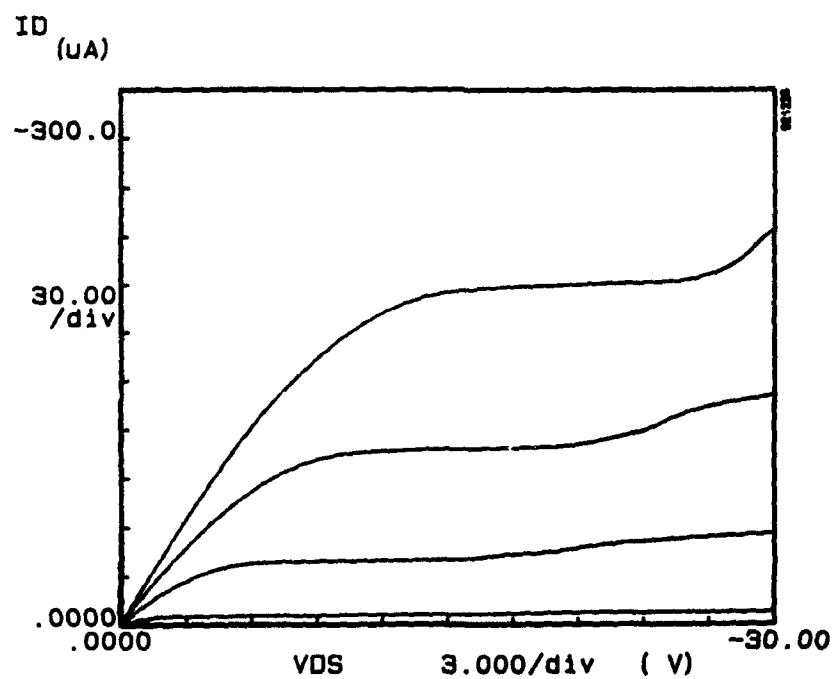
Figure 4-2. I_D vs. V_{DS} characteristics from quick turnaround devices fabricated on a) SIMOX without Ge implantation and b) SIMOX with Ge implantation.
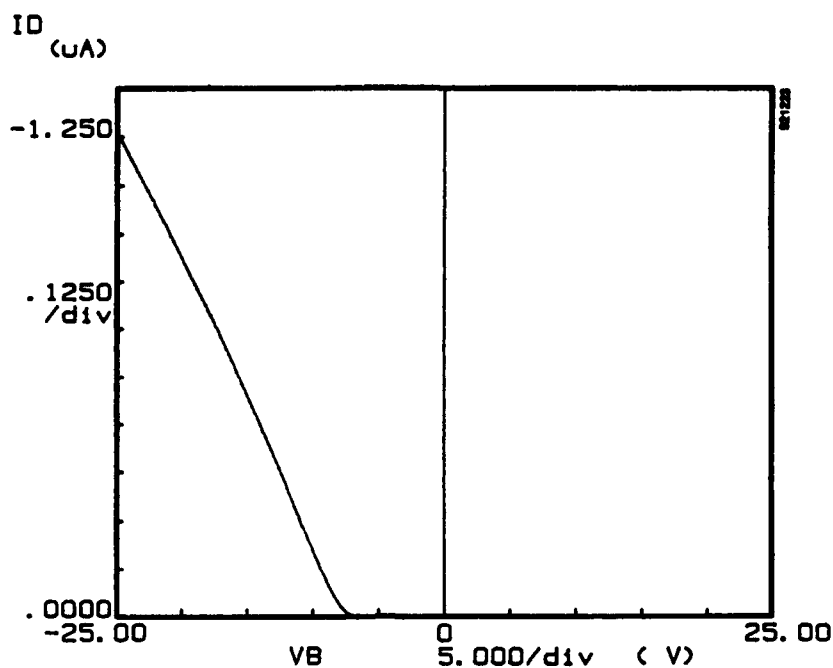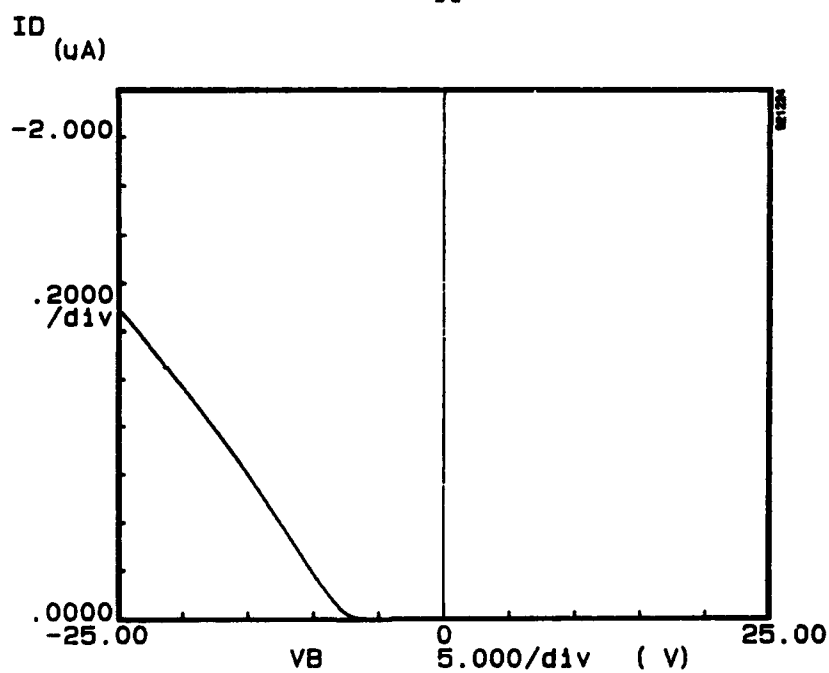
Figure 4-3. I_D vs. V_B characteristics from quick turnaround devices fabricated on a) SIMOX without Ge implantation and b) SIMOX with Ge implantation.

53

SECTION 5

DEVICE FABRICATION

This section includes five pages of information listing the SIMOX and bulk Si samples, as well as the process flow for fabricating Phase II devices at MIT. Below are additional details and explanations of the fabrication steps provided by MIT.

5.1 PREPARATION OF SIMOX WAFERS.

To demonstrate the universality of Ge implantation for improving the performance and radiation hardness of SIMOX devices and circuits, we purchased several four-inch standard single-implant SIMOX wafers from IBIS Corporation and SOITEC USA. All wafers were Ge-implanted at Spire and sent to MIT for device fabrication.

5.2 PROCESS FLOW.

We worked with MIT to generate an appropriate process flow for device fabrication on the above-described wafers. Devices and circuits were fabricated under identical conditions on different non-implanted and Ge-implanted wafers. Results from characterizing and comparing these devices and circuits aided in evaluating the Ge implantation process as a method for 65 reducing back-channel leakage and improving device performance.

Samples were implanted with Ge^+ and annealed under optimum conditions determined by previous studies. In most samples, only half of each wafer was implanted with Ge^+ while the other half was masked during implantation. By fabricating and testing identical devices over each entire wafer surface, we could evaluate the effect of Ge implantation on device performance without risking possible non-uniformities among different sample structures.

We divided the wafers into two groups, the first composed of five wafers and the second of 15. Processing these two sets of wafers differed: the first group was initially implanted with Ge, annealed, and, finally, isolated using the LOCalized Oxidation of Silicon (LOCOS) process, while the second group was first isolated using LOCOS and then received Ge implantation.

Ge was implanted into the device active regions before the gate oxidation step. A fractional-factorial Ge implantation matrix of nine elements, in terms of implant energy, dose, and top Si recrystallization-annealing temperature, was implemented in the device fabrication process in order to optimize the Ge-implant technology. The Ge implant energies used were 120 keV and 150 keV; Ge^+ doses were 10^{15}, 5×10^{15}, and 10^{16} /cm^2; and recrystallization annealing temperatures were at 850°C and 950°C. The matrix elements of 120 keV and annealing temperature of 850°C for all three doses were not included. The total time of recrystallization-annealing, which was performed immediately after the Ge implant, was 30 minutes.

The major thermal cycle after LOCOS consisted of the gate oxidation and source/drain drive-in steps for a total of 70 minutes at 900°C. As substitutional dopants in Si, Ge showed no evidence of redistribution at 850°C.[17] However, at 900°C or higher, the as-implanted Ge profile may have been broadened.

54

Thus in Phase II, Non-LDD, n-MOSFETs were fabricated on SIMOX wafers, along with bulk control devices. The gate oxide thickness was 120Å, the top silicon thickness was 2000Å, and the buried oxide thickness was 3850Å. The channel doping had three splits: Boron 1.5×10^{15} cm^{-3} (fully depleted), BF_2 7×10^{16} cm^{-3} (partially depleted), and BF_2 $2.1 \times {}^{17}cm^{-3}$ (partially depleted). Devices with body-contacts (H-gate) and edge-less gates were also fabricated.

We measured the layer thicknesses of a wafer from each SIMOX group using Spire's non-destructive optical reflectance analysis. Figures 5-1 and 5-2 show the optical reflectance results from regions near the edge and at the center, respectively, of the SOITEC SIMOX wafer. These results indicate an average Si top layer thickness of about 2095Å and a buried oxide layer thickness of about 3700Å. Figures 5-3 and 5-4 show the optical results measured from regions near and at the center, respectively, of the IBIS wafer. These results indicate an average Si top layer thickness of about 2190Å and a buried oxide layer thickness of about 3800Å. The results shown in Figures 5-1 through 5-4 agree with the layer thicknesses measured at SOITEC ($Si=2056Å$, $SiO_2=3985Å$) and IBIS ($Si=2190Å$, $SiO_2=3866Å$). The values for layer thickness are useful for determining the appropriate Ge implantation energy to create back-channel defects.

To: PTC
Subject: SIMOX NMOSFET with Ge-implantation process traveler
From: Hua-Fang Wei
Date: December 18, 1992

The purpose of this run is to build Ge-implanted NMOSFETs using SIMOX SOI
wafers, with non-fully depleted and fully depleted operation modes.
Some starting SOI wafers received Ge implantation in the top Si film. Some
starting SOI wafers without Ge-implant will be Ge-implanted after LOCOS is
formed. Ge implant will be preformed at SPIRE (only Ge is implanted and only
Si substrate is used in that implanter). Ge implantation recrystallization
annealing will be done at ICL.

According to previous SiGe work, tube A7 can be used for LTO, B5 for anneal,
and B7 for sintering, all after SiGe deposition.

The top target Si thickness is designed to be thickest possible so as to minimize
the interaction between the Ge-implant-damaged region and the top channel.
Non-fully depleted mode is achieved by channel implant with Boron.

Three Ge-implantation-related process variables are
considered in the design of experiment. There are:
Ge implantation dose (D1=1E15 cm^{-2}, D2=5E15, D3=1E16),
Ge implantation energy (E1 = 150 keV , E2=E1-30 KeV),
After Ge implantation recrystallization annealing temperature
(T1=850 C, T2=950 C).
Previous studies indicate D2 and T1 are more favored.
Notation "V" means virgin, or no Ge is implanted, which serves as controller.
Most single wafers have pairs of samples on them in terms of half wafer (divided
by '||' sign).
SOI-Wafer # is SOI wafer from Soytech, Ibis # is SOI wafer from IBIS. This run
can also compare wafers from different companies.

Experiment Matrix:
(1) Ge implantation before device process:
SOI-Wafer 1: V||D1/E1/T1
SOI-Wafer 2: D2/E2/T1||D2/E1/T1
SOI-Wafer 3: V||D3/E1/T1
Ibis 1, and bulk-wafer 1: V||D2/E1/T1

(2) Ge implantation after LOCOS:
SOI-Wafer 4: V||D1/E1/T1
SOI-Wafer 5: D1/E2/T2||D1/E1/T2
SOI-Wafer 6: D2/E2/T1||D2/E1/T1
Bulk-wafer 2: V||D2/E1/T1
SOI-Wafer 7: D2/E2/T1
SOI-Wafer 8: V||D2/E2/T2
SOI-Wafer 9, Ibis 2, and bulk-wafer 3: V||D2/E1/T2
SOI-Wafer 10 and Ibis 3: V||D3/E1/T1
SOI-Wafer 11: D3/E2/T2||D3/E1/T2
Bulk-wafer 4: D3/E1/T2||D1/E1/T2
Ibis 4: D2/E1/T1||D1/E1/T1

(3) No Ge implantation at all
SOI-Wafer 12: V and no T1/T2

Note: All virgin half wafers (no Ge implantation) also receive the after
Ge implantation annealling the other half wafers receive.
SOI-Wafer 7 is the duplication since the combination of D2 and T1 are important.
A full factorial experiment of D, E, and T will yield 12 total. In the design
above the combinations of D1/E2/T1 and D3/E2/T1 are not included.

SIX MASK NMOSFET PROCESS FOR 0.5 MICRON CHANNEL LENGTH SOI DEVICES

LOT # __spire__   LOT OWNER _Hua-Fang Wei_

RESISTIVITY __10-20_ ohm-cm   TOTAL NUMBER OF WAFERS:16 simoxs,4 bulks,13 dummies

STARTING SIMOX SOI WAFER: P-Si(2245 A)/SiO2(3794 A)/P-Si (Boron doped,2.5E14 cm^-3)
STARTING BULK WAFER: P SUBSTRATE (Boron doped, 2.5E14 cm^-3)

* indicates a step which needs to be modified from the NMOS baseline opset

STEP #	STEP DESCRIPTION	STATUS
1	Ge implantation for 4 wafers (done at SPIRE)	
2	Recrystallization anneal 850 C, 30 min, B5 recipe needs to be created	Number wafers _____ Opset start _____ Opset finish _____
3*	Stress Relief Oxide dsro220.set (recipe 230/A1) (950C, 38.75min in DryO2 950C, 30min in N2) Dummy #1 in for SRO monitoring, out Dummies #2,3 in; dummy #4 in, out	Number wafers _____ Opset start _____ Opset finish _____
4	LPCVD Silicon Nitride dnit1.5k.set (recipe 410/A5) (800C, 2hr) Dummies #2,3 for Nitride monitoring,out	Number wafers _____ Opset start _____ Opset finish _____
5	Active Area Pattern phfieldsor.set (Mask: SOI CD Job: ICL CWR1)	Number wafers _____ Opset start _____ Opset finish _____
6	Nitride Plasma Etch plnit1.5k.set Dummy #2 in, for etch monitoring, out	Number wafers _____ Opset start _____ Opset finish _____
7	P-Field Implant (p-bulk) ipfield1su.set (Boron, 3E13, 25 keV) dummy #4 and its twin in, out	Number wafers _____ Opset start _____ Opset finish _____
8	Resist Ash ash.set	Number wafers _____ Opset start _____ Opset finish _____
9*	Field Oxide (fox+SRO:t1 A SiO2) t1=11 0%(2245/.45) t1 is measured from dummy #4 dsfox.set (recipe 114/B1 or B2) (950C, 30min in DryO2 950C, time min in WetO2	Number wafers _____ Opset start _____ Opset finish _____ time is so decided to yield t1 A

SiO2
      950C, 30min in DryO2
      950C, 30min in N2)
      Dummy #4 in for fox monitoring, out

10   Nitride Wet Etch   Number wafers _____
      wnit1.5k.set   Opset start _____
      Dummy #3 in for etch monitoring, out   Opset finish _____

11   Stress Relief Oxide Wet Etch Number wafers _____
      wsro220.set   Opset start _____
                                    Opset finish _____
      Dummy #1 in for SRO etch monitoring, out

12*   Dummy Gate Oxide Growth   Number wafers _____
      dgate120.set (recipe 112/A2) Opset start _____
      (900C, 25min in DryO2   Opset finish _____
       900C, 25min in N2)
      Dummy #5 in for oxide monitoring, out
      Dummies #6 & #7 in, out

***************(repeat 13,14,15 for implant splits)***********************

13*   Channel Implant Pattern   Number wafers _____
      phchannel.set   Opset start _____
      (Mask: no mask   Opset finish _____
       Job: LSU,4 for HI vt)
            LSU,9 for MED vt)
      Decide channel implant dose now using known dummy oxide thickness
      and SUPREM, so as to have non-fully depleted mode for higher dose implants,
      lower dose implant and intrinsic are fully depleted modes.

14*   Channel Implant   Number wafers _____
      ipvtlsu.set   Opset start _____
         (BF2, 40keV, 3E12 for HI vt)   Opset finish _____
         (BF2, 40keV, 1E12 for MED vt)
      (no implants for low vt)
      Dummies #6 & #7 in, out

15   Resist Ash   Number wafers _____
      ash.set   Opset start _____
                                 Opset finish _____

***************(repeat 13,14,15 for implant splits)*******************

16   Dummy Gate Wet Etch   Number wafers _____
      wgate120.set   Opset start _____
      Dummy #5 in for etch monitoring, out   Opset finish _____
      Dummies #6 & #7 in

17*   Gate Oxide   Number wafers _____
      dgate109.set (recipe 112/A2) Opset start _____
      (900C, 25min in DryO2   Opset finish _____
       900C, 25min in N2)
      Dummies #6 & #7 out
      Dummies #8 & #9 in for oxide monitoring
      Dummy #10 in, out

18*   LPCVD Polysilicon   Number wafers _____
      poly3k.set (recipe 428/A6)   Opset start _____
      (625C)   Opset finish _____
      Dummies #8 & #9 for poly monitoring, out
      Dummy #11 in, out

58

19	Poly Gate Pattern phpolylsu.set (Mask: SOI CP Job: ICL CD1)	Number wafers _____ Opset start _____ Opset finish _____

20	Plasma Poly Etch plpoly3k.set Dummy #8 in for etch monitoring, out	Number wafers _____ Opset start _____ Opset finish _____

21	Resist Ash ash.set	Number wafers _____ Opset start _____ Opset finish _____

22	N+ Poly/S/D Pattern phn+lsu.set (Mask: SOI CN+ Job: ICL CP1)	Number wafers _____ Opset start _____ Opset finish _____

23*	Poly And S/D Implant inpsdhao.set (As: 25kev,4e15) Dummies #10 & #11 in, out	Number wafers _____ Opset start _____ Opset finish _____

24	Resist Ash ash.set	Number wafers _____ Opset start _____ Opset finish _____

25	P+ Poly/S/D Pattern pp+lsu.set (Mask: SOI CP+ Job: ICL CD1)	Number wafers _____ Opset start _____ Opset finish _____

26*	P+ Sub Contact Implant innsdlsu.set (BF2: 25kev,4e15) Dummy #9 in, out	Number wafers _____ Opset start _____ Opset finish _____

27	Resist Ash ash.set	Number wafers _____ Opset start _____ Opset finish _____

28*	Poly And S/D Diffusion ddrivehao.set (recipe 113/B5) (900C, 15min in Dry O2) (900C, 5 min in N2) Dummies #6,#7,#9,#10 & #11 in,out Dummy #10 for oxide increase (beyond gate oxide) monitoring	Number wafers _____ Opset start _____ Opset finish _____

29*	LTO Deposition dlto4k.set (recipe 437/A7, 400C) Dummies #12 &#13 in for LTO monitoring	Number wafers _____ Opset start _____ Opset finish _____

30	LTO densification dann.set (recipe 806/B5) (950C, 30min in N2) Dummies #12 & #13 out Dummies #6,#7,#9,#10 & #11 in,out	Number wafers _____ Opset start _____ Opset finish _____

31	Resist Coat phcoat.set	Number wafers _____ Opset start _____ Opset finish _____

32	Backside LTO Wet Etch	Number wafers _____

```
        wlto4k.set                          Opset start     _____
                                            Opset finish    _____
        Dummies #6 & #7 in for channel doping monitoring, out
        Dummy #9 in for P + sub contact doping monitoring, out
        Dummy #10 in for S/D doping monitoring, out
        Dummy #11 in for poly doping monitoring, out
```

33   **Backside Poly Plasma Etch**   Number wafers   _____
      plpoly3k.set   Opset start   _____
      (CCL4, 45sec/8sec)   Opset finish   _____

34   **Backside Oxide Wet Etch**   Number wafers _____
      wox5k.set   Opset start   _____
                                      Opset finish   _____

35   **Resist Ash**   Number wafers   _____
      ash.set   Opset start   _____
                                      Opset finish   _____

36   **Contact Pattern**   Number wafers   _____
      phconthao.set   Opset start   _____
      (Mask: SOI CC   Opset finish   _____
       Job: ICL CP1)

37   **LTO Plasma Etch**   Number wafers   _____
      pllto4k.set   Opset start   _____
      (CF4)   Opset finish   _____
      Dummies #12 & #13 in for etch monitoring

38   **LTO Wet Etch**   Number wafers   _____
      wlto4k.set   Opset start   _____
                                      Opset finish   _____
      Dummies #12 & #13 for etch monitoring, out

39   **Resist Ash**   Number wafers   _____
      ash.set   Opset start   _____
                                      Opset finish   _____

40   **Metal Deposition (Al)**   Number wafers   _____
      cvclugc.set   Opset start   _____
      (Use Varian.set)   Opset finish   _____
      Dummy #14 in for metal monitoring, out

41   **Metal Pattern**   Number wafers   _____
      phmetlsu.set   Opset start   _____
      (Mask: SOI CM1   Opset finish   _____
       Job: ICL CC)

42   **Metal Plasma Etch**   Number wafers   _____
      plmetal.set   Opset start   _____
                                      Opset finish   _____

43   **Resist Ash**   Number wafers   _____
      ash.set   Opset start   _____
                                      Opset finish   _____

44   **Sinter Metal**   Number wafers   _____
      dsinter.set (recipe 710/B8)   Opset start   _____
      (400C, 40min in H2+N2)   Opset finish   _____

REFLECTANCE DATA (SYMBOLS) AND FIT (LINE)

L551-CTL-E X^2 = .189E-03

DOSE = 1.69E+18   FWHM = 381 nm   DEPTH = 435 nm   CAP THICKNESS = 0 nm

IMPLANTED OXYGEN PROFILE

L551-E .SOI   P_3A2081.TRS

XC = 0 nm   XE = 210 nm   XF = .00349 nm   XI = 379 nm   XB = 70.9 nm

Figure 5-1. *Optical reflectance results measured on the region near edge of a SOITEC SIMOX wafer indicating a Si top layer 2100Å thick and a buried SiO_2 layer 3790Å thick.*

61

Figure 5-2. *Optical reflectance results measured at the center region of a SOITEC SIMOX wafer indicating an Si top layer 2090Å thick and a buried SiO$_2$ layer 3620Å thick.*

62

REFLECTANCE DATA (SYMBOLS) AND FIT (LINE)

1578-CTL-E   X² = .151E-03

DOSE = 1.72E+18   FWHM = 387 nm   DEPTH = 452 nm   CAP THICKNESS = 0 nm

IMPLANTED OXYGEN PROFILE

1578-E .SOI   P_5A20M1.TRS

XC = 0 nm   XE = 216 nm   XF = .0117 nm   XI = 385 nm   XB = 86.9 nm

Figure 5-3.   *Optical reflectance results measured on the region near edge of an IBIS SIMOX wafer indicating a Si top layer 2160Å thick and a buried SiO₂ layer 3850Å thick.*

63

REFLECTANCE DATA (SYMBOLS) AND FIT (LINE)

1578-CTL-C $X^2 = .134E-03$

DOSE = 1.68E+18   FWHM = 378 nm   DEPTH = 462 nm   CAP THICKNESS = 0 nm

IMPLANTED OXYGEN PROFILE

1578-C .SOI   P_5A2081.TRS

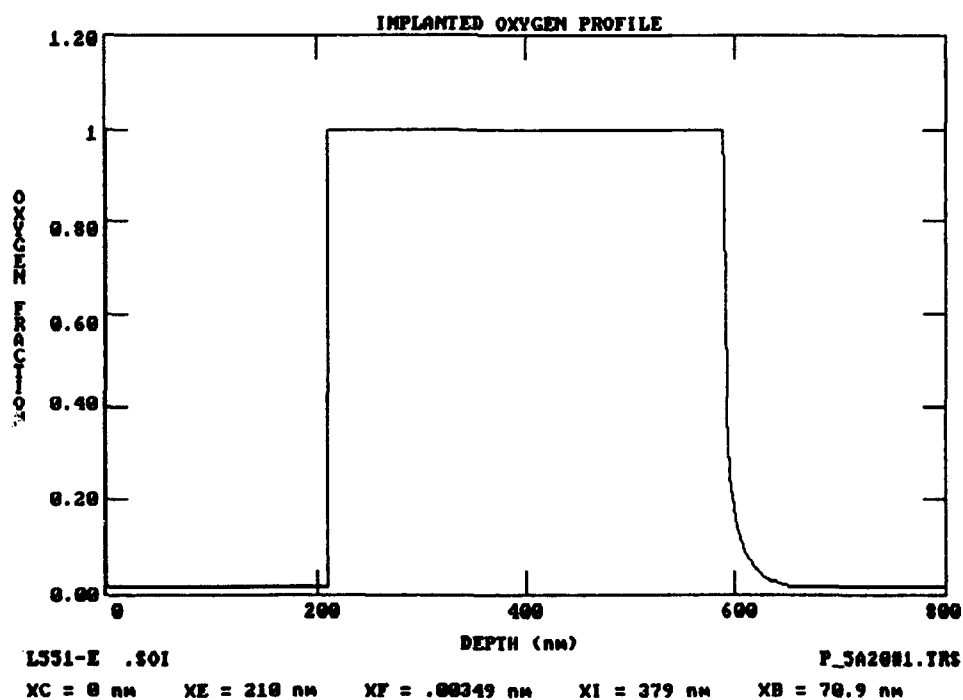XC = 0 nm   XE = 222 nm   XF = .0586 nm   XI = 375 nm   XB = 104 nm
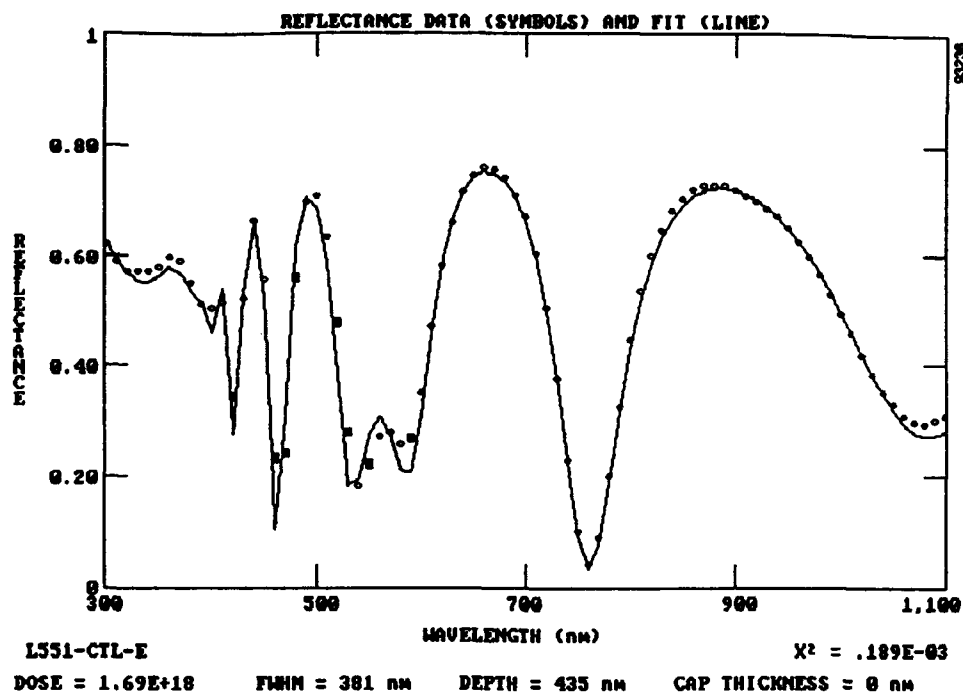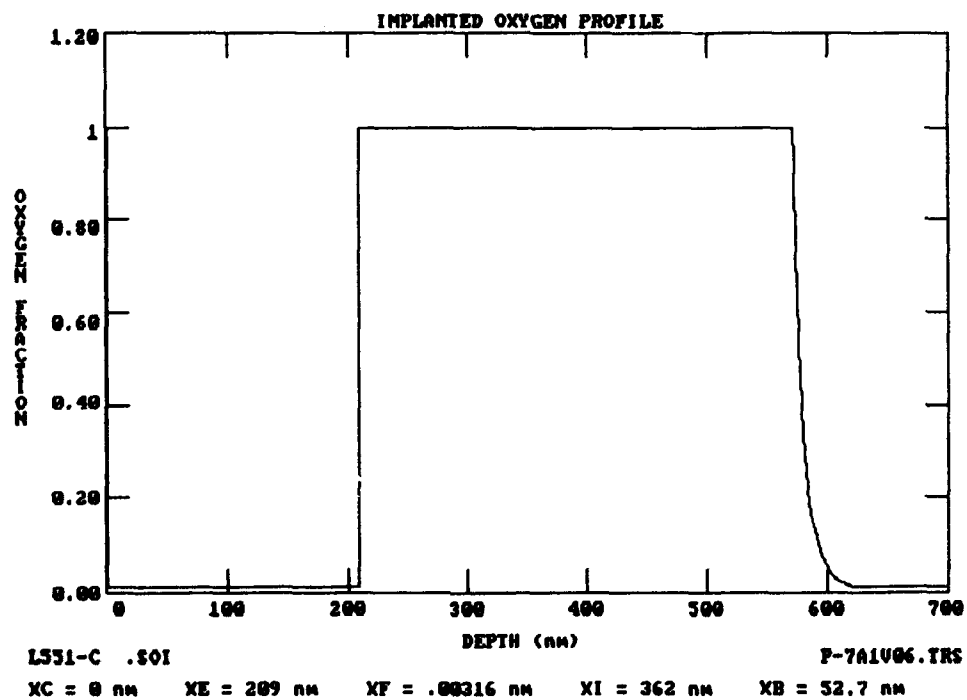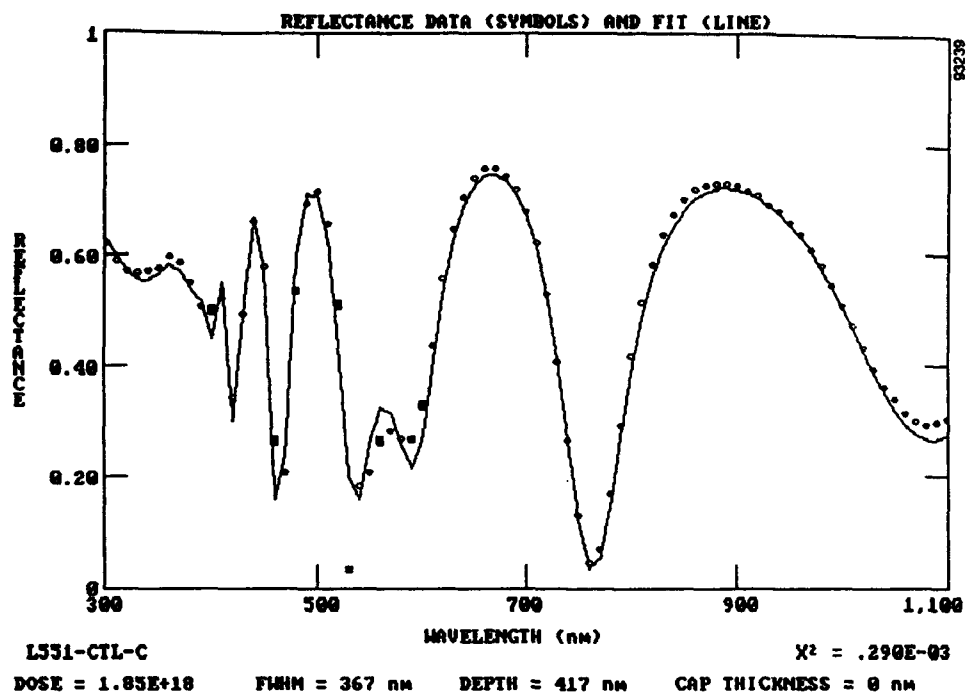
Figure 5-4. *Optical reflectance results measured at the center region of a SOITEC SIMOX wafer indicating an Si top layer 2200Å thick and a buried SiO_2 layer 3750Å thick.*
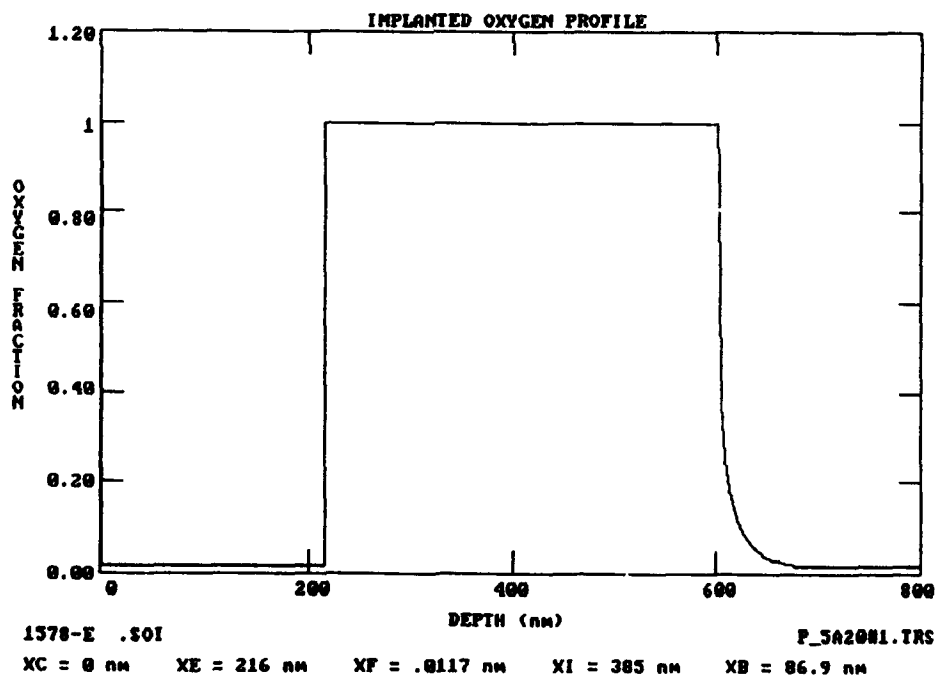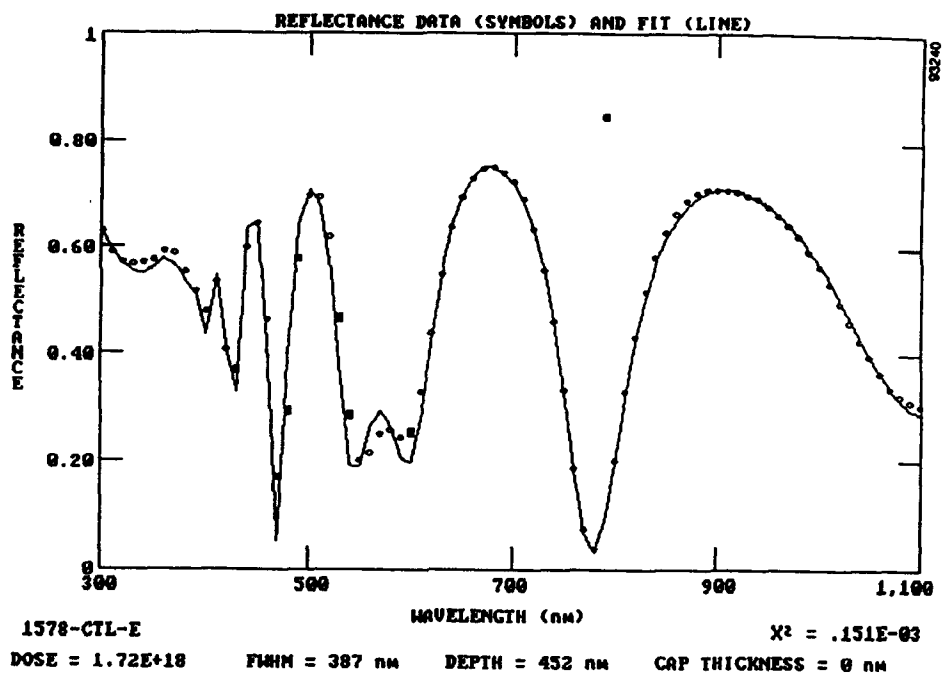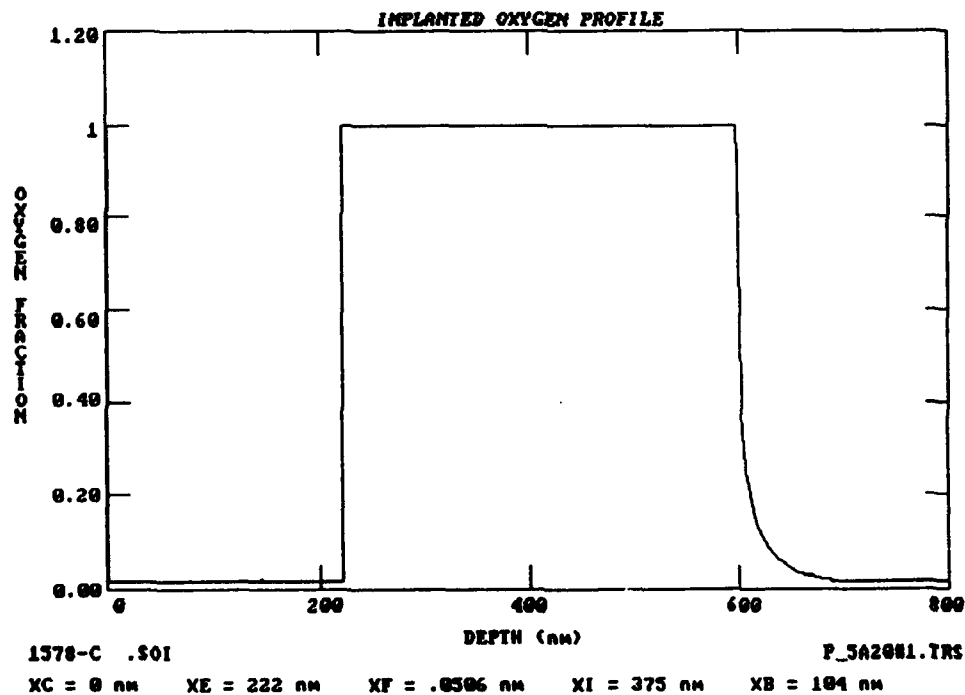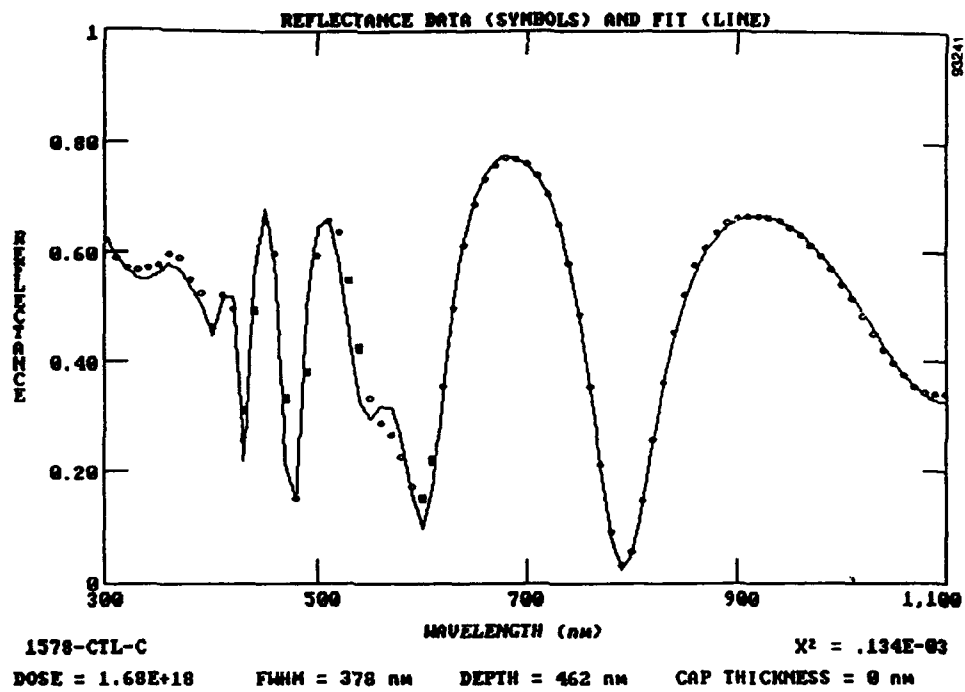
64

SECTION 6

DEVICE CHARACTERIZATIONS AND RESULTS

The material provided in this section was provided to Spire by the subcontractor (Department of Electrical Engineering and Computer Science at Massachusetts Institute of Technology, Cambridge, Massachusetts) under the supervision of Professor James Chung.

As indicated previously, SOI n-MOSFETs suffer from parasitic bipolar effects such as low break-down voltage,[18] amplification of GIDL (gate-induced-drain-leakage),[19] and back-channel off-state leakage which are caused by trapped positive charges in the buried oxide. These charges may originate from factors such device processing, hot-carrier degradation, and/or exposure to radiation-intensive environments.[18] Previous work has demonstrated the use of the DSFET (dual source SOI MOSFET) structure to eliminate the effects of the parasitic BJT.[20]

In this program, we have demonstrated a simple and well-controlled technique of channel defect engineering based on implanting Ge into SOI device channels to degrade the minority carrier lifetime killer and thus reduce the parasitic bipolar effect and improve the source-to-drain breakdown voltage. Furthermore, we have shown that Ge implantation creates Si structural defects in the back interface region which reduces the back channel off-state leakage and improves the radiation hardness of the device.

The success of the Ge-implantation technique requires that defect states be introduced at the back Si-SiO$_2$ interface without degrading the front channel Si quality. Figure 6-1 shows an XTEM micrograph of a SIMOX wafer implanted with a dose of 5×10^{15} Ge$^+$/cm^2 at 120 keV and annealed for 30 minutes at 850°C to form end-of-range damage dislocation loops near the buried SiO$_2$ interface while retaining a high quality Si layer near the surface for device fabrication.[21] The superimposed RBS profile of the implanted Ge in the Figure indicates the Ge dopant distribution from the front to back interface.

The following subsections summarize the work performed and results obtained by the MIT group for the Phase II devices before and after exposure to ionizing radiation. The radiation experiments were performed at the Rome Air Development Center, Hanscom Air Force Base, Massachusetts, with the permission and under the supervision of Dr. Walter Shedd.

6.1 PRE-IRRADIATION EXPERIMENTS AND RESULTS.

6.1.1 Improvement of Breakdown Voltage by Ge Implantation.

Our results indicate that due to the recombination centers introduced by the Ge dopants and defect states, all parasitic bipolar effects in SOI MOSFETs are reduced in the Ge-implanted devices. Figure 6-2 shows the suppression of bipolar gain in H-gate devices with the Ge-implant. The body is boron doped at 1.5×10^{15} cm^{-3} and the body tie serves as the base contact. Both front and back gates are biased at -2 V to insure that both interfaces are in accumulation mode and the field-effect component in I_c is eliminated.[22]

65

932677
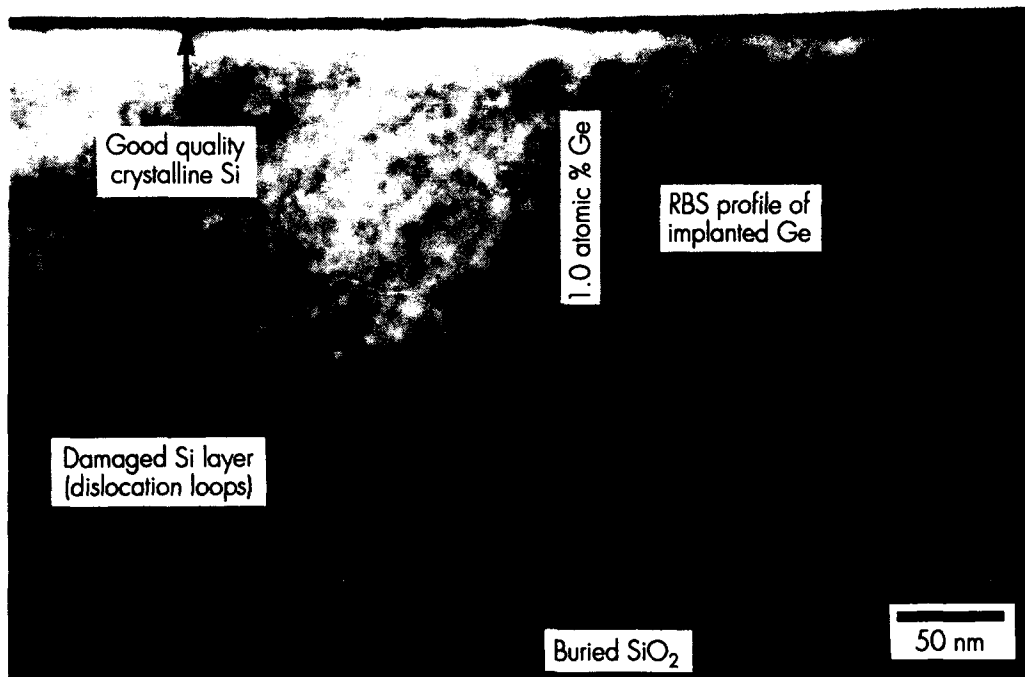
Figure 6-1. *XTEM micrograph and RBS profile of Ge in SIMOX wafer implanted with a dose of 5 x 10^{15} Ge$^+$/cm^2 at 120 keV and annealed for 30 minutes at 850°C.*

Figure 6-2. *Gummel plots for lateral SIMOX NPN BJTs (H-gate structures) with and without Ge-implant, $V_{GSf} = V_{GSb} = -2$ volts. The Ge was implanted with a dose of 5x10^{15} Ge$^+$/cm^2 implantation at 120 keV and the samples were annealed at 950°C for 30 minutes.*

66

As shown in Figure 6-3, the breakdown voltage is improved in the Ge implanted SIMOX devices compared with the ones without the Ge-implant. The source to drain breakdown voltage for SOI devices is defined at 2 mS output conductance and $V_{GS,f} = V_{T,f}$ while back gate is grounded. For bulk devices, the breakdown voltage definition remains the same except $V_{GS,f} = V_{T,f} + 2V$.
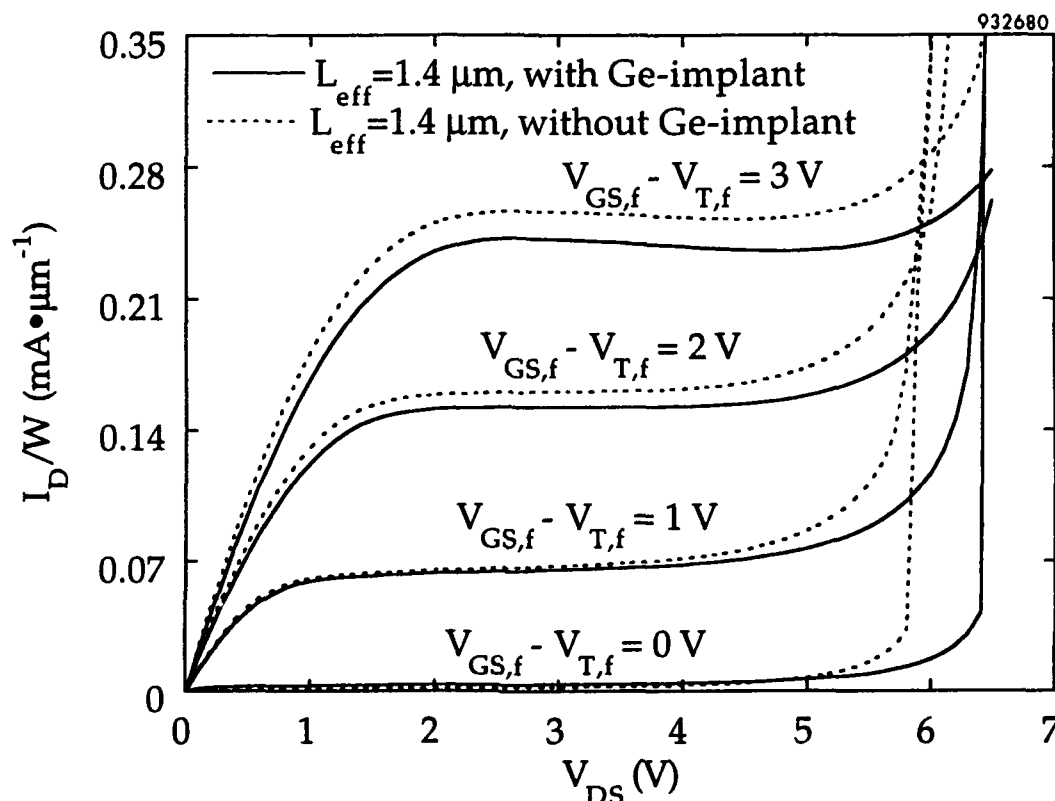
Figure 6-3. *Breakdown voltage improvement in SIMOX SOI n-MOSFETs due to Ge implantation ($5x10^{15}$ Ge^+/cm^2 at 150 keV, annealed at 950°C), $V_{GS,b} = 0$ volts.*

The channel-length-dependent improvement in breakdown voltages of both SOI devices and bulk controls is shown in Figures 6-4 and 6-5, respectively. Given th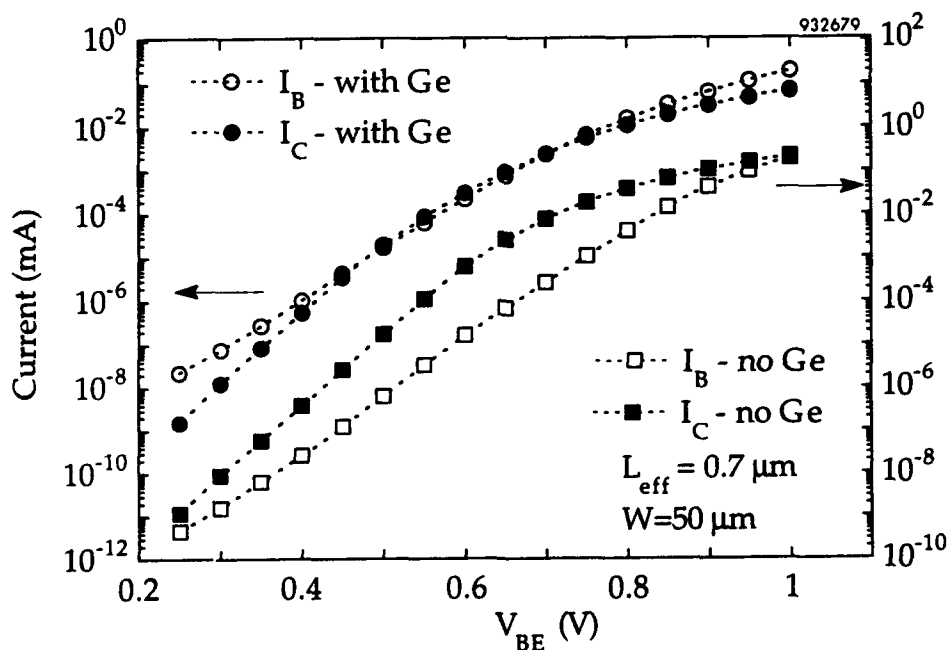e same reduction in the electron diffusion length, the amount of breakdown voltage improvement increases with increasing L_{eff}, as expected from open-base bipolar breakdown theory. For L_{eff} less than 0.5 μm, punch-through rather than bipolar breakdown dominates in bulk devices, as seen in Figure 6-5. The improvement in breakdown voltage with different Ge-implant technologies is shown in Figure 6-6, which indicates an optimal Ge-implant condition of 5 x 10^{15} cm^{-2} at 120 keV, annealed at 950°C.

Our studies show that GIDL is also suppressed in SOI devices with the Ge-implant, as shown in Figure 6-7. This improvement results because the gate-to-drain overlap area is smaller due to retarded arsenic diffusion in the Ge-implanted Si. The parasitic bipolar effect in GIDL is reduced because of the lower bipolar gain of Ge-implanted samples.
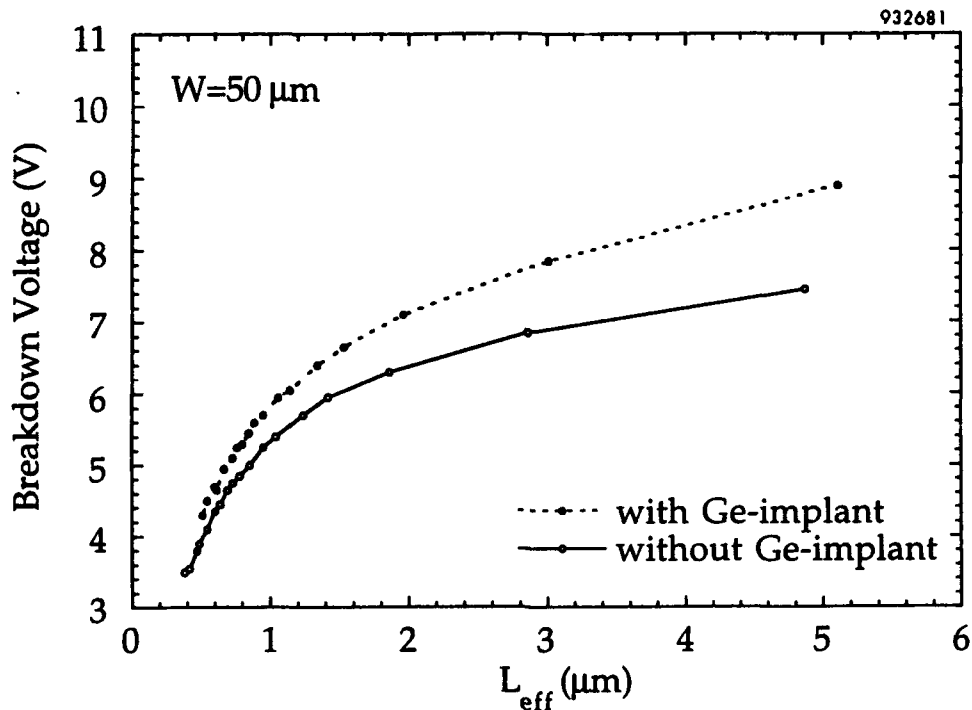
Figure 6-4. *Channel length-dependent breakdown voltage improvement in SIMOX SOI n-MOSFETs due to Ge implantation with a dose of 5 x 10^{15} Ge$^+$/cm^2 at 120 keV and annealing at 950°C.*
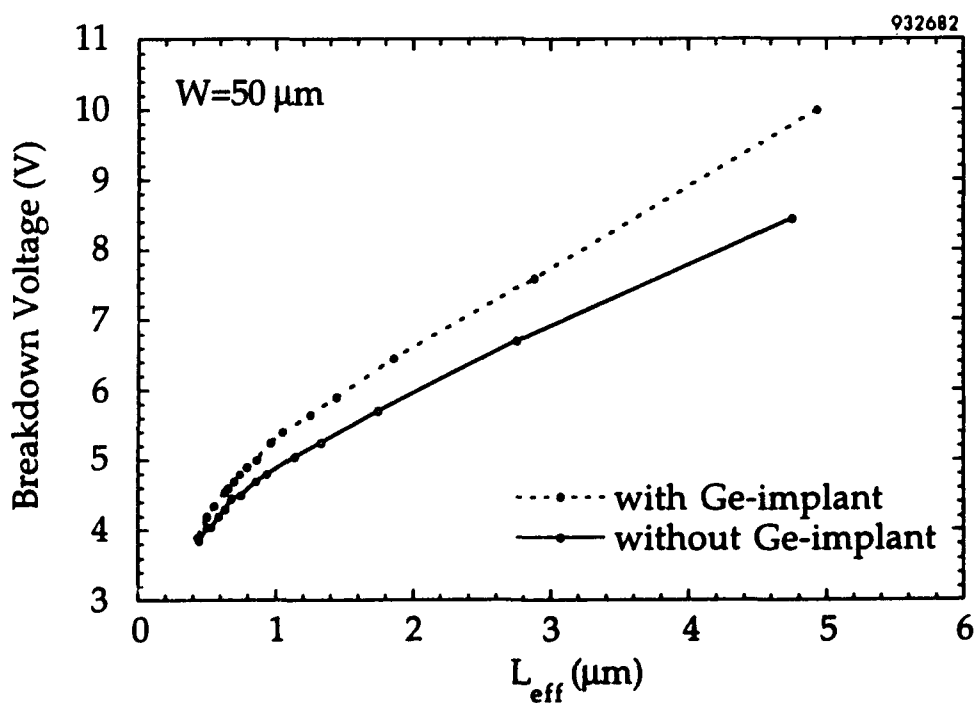
Figure 6-5. *Channel length-dependent breakdown voltage improvement in bulk n-MOSFETs due to Ge implantation with a dose of 5 x 10^{15} Ge$^+$/cm^2 at 150 keV and annealing at 950°C.*
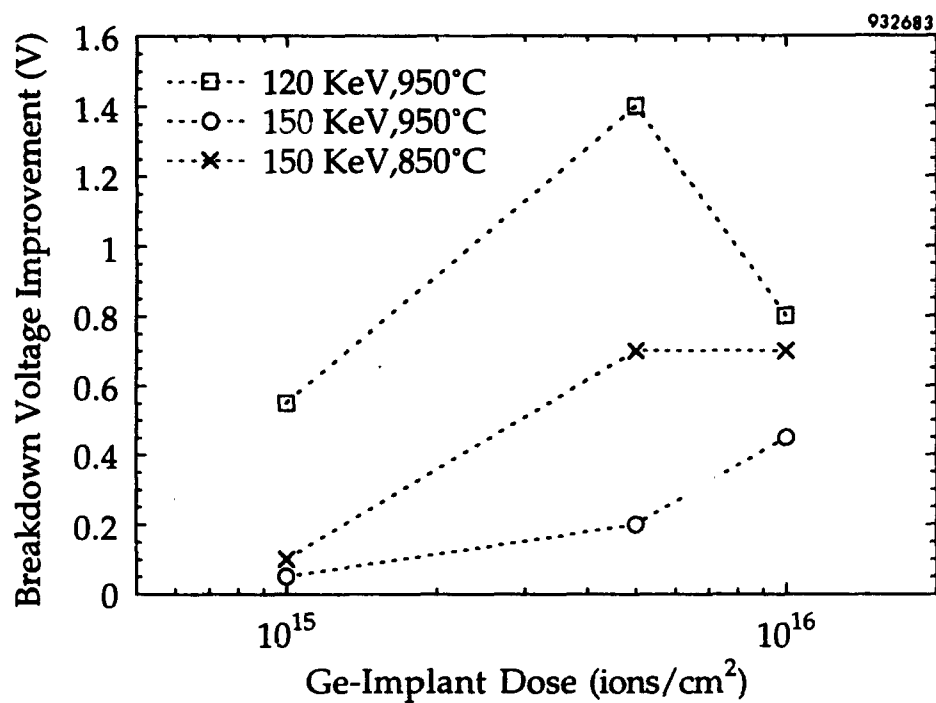
Figure 6-6. *Breakdown voltage improvement in SIMOX n-MOSFETs implanted with Ge and annealed under different conditions.*
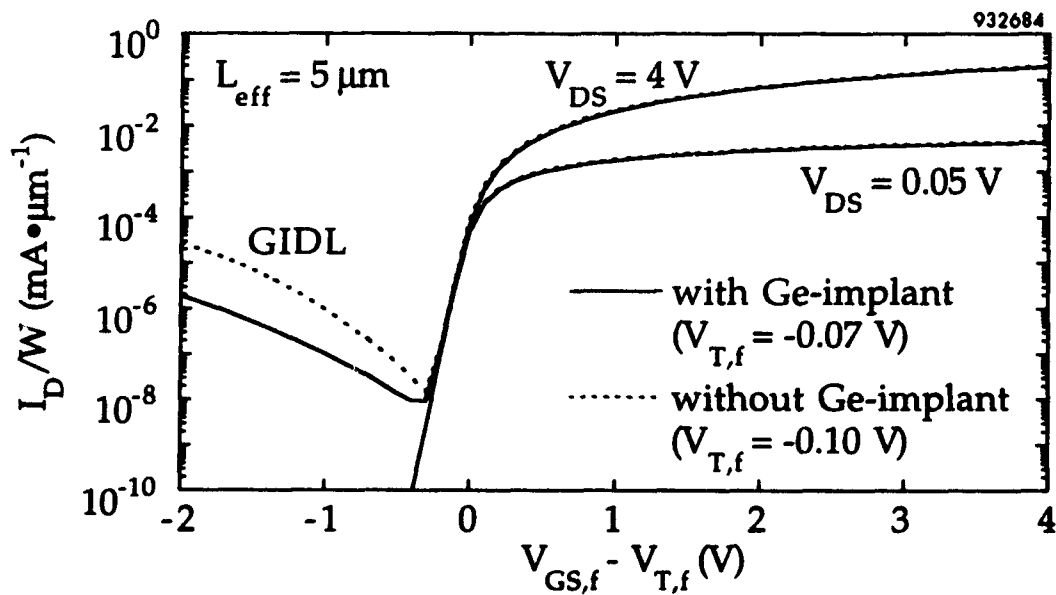
Figure 6-7. *Comparison of front channel performance in samples with and without Ge implantation (5 x 10^{15} Ge⁺/cm² at 120 keV, ann. at 950°C, with $V_{GS,b} = 0$ V).*

69

6.1.2 Off-State Leakage Improvement by Ge Implantation.

The defect states introduced at the back Si=SiO$_2$ interface region by Si structural defects and possible migrated Ge dopants can pin the Fermi level in the back interface region, as illustrated in Figure 6-8. For partially-depleted devices, positive back gate bias or trapped holes in the buried oxide can be initially supported by space charge formed by the ionized defect states. Further increase in the back bias or the amount of trapped holes will eventually cause band bending and back-channel inversion. As a result, the back-channel threshold-voltage (when the front-channel is biased in accumulation) is increased. For both partially- and fully-depleted devices with the Ge-implant, suppressed bipolar effects from impact ionization and reduced back channel mobility from Si-structural defects and Ge-related scattering also contribute to the overall reduction of back-channel leakage current. Indeed, the off-state leakage current is substantially suppressed, as shown in Figure 6-9. For fully-depleted devices, however, back-channel V$_T$ remains unchanged because the body effect does not change with doping, including the Ge-implantation.[2]
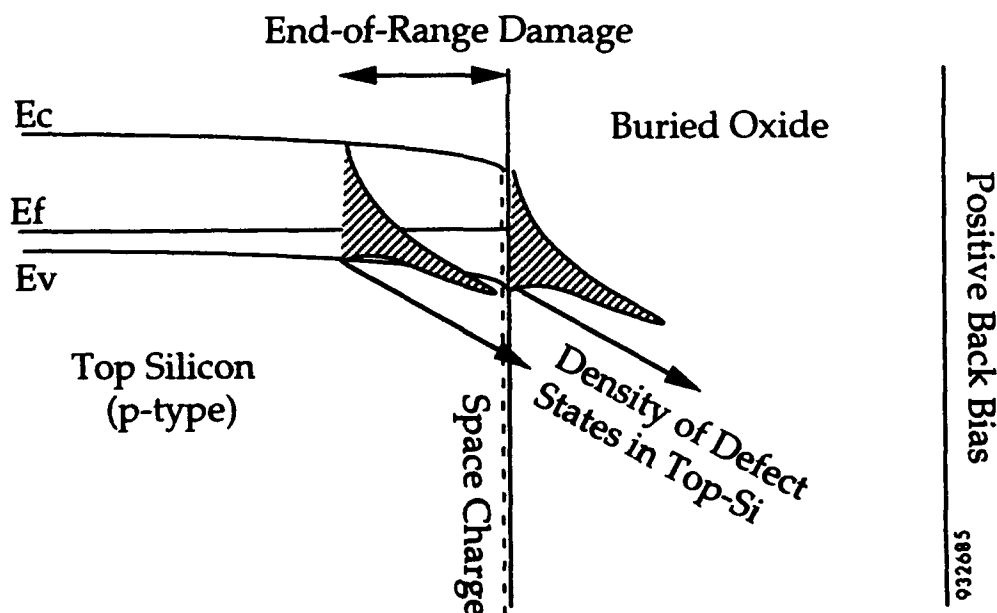
Figure 6-8. *Energy band diagram illustrating the back interface Fermi level pining in SIMOX SOI structures.*

70
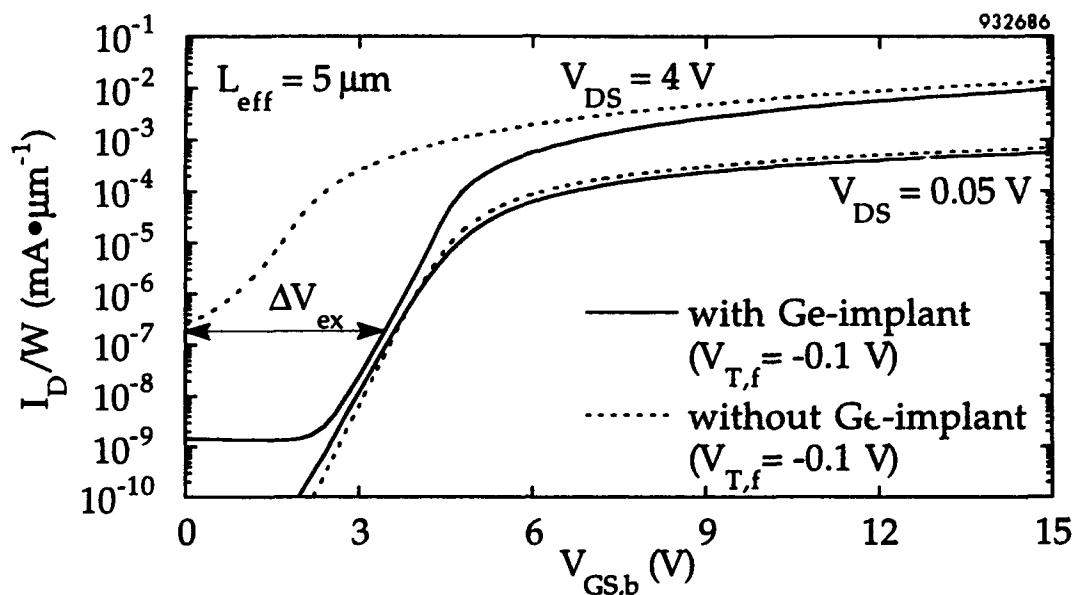
Figure 6-9. *Back channel leakage reduction in SIMOX devices due to Ge implantation ($5x10^{15}$ Ge^+/cm^2 at 120 keV, annealed at 950°C, $V_{GS,f}$).*

Also indicated in Figure 6-9, compared with non-implanted SOI devices, devices with Ge-implantation can sustain an extra back bias ($V_{ex}\Delta$) beyond the zero back bias condition. This extra back bias can be viewed to represent the total extra positive charge sustainable by the device due to trapped holes in the buried oxide. Shown in Figure 6-10, is ΔV_{ex} for different Ge-implant technologies. To achieve the largest ΔV_{ex}, an optimal Ge-implant condition of 5 x 10^{15} Ge^+/cm^2 dose at 120 keV annealed at 950°C is necessary. Notice this optimal Ge-implant condition is the same as that required for the greatest breakdown voltage improvement shown in Figure 6-6. The similar bell-shaped trend in both Figure 6-10 and Figure 6-6 indicates the important role played by the Si defect states created during the Ge-implant. A lower implant energy results in a larger volume of Si defects between the Ge-implant end-of-range and the buried oxide because the threading dislocations are terminated at the strain-induced interfaces ($SiGe/Si$ and Si/SiO_2). A smaller thermal cycle, using lower recrystallization temperatures will retain more Si defect structures. All these effects are observable in Figures 6-6 and 6-10.

Figure 6-10. *Extra back bias levels resulting from Ge⁺ implantation with different dose, energy, and annealing temperature (V_{GSf} = -0.8V).*

6.1.3 Further Evaluation of the Ge-Implant Technology.

It is important that the Ge-implant-induced damage in the channel does not change the body effect of the front threshold voltage. As seen in Figure 6-11, th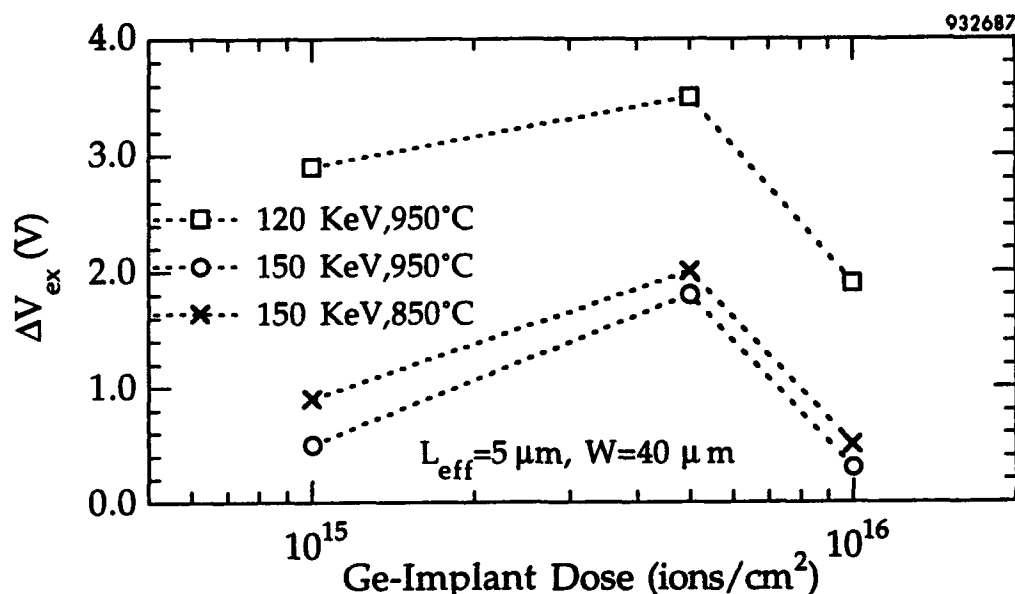e front threshold voltage with back bias remains unchanged by the Ge-implant for fully-depleted SOI devices. The front channel subthreshold slope also remains the same in SOI devices with the Ge-implant compared with the non-implanted ones, as shown in Figure 6-7.

Finally, it is also important that the optimal Ge-implant technology does not significantly degrade the front-channel current-drive. Shown in Figure 6-12 are the extreme cases of SOI front-channel μ_{eff} (effective mobility) degradation due to the Ge-implant, compared with μ_{eff} in a corresponding bulk n-MOSFET without the Ge-implant. The mobility was measured using a procedure in which the channel normal field E_{eff} is compensated with a non-zero field at the back interface for SOI devices.[23] Front-channel low- and high-field mobility degradation are shown in Figures 6-13 and 6-14, respectively, for different Ge-implant technologies. Low-field mobility is observed to be more sensitive to the particular Ge-implant conditions indicating that impurity (Ge) scattering is the major cause for μ_{eff} degradation. Indeed, this point is consistent with the overall μ_{eff} degradation trend observed in Figures 6-13 and 6-14. Higher Ge doses, lower implant energies (with resulting shorter projection ranges), and higher annealing temperatures (which broaden the Ge profile) result in more Ge dopants near the front-channel thus produce more μ_{eff} degradation in the front channel.

L_{eff}=5 μm, w=40 μm

with Ge-implant

without Ge-implant

$V_{T,f}$ (V)

$V_{GS,b}$ (V)
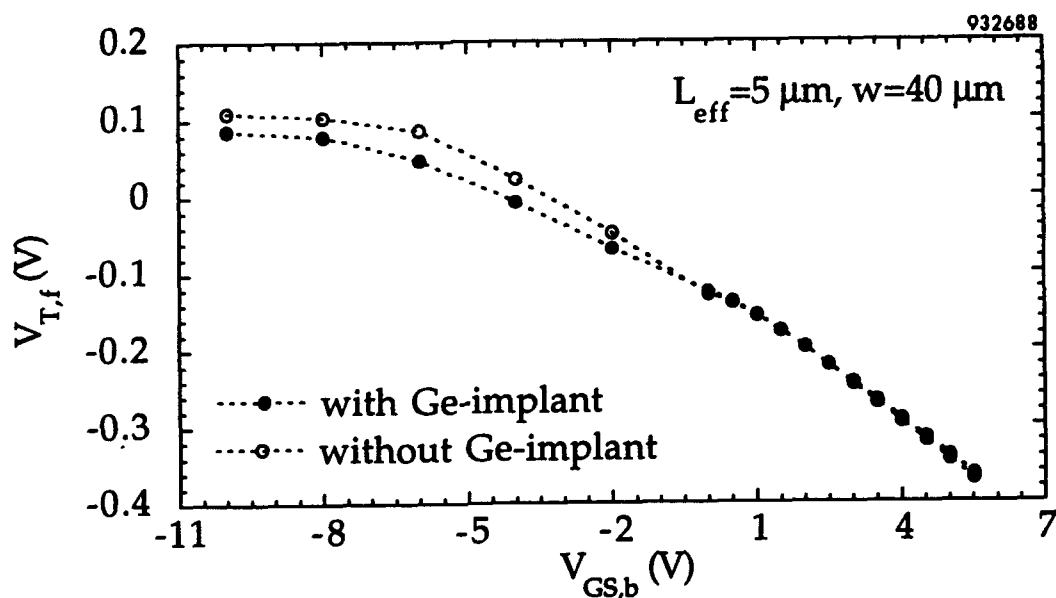
Figure 6-11. *Impact of Ge-implantation (5x10^{15} Ge$^+$/cm^2 at 150 keV and annealed at 950°C on front channel threshold voltage (V$_{Tf}$) body effect in SIMOX devices.*

SOI, with Ge-implant
10^{16} cm^{-2}/120 Kev/950°C
SOI, with Ge-implant
10^{15} cm^{-2}/150 Kev/850°C

Bulk, no Ge
SOI, no Ge

μ_{eff} (cm^2•v^{-1}•sec^{-1})

E_{eff} (MV/cm)

Figure 6-12. *Extreme degradation cases of front-channel μ$_{eff}$ versus channel effective normal field due to Ge-implant.*
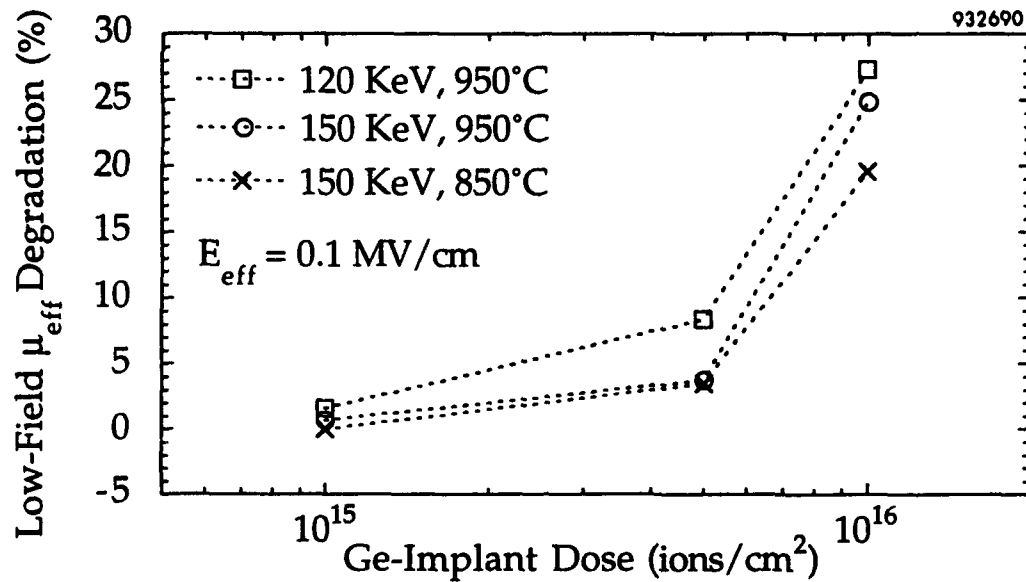
Figure 6-13. *Front-channel low-field mobility degradation resulting from Ge implantation into SIMOX and annealing at different conditions.*
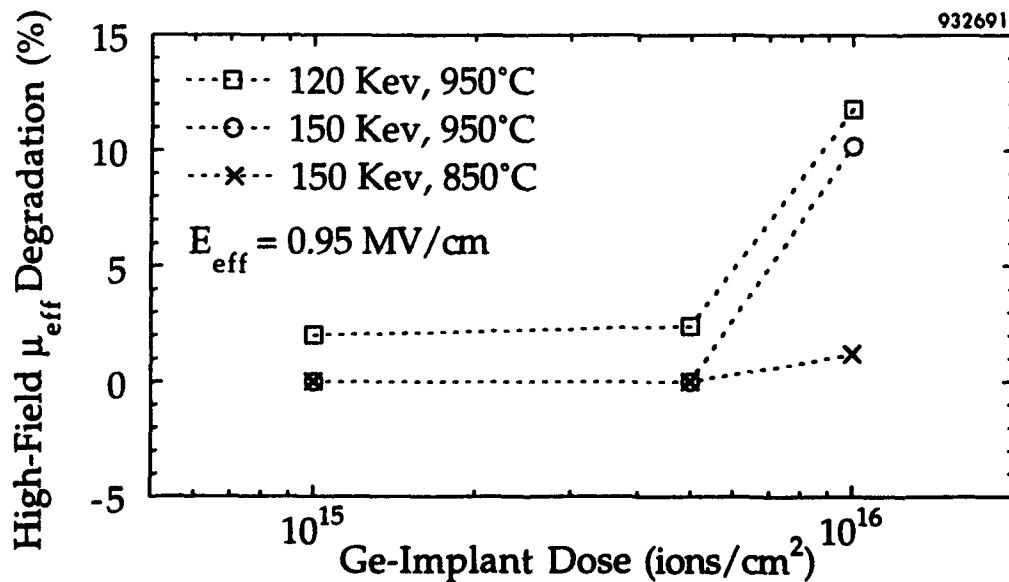
Figure 6-14. *Front-channel high-field mobility degradation resulting from Ge implantation into SIMOX and annealing at different conditions.*

74

6.2 POST-IRRADIATION EXPERIMENTS AND RESULTS.

6.2.1 Results from Testing Fully-Depleted Edge-Less Devices.

As discussed in Sections 6.1.2 and 6.1.3, the body effect remains unchanged for fully-depleted devices. Therefore after radiation, the shift of back-channel threshold voltage is the same for Ge-implanted SOI devices and non-implanted ones. However, the reduced bipolar effect and back-channel mobility degradation effect in off-state leakage can still be observed after irradiation. Figures 6-15a and 6-15b show the pre-irradiation back-channel subthreshold characteristics for Ge-implanted and non-implanted fully-depleted SIMOX devices. Both devices have a b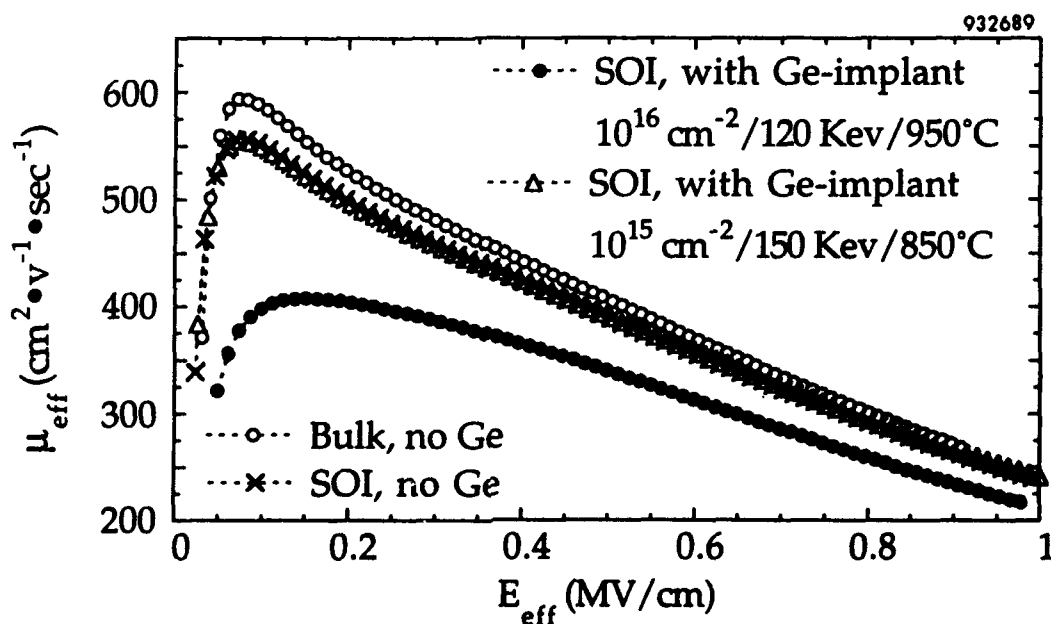ack-channel V_T value of about 3V (germanium implantation has little influence on the body effect). Figures 6-16a and 6-16b show the post-irradiation (100 Krad) changes of back threshold voltage and off-state leakage. As seen, the amount of back-channel V_T shift is the same for both Ge-implanted and non-implanted devices because the same amount of holes are trapped in buried oxide and device regions. But, the off-state leakage at $V_{DS} = 4V$ is almost three orders of magnitude less at $V_{sub} = V_{T,b}$, for Ge-implanted devices. Notice the large shift in $V_{T,b}$ resulting from the 4V bias on back gate during irradiation which pushes the trapped holes to the back interface.

6.2.2 Results from Partially-Depleted Edge-Less Devices.

For partially-depleted devices, the Ge-implanted SIMOX devices always showed higher back-channel V_T due to the back-interface Fermi level pinning effect discussed in Section 6.1.2. This effect still exists after the irradiation. Pre-irradiation subthreshold characteristics for partially-depleted Ge-implanted and non-implanted SIMOX devices are shown in Figures 6-17a and Figure 6-17b. The starting $V_{T,b}$ values for Ge-implanted and non-implanted devices were 3.3V, and 2.4V, respectively. After 170 Krad X-ray irradiation, a 4V shift in $V_{T,b}$ was observed in both devices, thus preserving the higher $V_{T,b}$ value for the Ge-implanted device. Off-state leakage reduction effect is also retained after the irradiation for Ge-implanted devices, as shown in Figure 6-18. The back gate bias was 0V during radiation, so trapped holes in the buried oxide were not concentrated at the back interface region, resulting in a much smaller shift in $V_{T,b}$ compared with the shift described in Section 6.2.1.

6.3 SUMMARY OF RESULTS.

In conclusion, we have demonstrated channel defect engineering in SIMOX SOI and bulk Si devices using Ge-implantation in order to suppress parasitic bipolar effects and to reduce off-state leakage, and have discussed the physical mechanisms involved in this simple and well-controlled technique.

Figure 6-15. *Comparison of pre-irradiation subthreshold characteristics of fully-depleted SIMOX devices a) with, and b) without the Ge implantation (L_{eff}=5 μm and W=40μm).*

Figure 6-16. *Comparison of post-irradiation, 100 Krads (Si), back-channel V_T vs. leakage current plots for fully-depleted SIMOX devices a) with, and b) without Ge implantation (V_{Gf}=-0.8V, V_{sub}, or V_{Gb}=4V during irradiation).*

77
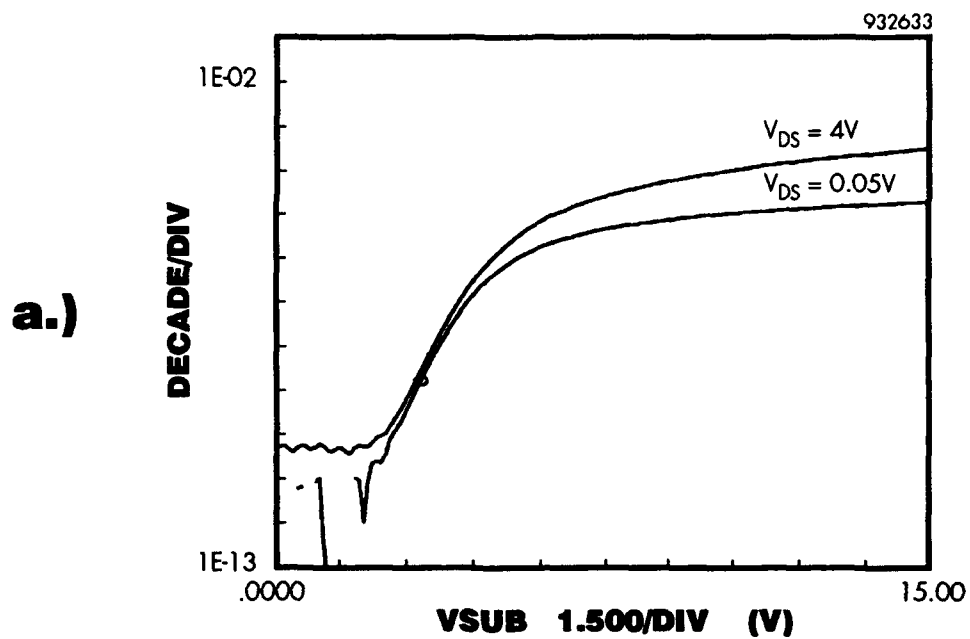
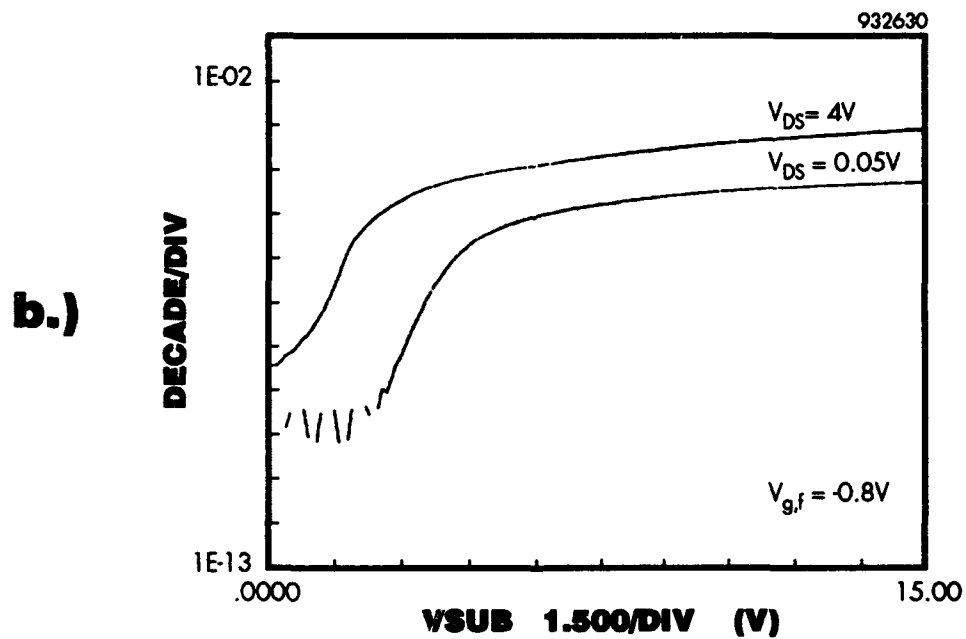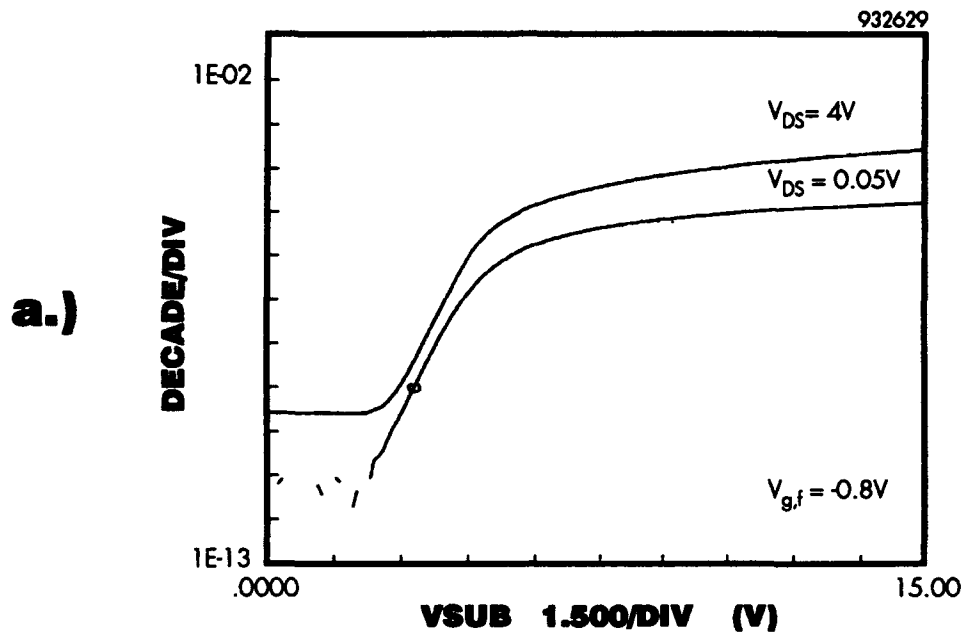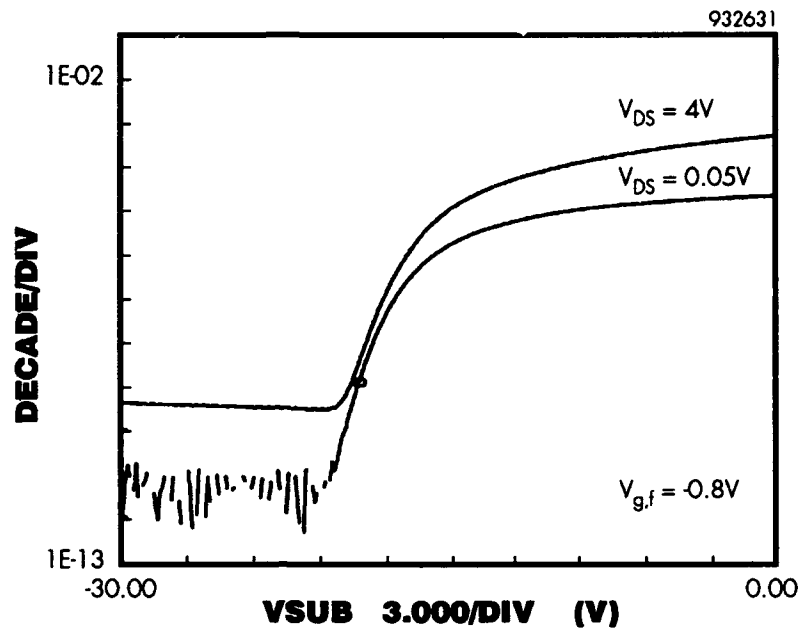**Figure 6-17.** *Comparison of pre-irradiation subthreshold characteristics of partially-depleted SIMOX devices a) with, and b) without the Ge implantation (L_{eff}=5 μm, and W= 40 μm).*
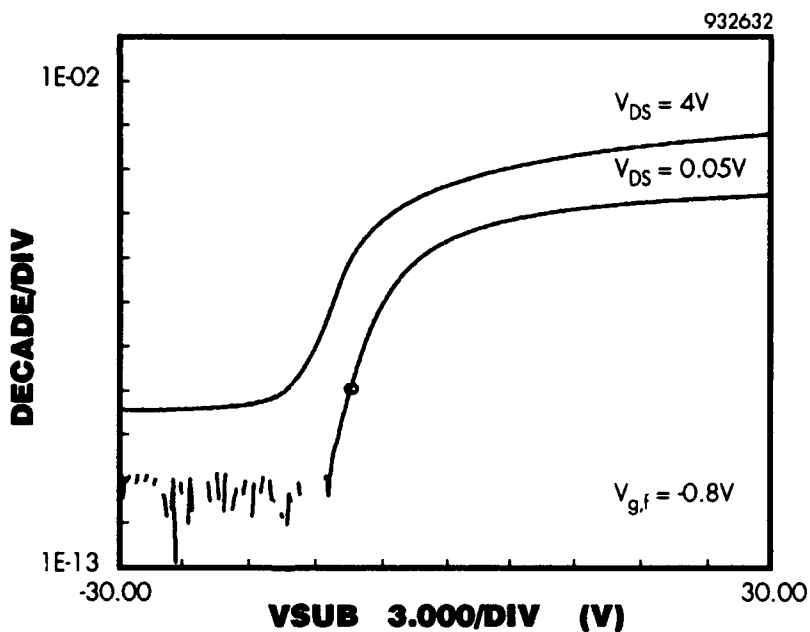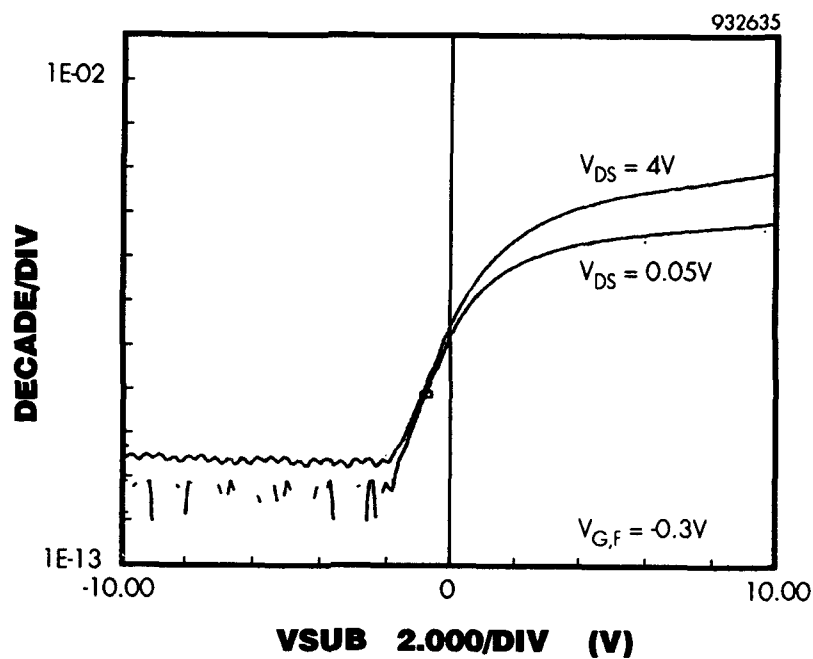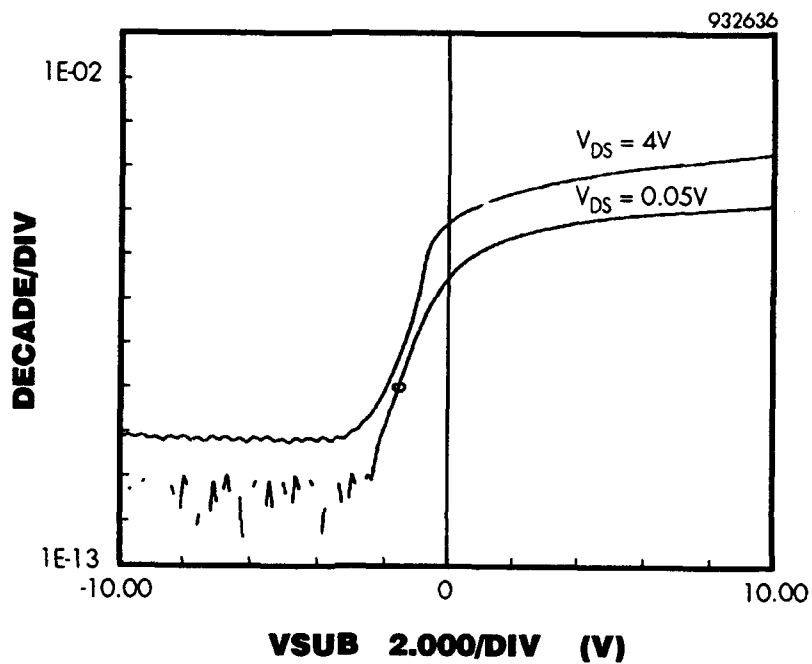
Figure 6-18. *Comparison of post-irradiation, 170 Krads (Si), back-channel V_T vs. leakage current plots for partially-depleted SIMOX devices a) with, and b) without Ge implantation (V_{G_f}=-0.3V, V_{sub}=0V during irradiation).*
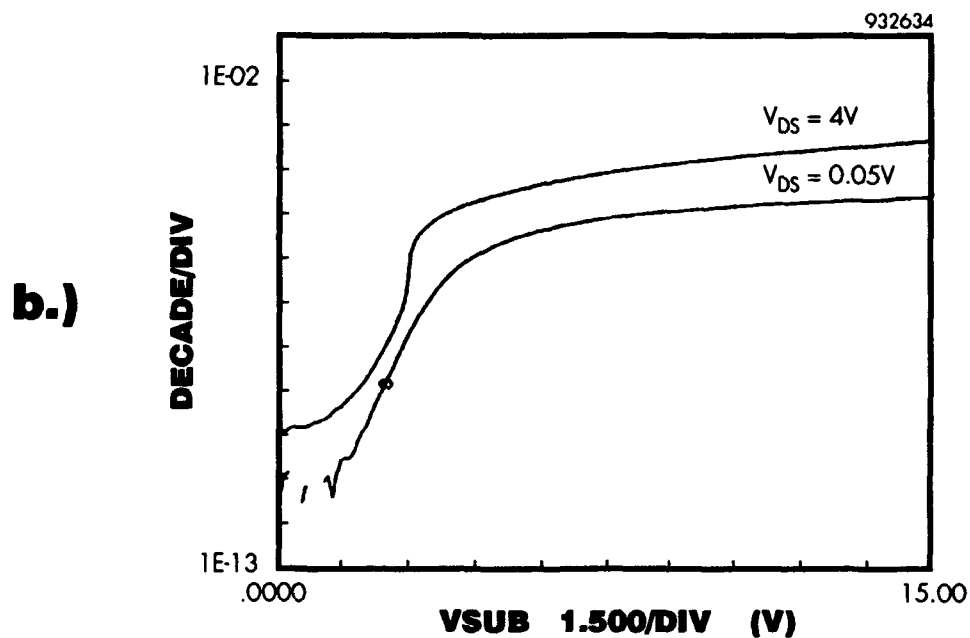
79

SECTION 7

CONCLUSIONS

In this program we demonstrated the improvement of the crystalline quality of the Si top layer and the degradation of Si at the Si/buried SiO_2 interface for SIMOX wafers implanted with Ge. Improving the crystalline quality of the surface region is essential for high performance device fabrication. In addition, degradation of the Si/buried SiO_2 interface region significantly reduces back channel leakage current in devices exposed to ionizing radiation.

In order to demonstrate applications of Ge-implantation into SIMOX, we have fabricated n-MOSFET devices on SIMOX and Si, with and without Ge implantation. No degradation in device performance was observed for devices fabricated on SIMOX substrates implanted with Ge, as compared to substrates without Ge implantation. Our results clearly indicate that off-state leakage and parasitic bipolar effects were reduced in the Ge-implanted SIMOX substrates. Electrical testing was also performed before and after irradiation of devices at 100 krad X-ray at RADC. Our electrical testing after irradiation shows that off-state leakage current for devices fabricated on SIMOX with Ge implantation was about 1000 times less than that for devices fabricated on SIMOX without Ge implantation. Lastly, our results indicate that Ge implantation into SIMOX resulted in the suppression of the gate-induced drain leakage of n-MOSFETs and the the source-to-drain voltage was significa ly improved.

SECTION 8

REFERENCES

1. B.Y. Tsaur, "SOI Technologies: Device Applications and Future Prospects" (U), Lincoln Labs., MIT (Lexington, MA), *Mat. Res. Soc. Symp. Proc.* **35**, 641 (1985). (Unclassified).

2. G.K. Celler, P.L.F. Hemment, K.W. West, and J.M. Gibson, "High Quality Si-on-SiO$_2$ Films by Large Dose Oxygen Implantation and Lamp Annealing" (U), AT&T Bell Labs. (Murray Hill, NJ), *Appl. Phys. Lett.* **48** (8), 532 (24 February 1986). (Unclassified).

3. B.Y. Mao, P.H. Chang, H.W. Lam, B.W. Shen, and J.A. Keenan, "Microstructure of High-Temperature Annealed Buried Oxide Silicon-on-Insulator" (U), Texas Instruments (Dallas, TX), *Appl. Phys. Lett.* **48** (12), 794 (24 March 1986). (Unclassified).

4. S.S. Lau, S. Matteson, J.W. Mayer, P. Revesz, J. Gyulai, J. Roth, T.W. Sigmon, and T. Cass, "Improvement of Crystalline Quality of Epitaxial Si Layers by Ion-implantation Techniques" (U), California Institute of Technology (Pasadena, CA), *Appl. Phys. Lett.* **34** (1), 76 (1 January 1979). (Unclassified).

5. W.E. Ham, M.S. Abrahams, C.J. Buiocchi, and J. Blanc, "Direct Observation of the Structure of Thin, Commercially Useful Silicon on Sapphire Films by Cross Section Transmission Electron Microscopy" (U), RCA Labs., David Sarnoff Research Center (Princeton, NJ), *J. Electrochem. Soc.* **124** (4), 634 (April 1977). (Unclassified).

6. H. Beneking, P. Narozny, N. Emeis, and K.H. Goetz, "Reduction of Dislocations in GaAs and InP Epitaxial Layers by Quasi Ternary Growth and its Effect on Device Performance" (U), Institute of Semiconductors Electronics, Aachen Technical Univ. (Aachen, Germany), *J. Electronic Materials* **15** (4), 247 (July 1986). (Unclassified).

7. Dale Hill, Phil Fraundorf, and Gail Fraundorf, "The Reduction of Dislocations in Oxygen Implanted Silicon-on-Insulator Layers by Sequential Implantation and Annealing" (U), Monsanto Electronic Materials Co. (St. Peters, Missouri), *J. Appl. Phys.* **63** (10), 4933 (15 May 1988). (Unclassified).

8. Tom F. Cheek, Jr., and Daniel Chen, "Dislocation Reduction on SIMOX Substrates by Using Multiple Implants" (U), Texas Instruments Inc. (Dallas, TX), in Silicon-on-Insulator and Buried Metals in Semiconductors, eds. J.C. Sturm, C.K. Chen, L. Pfeiffer, and P.L.F. Hemment, *Mat. Res. Soc. Symp. Proc.* **107**, 53 (1987). (Unclassified).

9. J. Margail, J. Stoemenos, C. Jaussaud, and M. Bruel, "Reduced Defect Density in Silicon-on-Insulator Structures Formed by Oxygen Implantation in Two Steps" (U), Centre d'Etudes Nucleaires de Grenoble (France), *Appl. Phys. Lett.* **54** (6), 526 (6 February 1989). (Unclassified).

10. Fereydoon Namavar, Elisabetta Cortesi, and Piran Sioshansi, "Recent Advances in SIMOX Defect Reduction and Novel Structures" (U), Spire Corporation (Bedford, MA), in Selected Topics in Electronic Materials, eds. B.R. Appleton, D.K. Biegelsen, W.L.

Brown, and J.A. Knapp, (*Mat. Res. Soc. Extended Abstract*, Pittsburg, PA, 1988), 109. (Unclassified).

11. Fereydoon Namavar, Elisabetta Cortesi, and Piran Sicshansi, "Low Defect, High Quality SIMOX Produced by Multiple Oxygen Implantation with Substoichiometric Total Dose" (U), Spire Corporation (Bedford, MA), *Mat. Res. Soc. Symp. Proc.* **128**, 623 (1989). (Unclassified).

12. Bobby L. Buchanan, Donald A. Neamen, and Walter M. Shedd, "SOS Device Radiation Effects and Hardening" (U), Rome Air Dev. Ctr. (Hanscom AFB, MA), *IEEE Trans. Electron Devices* **ED-25** (8), 959 (August 1978). (Unclassified).

13. Bobby L. Buchanan, "Chapter 32: Radiation Effects and Radiation-Hardening of VLSI Circuits" (U), Rome Air Development Center (Hanscom AFB, MA), pp. 565-579 in VLSI Handbook, ed. Norman G. Einspruch (Academic Press, Inc., Orlando, FL, 1985), 571. (Unclassified).

14. G.E. Davis, L.R. Hite, T.G.W. Blake, C.-E. Chen, H.W. Lam, and R. DeMoyer, Jr., "Transient Radiation Effects in SOI Memories" (U), Naval Research Lab. (Washington DC), *IEEE Trans. Nucl. Sci.* **NS-32** (6), 4432 (December 1985). (Unclassified).

15. J.R. Srour, O.L. Curtis, Jr., and K.Y. Chiu, "Charge Transport Studies in SiO_2: Processing Effects and Implications for Radiation Hardening" (U), Northrop Research and Technology Ctr. (Hawthorne, CA), *IEEE Trans. Nucl. Sci.* **NS-21** (6), 73 (December 1974). (Unclassified).

16. R.C. Hughes, E.P. EerNisse, and H.J. Stein, "Hole Transport in MOS Oxides" (U), Sandia Labs. (Albuquerque, NM), *IEEE Trans. Nucl. Sci.* **NS-22** (6), 2227 (December 1975). (Unclassified).

17. F. Namavar *et al.*, *Mat. Res. Soc. Symp. Proc.*, Vol. 201, p. 337, 1991.

18. J.P. Colinge, Silicon-On-Insulator Technology: Materials to VLSI, Kluwer Academic Publishers, 1991.

19. J. Chen *et al.*, *IEEE Inter. SOI Conf.*, p. 84, 1992.

20. E.P. VerPloeg *et al.*, *IEDM Tech. Dig.*, p. 337, 1992.

21. F. Namavar *et al.*, *Mat. Res. Soc. Symp. Proc.*, Vol. 147, p. 235, 1989.

22. M. Rodder *et al.*, *IEEE Elect. Dev. Lett.*, Vol. EDL-4, no. 6, p. 193, 1983.

23. M.J. Sherony *et al.*, in press, *IEEE Elect. Dev. Lett.*, 1993.

DISTRIBUTION LIST

DEPARTMENT OF DEFENSE

ADVANCED RESEARCH PROJECT AGENCY
    ATTN: ASST DIR ELECTRONIC SCIENCES DIV
    ATTN: R REYNOLDS

ASSISTANT TO THE SECRETARY OF DEFENSE
    ATTN: EXECUTIVE ASSISTANT

DEFENSE ELECTRONIC SUPPLY CENTER
    ATTN: DESC-E

DEFENSE INTELLIGENCE AGENCY
    ATTN: DIW-4
    ATTN: DT-1B

DEFENSE NUCLEAR AGENCY
 2 CY ATTN: IMTS
    ATTN: RAES

DEFENSE SYSTEMS SUPPORT ORGANIZATION
    ATTN: JNGO

DEFENSE TECHNICAL INFORMATION CENTER
 2 CY ATTN: DTIC/OC

DNA PACOM LIAISON OFFICE
    ATTN: DNALO

FIELD COMMAND DEFENSE NUCLEAR AGENCY
    ATTN: FCINI
    ATTN: FCTO
    ATTN: FCTT-T W SUMMA
    ATTN: FCTT DR BALADI

DEPARTMENT OF THE ARMY

ARMY RESEARCH LABORATORIES
    ATTN: AMSRL-WT-NJ
    ATTN: SLCHD-NW-RP
    ATTN: SLCHD-NW-TN

U S ARMY MISSILE COMMAND
    ATTN: AMCPM-HA-SE-M

U S ARMY NUCLEAR & CHEMICAL AGENCY
    ATTN: MONA-NU DR D BASH

U S ARMY RESEARCH OFFICE
    ATTN: R GRIFFITH

U S ARMY SPACE & STRATEGIC DEFENSE CMD
    ATTN: CSSD-SL

U S ARMY STRATEGIC SPACE & DEFENSE CMD
    ATTN: CSSD-SA-E
    ATTN: CSSD-SD-A

U S MILITARY ACADEMY
    ATTN: LTC AL COSTANTINE

USAISC
    ATTN: ASOP-DO-TL

DEPARTMENT OF THE NAVY

NAVAL COMMAND CONTROL & OCEAN
SURVEILLANCE CTR
    ATTN: CODE 250

NAVAL POSTGRADUATE SCHOOL
    ATTN: CODE 52 LIBRARY

NAVAL RESEARCH LABORATORY
    ATTN: CODE 4600 D NAGEL
    ATTN: CODE 4653 A NAMENSON
    ATTN: CODE 6613 A B CAMPBELL
    ATTN: CODE 6813 N SAKS
    ATTN: CODE 6816 H HUGHES

NAVAL SEA SYSTEMS COMMAND
    ATTN: NAVSEA-081 A NEWHOUSE

NAVAL SURFACE WARFARE CENTER
    ATTN: CODE H21 F WARNOCK
    ATTN: CODE H23 R SMITH

NAVAL SURFACE WARFARE CENTER
    ATTN: CODE H-21

NAVAL TECHNICAL INTELLIGENCE CTR
    ATTN: LIBRARY

NAVAL WEAPONS SUPPORT CENTER
    ATTN: CODE 6054 D PLATTETER

NAWCWPNSDIV DETACHMENT
    ATTN: CLASSIFIED LIBRARY

PROGRAM EXECUTIVE OFFICE
    ATTN: AIR-536T

STRATEGIC SYSTEMS PROGRAM
    ATTN: JIM HOWARD SP-23

DEPARTMENT OF THE AIR FORCE

AERONAUTICAL SYSTEMS CENTER
    ATTN: ASD/ENSS

AIR FORCE CTR FOR STUDIES & ANALYSIS
    ATTN: AFSAA/SAI

AIR UNIVERSITY LIBRARY
    ATTN: AUL-LSE

PHILLIPS LABORATORY
    ATTN: PL/VTE
    ATTN: PL/VTEE S SAMPSON

ROME LABORATORY
    ATTN: ESR

USAF ROME LABORATORY TECHNICAL LIBRARY FL2810
    ATTN: RBR

WL/MLPJ BLDG 651
    ATTN: AFWAL/ELE
    ATTN: WRDC/MTE

DEPARTMENT OF ENERGY

DEPARTMENT OF ENERGY
ALBUQUERQUE OPERATIONS OFFICE
    ATTN: NESD

LAWRENCE LIVERMORE NATIONAL LAB
    ATTN: J YEE
    ATTN: G POMYKAL
    ATTN: W ORVIS

LOS ALAMOS NATIONAL LABORATORY
    ATTN: E LEONARD

SANDIA NATIONAL LABORATORIES
    ATTN: DEPT 1332 F SEXTON
    ATTN: L D POSEY DIV 9351
    ATTN: ORG 2146 T A DELLIN
    ATTN: P WINKUR DIV 1332
    ATTN: T F WROBEL DIV 9341
    ATTN: 2140 J WOODARD

OTHER GOVERNMENT

CENTRAL INTELLIGENCE AGENCY
    ATTN: OSWR/NED
    ATTN: OSWR/STD/MTB

DEPARTMENT OF TRANSPORTATION
    ATTN: ARD-350

NASA
    ATTN: CODE 313 V DANCHENKO
    ATTN: CODE 900 E STASSINOPOULOS

NATIONAL INSTITUTE OF STANDARDS & TECHNOLOGY
    ATTN: P ROITMAN

DEPARTMENT OF DEFENSE CONTRACTORS

ADVANCED RESEARCH & APPLICATIONS CORP
    ATTN: R ARMISTEAD

AEROSPACE CORP
    ATTN: A AMRAM
    ATTN: C RICE
    ATTN: D SCHMUNK
    ATTN: G CUEVAS
    ATTN: K G HOLDEN
    ATTN: LEE MENDOSA
    ATTN: N SRAMEK
    ATTN: R KOGA

ALLIED-SIGNAL, INC
    ATTN: DOCUMENT CONTROL

ANALYTIC SERVICES, INC (ANSER)
    ATTN: A HERNDON
    ATTN: A SHOSTAK

BDM FEDERAL INC
    ATTN: D WUNSCH

BOEING CO
    ATTN: D KINGSBURY
    ATTN: D EGELKROUT
    ATTN: ROS WOOD
    ATTN: O MULKEY

BOOZ ALLEN & HAMILTON INC
    ATTN: D VINCENT
    ATTN: L ALBRIGHT

CALIFORNIA INSTITUTE OF TECHNOLOGY
    ATTN: C BARNES

COMPUTER SCIENCES CORP
    ATTN: A SCHIFF

DAVID SARNOFF RESEARCH CENTER, INC
    ATTN: R SMELTZER

E-SYSTEMS, INC
    ATTN: MAIN LIBRARY

EATON CORP
    ATTN: R BRYANT

ELECTRONIC INDUSTRIES ASSOCIATION
    ATTN: J KINN

GENERAL ELECTRIC CO (ASD)
    ATTN: D SWANT
    ATTN: D TASCA
    ATTN: H O'DONNELL
    ATTN: J ANDREWS
    ATTN: J LINNEN
    ATTN: J LOMAN

GENERAL ELECTRIC CO
    ATTN: B FLAHERTY
    ATTN: L HAUGE

GENERAL RESEARCH CORP
    ATTN: A HUNT

HARRIS CORP
    ATTN: N VAN VONNO

HARRIS CORPORATION
    ATTN: E YOST
    ATTN: W ABARE

HONEYWELL INC
    ATTN: C SANDSTROM

HONEYWELL, INC
    ATTN: MS 725-5

HUGHES AIRCRAFT COMPANY
    ATTN: E KUBO

IBM CORP
    ATTN: DEPT L75

IBM CORP
    ATTN: A SADANA

IBM CORP
ATTN: N HADDAD

INSTITUTE FOR DEFENSE ANALYSES
ATTN: TECH INFO SERVICES

JAYCOR
ATTN: D WALTERS

JAYCOR
ATTN: CYRUS P KNOWLES
ATTN: R SULLIVAN

JAYCOR
ATTN: R POLL

JOHNS HOPKINS UNIVERSITY
ATTN: R MAURER

KAMAN SCIENCES CORP
ATTN: DASIAC

KAMAN SCIENCES CORPORATION
ATTN: DASIAC
ATTN: R RUTHERFORD

KEARFOTT GUIDANCE AND NAVIGATION CORP
ATTN: J D BRINKMAN

LITTON SYSTEMS INC
ATTN: F MOTTER

LOCKHEED MISSILES & SPACE CO, INC
ATTN: TECHNICAL INFORMATIION CENTER

LOCKHEED MISSILES & SPACE CO, INC
ATTN: E HESSEE
ATTN: G LUM ORG 81-63
ATTN: J CAYOT DEPT 81-63
ATTN: L ROSSI
ATTN: P BENE

LOGICON R & D ASSOCIATES
ATTN: D CARLSON

LORAL AERONUTRONIC
ATTN: TECHNICAL LIBRARY

LTV AEROSPACE & DEFENSE COMPANY
2 CY ATTN: LIBRARY EM-08

MARTIN MARIETTA DENVER AEROSPACE
ATTN: P KASE
ATTN: RESEARCH LIBRARY

MARTIN MARIETTA TECHNOLOGIES INC
ATTN: J TANKE
ATTN: TIC/MP-30

MARTIN MARIETTA TECHNOLOGIES, INC
ATTN: H SCHISLER

MAXWELL LABORATORIES INC
ATTN: J M WILKENFELD

MCDONNELL DOUGLAS CORPORATION
ATTN: P ALBRECHT

MISSION RESEARCH CORP
ATTN: D ALEXANDER

MISSION RESEARCH CORP
ATTN: J LUBELL
ATTN: W WARE

MITRE CORPORATION
ATTN: J R SPURRIER
ATTN: M FITZGERALD

NORDEN SYSTEMS, INC
ATTN: N RIEDERMAN
ATTN: TECHNICAL LIBRARY

NORTHROP GRUMMAN CORPORATION
ATTN: J R SROUR

PACIFIC-SIERRA RESEARCH CORP
ATTN: H BRODE

PHYSITRON INC
ATTN: MARK CHRISTOPHER

RAND CORP
ATTN: C CRAIN

RAYTHEON CO
ATTN: D D LEE
ATTN: JOSEPH SURRO

RESEARCH TRIANGLE INSTITUTE
ATTN: M SIMONS

ROCKWELL INTERNATIONAL CORP
ATTN: V DE MARTINO

SCIENCE APPLICATIONS INTL CORP
ATTN: D MILLWARD
ATTN: DAVID LONG

SCIENCE APPLICATIONS INTL CORP
ATTN: J RETZLER

SCIENCE APPLICATIONS INTL CORP
ATTN: W CHADSEY

SCIENTIFIC RESEARCH ASSOC, INC
ATTN: H GRUBIN

SPIRE CORP
2 CY ATTN: F NAMAVAR

SUNDSTRAND CORP
ATTN: C WHITE

SYSTRON-DONNER CORP
ATTN: SECURITY OFFICER

TECHNOLOGY DEVELOPMENT ASSOCIATES
ATTN: R V BENEDICT

TELEDYNE BROWN ENGINEERING
ATTN: G R EZELL
ATTN: LEWIS T SMITH

TEXAS INSTRUMENTS, INC
ATTN: J SALZMAN

TRW INC
    ATTN: TIC

TRW S. I. G.
    ATTN: C BLASNEK
    ATTN: DR D R GIBSON

UNISYS CORPORATION-DEFENSE SYSTEMS
    ATTN: P MARROFFINO

VISIDYNE, INC
    ATTN: C H HUMPHREY
    ATTN: W P REIDY